NASA/TP—2014–218197

Liquid Methane Testing With a Large-Scale Spray Bar Thermodynamic Vent System

L.J. Hastings
Alpha Technology Inc., Huntsville, Alabama

L.G. Bolshinskiy
Jacobs Engineering MSFC Group, Marshall Space Flight Center, Huntsville, Alabama

A. Hedayat, R.H. Flachbart (retired), J.D. Sisco, and A.R. Schnell
Marshall Space Flight Center, Huntsville, Alabama

July 2014

The NASA STI Program…in Profile

Since its founding, NASA has been dedicated to the advancement of aeronautics and space science. The NASA Scientific and Technical Information (STI) Program Office plays a key part in helping NASA maintain this important role.

The NASA STI Program Office is operated by Langley Research Center, the lead center for NASA's scientific and technical information. The NASA STI Program Office provides access to the NASA STI Database, the largest collection of aeronautical and space science STI in the world. The Program Office is also NASA's institutional mechanism for disseminating the results of its research and development activities. These results are published by NASA in the NASA STI Report Series, which includes the following report types:

- TECHNICAL PUBLICATION. Reports of completed research or a major significant phase of research that present the results of NASA programs and include extensive data or theoretical analysis. Includes compilations of significant scientific and technical data and information deemed to be of continuing reference value. NASA's counterpart of peer-reviewed formal professional papers but has less stringent limitations on manuscript length and extent of graphic presentations.

- TECHNICAL MEMORANDUM. Scientific and technical findings that are preliminary or of specialized interest, e.g., quick release reports, working papers, and bibliographies that contain minimal annotation. Does not contain extensive analysis.

- CONTRACTOR REPORT. Scientific and technical findings by NASA-sponsored contractors and grantees.

- CONFERENCE PUBLICATION. Collected papers from scientific and technical conferences, symposia, seminars, or other meetings sponsored or cosponsored by NASA.

- SPECIAL PUBLICATION. Scientific, technical, or historical information from NASA programs, projects, and mission, often concerned with subjects having substantial public interest.

- TECHNICAL TRANSLATION. English-language translations of foreign scientific and technical material pertinent to NASA's mission.

Specialized services that complement the STI Program Office's diverse offerings include creating custom thesauri, building customized databases, organizing and publishing research results…even providing videos.

For more information about the NASA STI Program Office, see the following:

- Access the NASA STI program home page at <http://www.sti.nasa.gov>

- E-mail your question via the Internet to <help@sti.nasa.gov>

- Phone the NASA STI Help Desk at 757–864–9658

- Write to:
  NASA STI Information Desk
  Mail Stop 148
  NASA Langley Research Center
  Hampton, VA 23681–2199, USA

NASA/TP—2014–218197

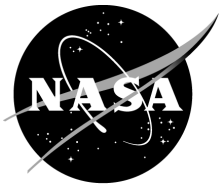

Liquid Methane Testing With a Large-Scale Spray Bar Thermodynamic Vent System

L.J. Hastings
Alpha Technology Inc., Huntsville, Alabama

L.G. Bolshinskiy
Jacobs Engineering MSFC Group, Marshall Space Flight Center, Huntsville, Alabama

A. Hedayat, R.H. Flachbart (retired), J.D. Sisco, and A.R. Schnell
Marshall Space Flight Center, Huntsville, Alabama

National Aeronautics and
Space Administration

Marshall Space Flight Center • Huntsville, Alabama 35812

July 2014

TRADEMARKS

Trade names and trademarks are used in this report for identification only. This usage does not constitute an official endorsement, either expressed or implied, by the National Aeronautics and Space Administration.

Available from:

NASA STI Information Desk
Mail Stop 148
NASA Langley Research Center
Hampton, VA 23681-2199, USA
757–864–9658

This report is also available in electronic form at
<http://www.sti.nasa.gov>

TABLE OF CONTENTS

TABLE OF CONTENTS (Continued)

LIST OF FIGURES

LIST OF FIGURES (Continued)

LIST OF FIGURES (Continued)

LIST OF TABLES

LIST OF ABBREVIATIONS, ACRONYMS, AND SYMBOLS

GHe	gaseous helium
GN_2	gaseous nitrogen
HEX	heat exchanger
J-T	Joule-Thompson
LCH_4	liquid methane
LH_2	liquid hydrogen
LN_2	liquid nitrogen
MHTB	multipurpose hydrogen test bed
MLI	multilayer insulation
NPSP	net positive suction pressure
TankSIM	Tank System Integrated Model
TVS	thermodynamic vent system

NOMENCLATURE

m_{GHe}	computed helium mass
$P_{\max}$	pressure control band maximum
P_{meas}	measured pressure
$P_{\min}$	pressure control band minimum
T_{meas}	measured temperature
T_{sat}	saturation temperature
ΔP	delta pressure
ΔT	delta temperature

TECHNICAL PUBLICATION

LIQUID METHANE TESTING WITH A LARGE-SCALE SPRAY BAR THERMODYNAMIC VENT SYSTEM

1. INTRODUCTION

Maintaining propellant tank pressure control while minimizing propellant loss is a significant challenge associated with the storage of cryogens in the reduced gravity environment of space. Thermodynamic vent systems (TVSs) are frequently considered as a concept for addressing this issue. A TVS typically includes a Joule-Thompson (J-T) expansion device, a two-phase heat exchanger, and a mixing pump to destratify and extract thermal energy from the tank contents with liquid losses minimized. The multipurpose hydrogen test bed (MHTB) spray bar was designed for operation in liquid hydrogen (LH_2) such that sufficient heat energy is removed for saturation conditions remaining within the prescribed control limits. Further, the design was for a system wherein the ullage was hydrogen vapor only, i.e., a single component gas. Although the MHTB spray bar TVS design was optimized for LH_2, the already existing test hardware offered a low-cost, near-term means for evaluating TVS operations with liquid methane (LCH_4) propellant. Furthermore, in order to reveal any unique or unexpected challenges associated with LCH_4 propellant management, two primary conditioning requirements were imposed during the testing: (1) Propellant densification and (2) helium pressurant. Specifics regarding test objectives, hardware, and approach are described in section 2.

To avoid confusion, it should be noted that two other subjects were addressed in a preliminary fashion or 'piggybacked' onto the TVS testing: (1) Radio frequency mass gauging and (2) a subsystem for conditioning the LCH_4 as it was loaded into the MHTB tank. Even though there are occasional references to these subjects throughout the test planning documentation, the two subjects are separately addressed.

2. TEST OBJECTIVES

Because gaseous helium (GHe) pressurant is frequently considered to enable orbital and lunar surface engine starts, testing the effects of GHe on methane TVS operations was required. The LCH_4 saturation conditions were reduced for two reasons: (1) To simulate densified methane in-space storage conditions and (2) to maximize the difference between the GHe partial pressure and the methane partial or vapor pressure to thereby simulate in-flight storage conditions as closely as possible. Further, when GHe pressurant and maintaining saturation conditions were introduced as operating conditions, the control algorithm had to be rewritten. Therefore, the primary objective of this program was to address TVS performance with densified LCH_4 pressurized with GHe. Specific goals associated with the primary objective were as follows:

- Evaluate/define a control algorithm for controlling both tank pressure and LCH_4 densification level.
- Anchor TVS analytical modeling.
- Define operational challenges unique to LCH_4.

3. TEST HARDWARE AND INSTRUMENTATION UTILIZATION

The test facilities, MHTB, and spray bar TVS are described in detail in references 1 and 2, and are therefore only briefly described herein. The major test article elements consisted of the test bed tank and its supporting equipment (including an environmental shroud), the cryogenic insulation subsystem, and the test bed instrumentation. The primary test subassemblies or subsystems of interest were the TVS spray bar heat exchanger assembly, recirculation pump, and 'TVS-dedicated' instrumentation.

3.1 Multipurpose Hydrogen Test Bed and Test Facility

The MHTB is pictured in figure 1 and schematically depicted in figure 2. The MHTB tank is enclosed within an environmental shroud, shown in figure 3, that simulates a ground hold conditioning purge (similar to that in a payload bay) and enables the imposition of a range of uniform temperatures on the multilayer insulation (MLI) external surfaces. The shroud is 4.57 m (15 ft) high by 3.56 m (12 ft) in diameter and contains a purge ring for distributing dry gaseous nitrogen (GN_2). The shroud heater strips/cooling loops can impose either constant or time-dependent boundary temperatures ranging from 80 to 320 K (144 to 576 °R). The 15083 aluminum tank is cylindrical in shape with a height of 3.05 m (10 ft), a diameter of 3.05 m (10 ft), and 2:1 elliptical domes. It has an internal volume of 18.09 m^3 (639 ft^3) and a surface area of 35.74 m^2 (379 ft^2), with a resultant surface area-to-volume ratio of 1.92 L/m (0.58 L/ft) that is reasonably representative of full-scale vehicle tanks. The MHTB tanking table is presented in appendix A, which defines fill height versus ullage volume, liquid volume, distance from bottom, and percent fill. The MHTB insulation concept consists of a foam/multilayer combination. The foam element enables the use of a payload bay-type GN_2 purge during ground hold periods. The 45-layer, double-aluminized Mylar® MLI provides thermal radiation protection while at vacuum conditions on-orbit. As reported in reference 2, which describes the insulation in more detail, the combined effects of the MLI variable density, large vent hole pattern, and installation technique resulted in substantial performance improvements over conventional insulation configurations. However, in this application, the insulation system performance was of secondary interest as discussed in section 4.

Figure 1. MHTB test article.

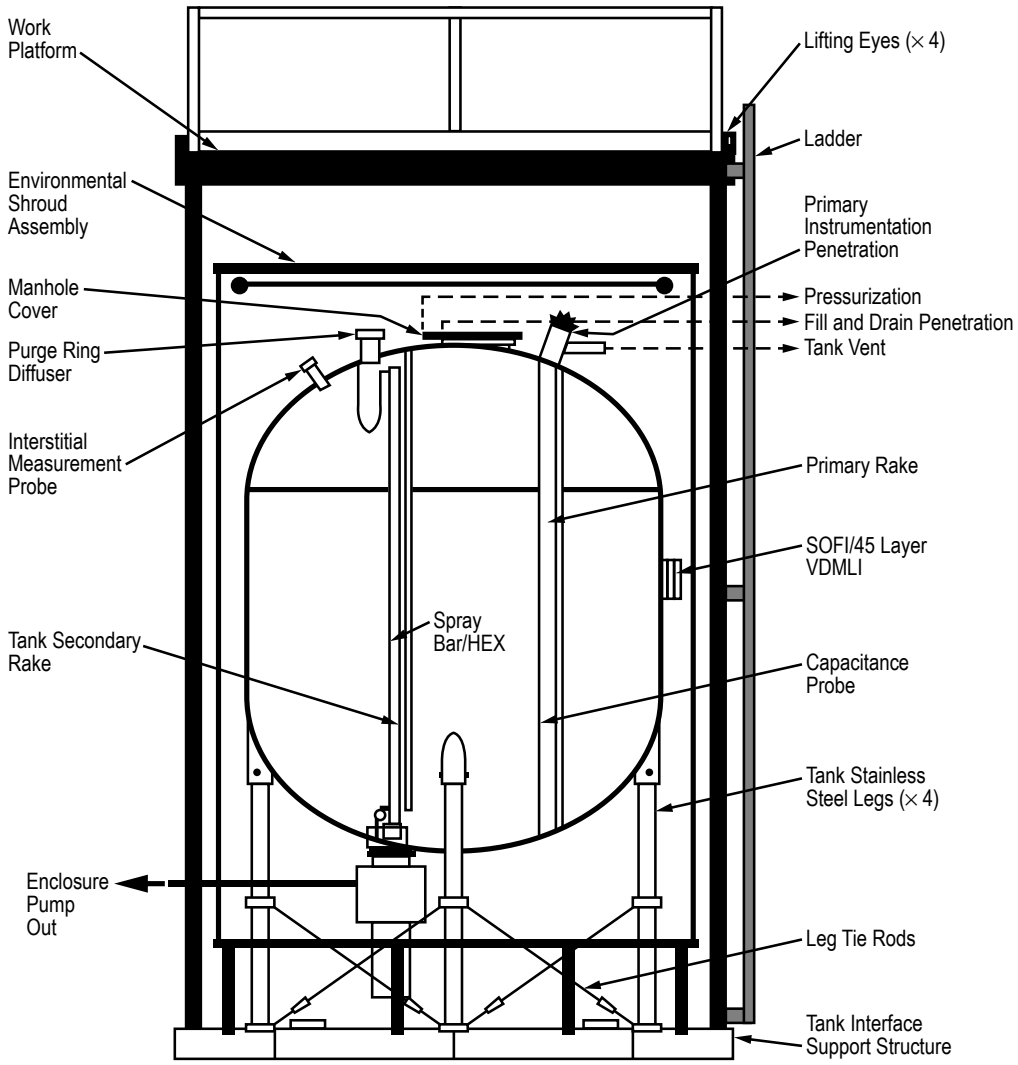

Figure 2. MHTB schematic.

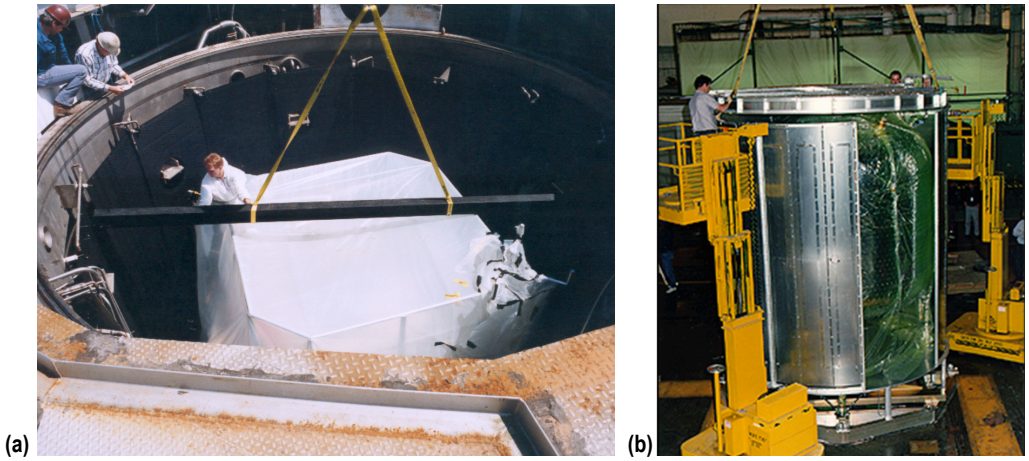

Figure 3. MHTB (a) installation in vacuum chamber and (b) shroud assembly.

Testing was performed at the Marshall Space Flight Center east test area thermal vacuum facility, Test Stand 300. The vacuum chamber is cylindrical in shape and has usable internal dimensions of 5.5 m (18 ft) in diameter and 7.9 m (26 ft) in height. Personnel access is through a small side-entry door, but the chamber lid is removable for installation of large test articles. The chamber pumping train consists of a single-stage GN_2 ejector, three mechanical roughing pumps (rated at 140 L/s (300 ft^3/min each)) with blowers (rated at 610 L/s (1,300 ft^3/min) each), and two 1.2-m (48-in) oil diffusion pumps (rated at 95,000 L/s (200,000 ft^3/min) nitrogen each). Liquid nitrogen (LN_2) cold walls provide cryopumping and thermal conditioning capability and are composed of five parallel zones that totally surround the usable chamber volume with a surface emissivity of ≈0.95. The facility systems in combination with the test article shroud enable simulation of orbit environmental conditions by providing vacuum levels of 10^{-8} torr and a temperature range of 80 to 320 K (140 to 576 °R).

3.2 Spray Bar Heat Exchanger Assembly

The spray bar heat exchanger and spray injection assembly schematic is presented in figure 4, and the installation within the MHTB is pictorially presented in figures 5 and 6. The heat exchanger element consists of two concentric stainless steel tubes. The outer and inner tubes have 3.81 and 3.18 cm (1.5 and 1.25 in) outside diameters, respectively, and both have a wall thickness of 0.089 cm (0.035 in). The overall length of the assembly is 2.67 m (105 in) with an area of 0.27 m^2 (2.9 ft^2) for energy exchange between the recirculated and vented fluids. The external area available for energy exchange between the vented and tank or bulk fluids is 0.287 m^2 (3.1 ft^2).

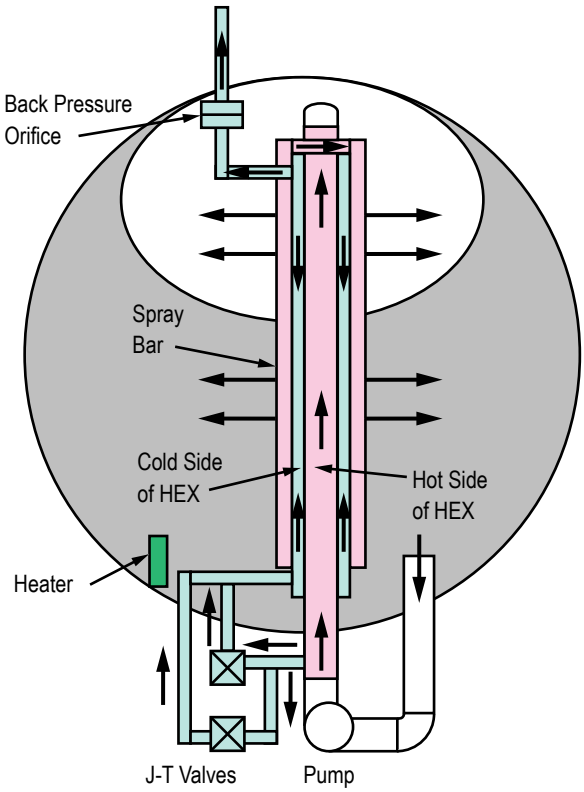

Figure 4. Spray bar heat exchanger and spray injection assembly schematic.

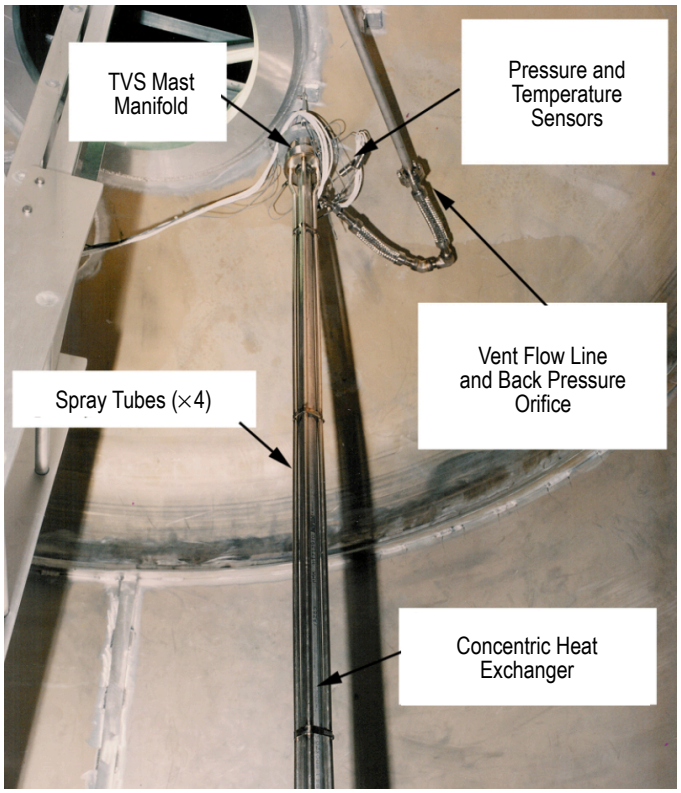

Figure 5. TVS spray bar assembly MHTB installation—top.

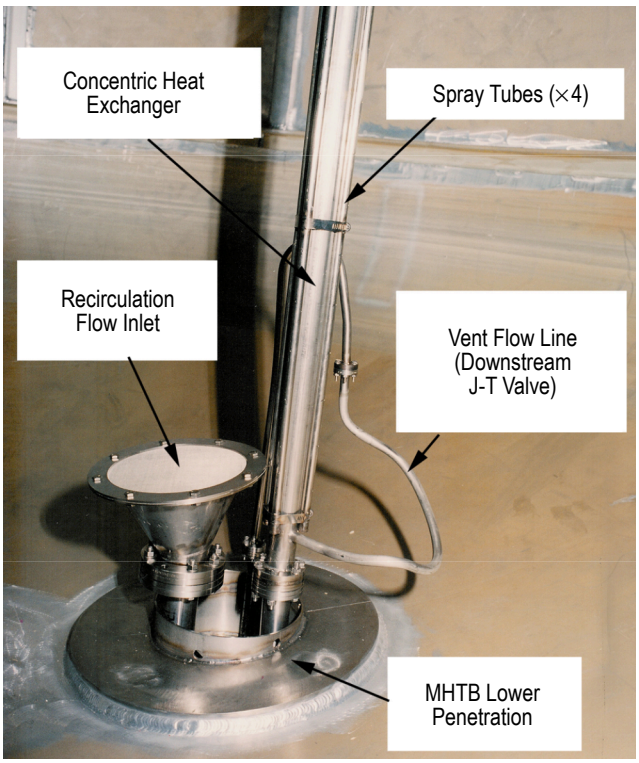

Figure 6. TVS spray bar assembly MHTB installation—bottom.

The spray injection design consists of four 1.27-cm (0.5-in) outside diameter tubes manifolded together at the heat exchanger outlet. Each tube contains 43 orifices equally spaced 6.1 cm (2.4 in) apart which enable spray injection in four directions. Additionally, eight orifices (two per axis) were included in the area above the heat exchanger outlet to increase injection cooling in the upper tank dome area.

3.3 Recirculation Pump

A Barber-Nichols, Inc., BNHP-08B-000 centrifugal cryogenic pump (operating characteristics: table 1; manual: appendix B) was used for the recirculation process. The pump delivers 114 LPM with a delta pressure (ΔP) of 33 kPa. The recirculation line and pump assembly were contained within an enclosure attached to the tank bottom, depicted in figures 7 and 8, so that any leakage could be entrapped and pumped out without compromising the chamber vacuum levels. Such an enclosure would not be required in an actual application.

Table 1. Barber-Nichols pump operating characteristics.

Barber-Nichols BNHP-08B-000 Pump Design Point Operating Conditions
Reference fluid: LN_2
Inlet pressure: 159 kPa (23 psia)
Inlet temperature: 81 K (146 R)
Flow rate: 114 LPM (30 GPM)
Differential pressure: 33 kPa (4.8 psid)
Approximate operating speed: 3,100 rpm
Motor Name Plate Data
Three-phase, inverter duty motor. In this application, operates at fraction of 200 VAC (400 Hz) design speed
Manufacturer: Lucas Western
Motor series: 181RA50
Volts, AC: 57; Amps: 1.1; Phase: 3; Hertz: 110; Poles: 4
Horsepower: 0.07 (0.15 hp at cryogenic temperatures)
Speed: 3,100 rpm
Ambient temperature: 313 K (564 R)
Duty: Continuous
Insulation class: Hs
Enclosure: TELC submerged

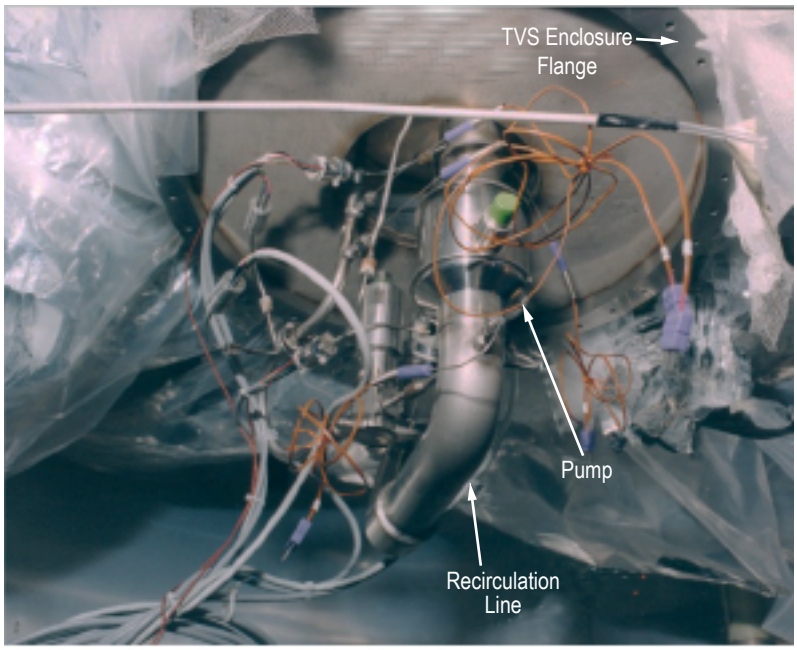

Figure 7. TVS recirculation line and pump.

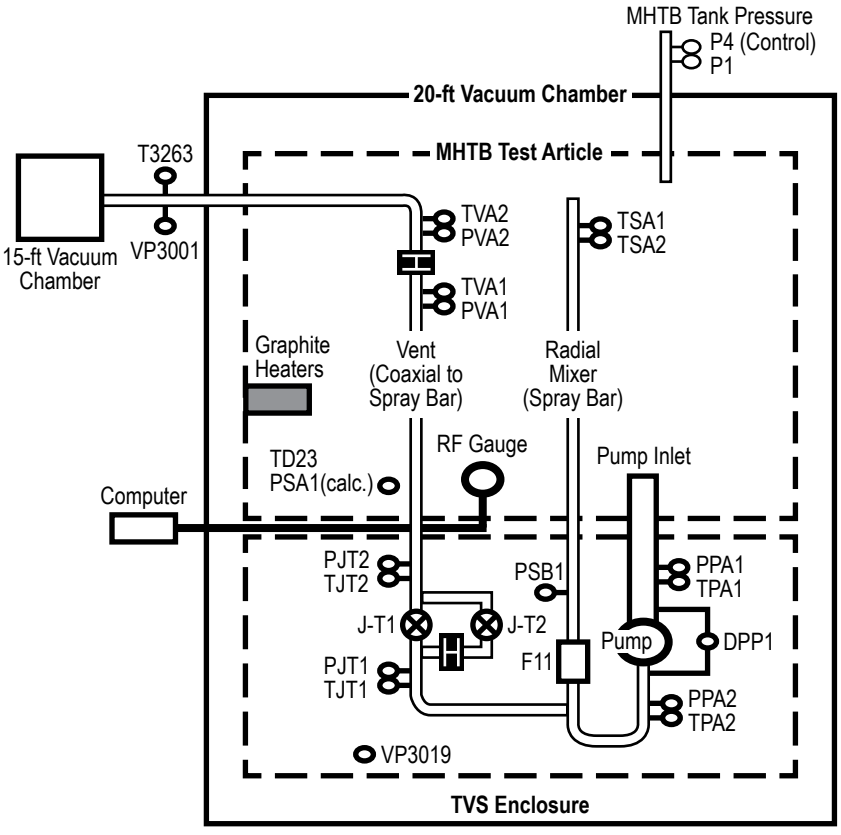

Figure 8. Spray bar TVS schematic with instrumentation and Test Stand 300 interfaces.

3.4 Test Bed Instrumentation

The test article and environmental shroud instrumentation details are presented in appendix C; however, the instrumentation arrangement for each primary segment is summarized in this section. The test article instrumentation consists primarily of thermocouple and silicon diodes to measure insulation, fluid, and tank wall temperatures. Typically, silicon diode (Lake Shore type DT-470-11A) temperature transducers are positioned in areas of lowest temperatures, which provide higher accuracy as compared to thermocouples. MLI temperature profiles or gradients are measured at seven positions with one silicon diode and four thermocouples placed at each of the seven measurement positions. The MLI interstitial pressure is measured at the foam/MLI interface, and a sampling port for both dew point and gas species is provided. The tank is internally equipped with two instrumentation rakes (table 2) and a capacitance liquid level probe, all supported from the top of the tank (fig. 9). The rakes, constructed from a fiberglass epoxy channel section, are equipped with silicon diodes attached at 22.9-cm (9-in) intervals using nylon rod offsets and cryogenic-compatible epoxy. The instrumentation rakes provide temperature gradient measurements within both ullage and liquid and serve as a backup to the continuous liquid level capacitance probe. The tank penetrations, including the vent, fill/drain, pressurization, pressure sensor probe, manhole pump-out, and support legs, are instrumented to determine the solid conduction component of heat leak. During the TVS performance testing, the bulk liquid temperature relative to ullage saturation conditions was monitored using silicon diode TD23 on rake 2 (fig. 9) and ullage pressure sensor, P4 (see sec. 3.5). P4 is an MKS Instruments, Inc., Baratron 0–666 kPa (0–96 psia) absolute pressure transducer with an accuracy of ±0.02%. The environmental shroud is composed of 17 individual panels, each equipped with a minimum of two thermocouples attached to the inner surfaces and placed beneath the electrical heating strips. These thermocouples are used with a test facility closed-loop control system to regulate each shroud panel temperature. The application of TVS-specific or dedicated instrumentation is discussed in section 3.5.

Table 2. Silicon diode positions on MHTB instrumentation rakes.

Rake 1			Rake 2		
	in	%		in	%
TD1	109.25	97.11	TD13	110	97.52
TD2	100.25	90.55	TD14	101	91.19
TD3	91.25	81.96	TD15	92	82.71
TD4	82.25	72.9	TD16	83	73.66
TD5	73.25	63.84	TD17	74	64.6
TD6	64.25	54.78	TD18	65	55.54
TD7	55.25	45.72	TD19	56	46.48
TD8	46.25	36.66	TD20	47	37.42
TD9	37.25	27.6	TD21	38	28.36
TD10	28.25	18.54	TD22	29	19.3
TD11	19.25	9.9	TD23	20	10.57
TD12	10.25	3.18	TD24	11	3.62

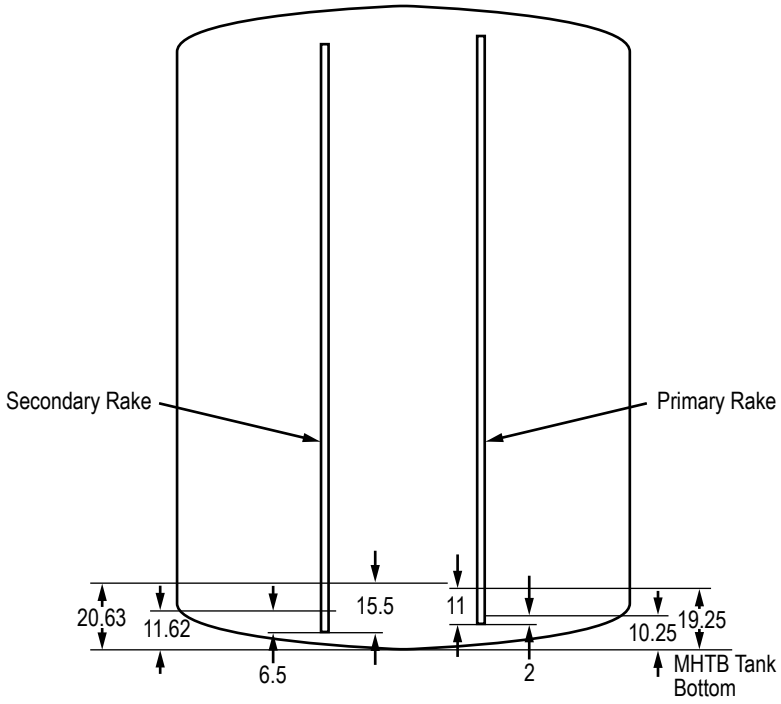

Figure 9. MHTB internal instrumentation rakes (dimensions in inches).

3.5 Thermodynamic Vent System Instrumentation Application

The combination of test bed and TVS-dedicated instrumentation was arranged to provide input to the TVS controller and to define the TVS performance characteristics. As described in section 3.4, a bulk temperature measurement was used to monitor the bulk liquid saturation conditions relative to the measured ullage pressure and as an input to the TVS controller. The sensor, TD23, at the 11.5% fill level, or 53.3 cm (21 in) above the tank bottom, was considered to be representative of the bulk liquid temperature. The TD23 temperature output was corrected to account for hydrostatic pressure, converted to a corresponding saturation pressure (termed PSA1), and compared with the ullage pressure, P4.

The TVS performance characterization, using the TVS-dedicated instrumentation shown in figure 8, included definitions of three elements: (1) Spray bar heat exchanger performance, (2) spray bar injection flow, and (3) vent flow rate. The planned approach for determination of each element using the TVS instrumentation was as follows:

(1) Spray bar recirculation flow—The total flow rate can be estimated based on the pump speed indication and the pump ΔP measurement. The recirculated or spray injection flow rate (total minus the vent flow) is directly measured by a turbine flowmeter (F11), and the spray bar inlet pressure is measured by PSB1, positioned just downstream of the flowmeter. The spray injection temperature is measured by redundant silicone diode transducers (TSA1 and TSA2) located at the inlet to the four spray tubes. These spray injection temperature measurements provide key inputs for thermodynamic reconstruction analysis to correlate ullage pressure reductions during mixing cycles.

(2) Vented flow conditions—The J-T valve inlet pressure and temperature are measured by PJ1 and TJ1, respectively, and outlet conditions by PJ2 and TJ2. The vented flow downstream of the J-T valve then enters the spray bar heat exchanger inlet, normally the cold side. After passing through the heat exchanger, the normally warmed vented fluid exits the spray bar and enters the back pressure orifice positioned within the MHTB tank. The back pressure orifice inlet pressure and temperature are measured by PVA1 and TVA1, respectively, and outlet conditions are measured by PVA2 and TVA2. The vented fluid is routed from the 20-ft chamber through a vacuum jacketed line into the 15-ft vacuum chamber where the vent line exit temperature and pressure are measured by facility measurements T3263 and VP300. A comparison of pressure and temperature measured at the J-T valve outlet (PJ2 and TJ2), with conditions entering the back pressure orifice (PVA1 and TVA1), provide an indication of spray bar energy extraction or heat exchanger performance. For example, whether or not the vented fluid exiting is superheated or two-phase can be determined. Ideally, the vented fluid entering the back pressure orifice should be single-phase vapor, slightly superheated. Assuming 100% vapor at the back pressure orifice inlet, the vented flow rate can be computed using choked flow calculations based on the calibrated back pressure orifice discharge, coefficient-area product. Then, the total MHTB energy extraction rate can be calculated based on change in inlet-to-outlet enthalpy times the vent flow rate.

Therefore, the overall strategy was that, although the spray bar was not optimized for operation with methane, the system setup could be adjusted to operate within appropriate thermodynamic regimes for measured data correlations with analytical modeling.

4. TEST APPROACH AND INITIAL OBSERVATIONS

Although minimizing the total heat leak was not critical, the heat leak into the tank was measured to support the subsequent testing and data evaluation. The heat leak testing was followed by propellant conditioning using the TVS (TVS test phase I) to reduce the LCH_4 saturation pressure, followed by pressurization conditioning. Then, the remaining TVS testing was conducted with the conditioned LCH_4 in four additional phases as various techniques were attempted to achieve the expected level of performance from the spray bar system. The objectives, test conditions, hardware adjustments, and preliminary test results associated with each test element or phase are described in the following sections.

4.1 Baseline Boiloff Measurement

Heaters were activated during the TVS testing to decrease the cycle durations, thereby enabling the accumulation of more cycles within the allotted test time. Therefore, minimizing tank heat leak was not a priority. The baseline heat leak of 120 W (without the heaters activated) was measured with a fill level of about 37 %, and the ullage pressure held constant at 166 ± 0.0069 kPa by the Test Stand 300 facility back pressure control system. It should also be noted that the ambient heat leak was elevated in comparison to the more typical range of 20 to 50 W because the chamber cold walls and the tank leg heat guards were not activated.

4.2 Phase I—Propellant Conditioning

4.2.1 Saturation Conditioning

As previously stated, LCH_4 saturation conditions were reduced to simulate densified in-space storage conditions. Starting with a 90% tank fill level, the pump and J-T2 remained on to reduce the liquid saturation pressure. As shown in figure 10, after 14 hr and 40 min, the liquid saturation pressure was reduced from 110 kPa (16 psia) to 54.3 kPa (7.9 psia).

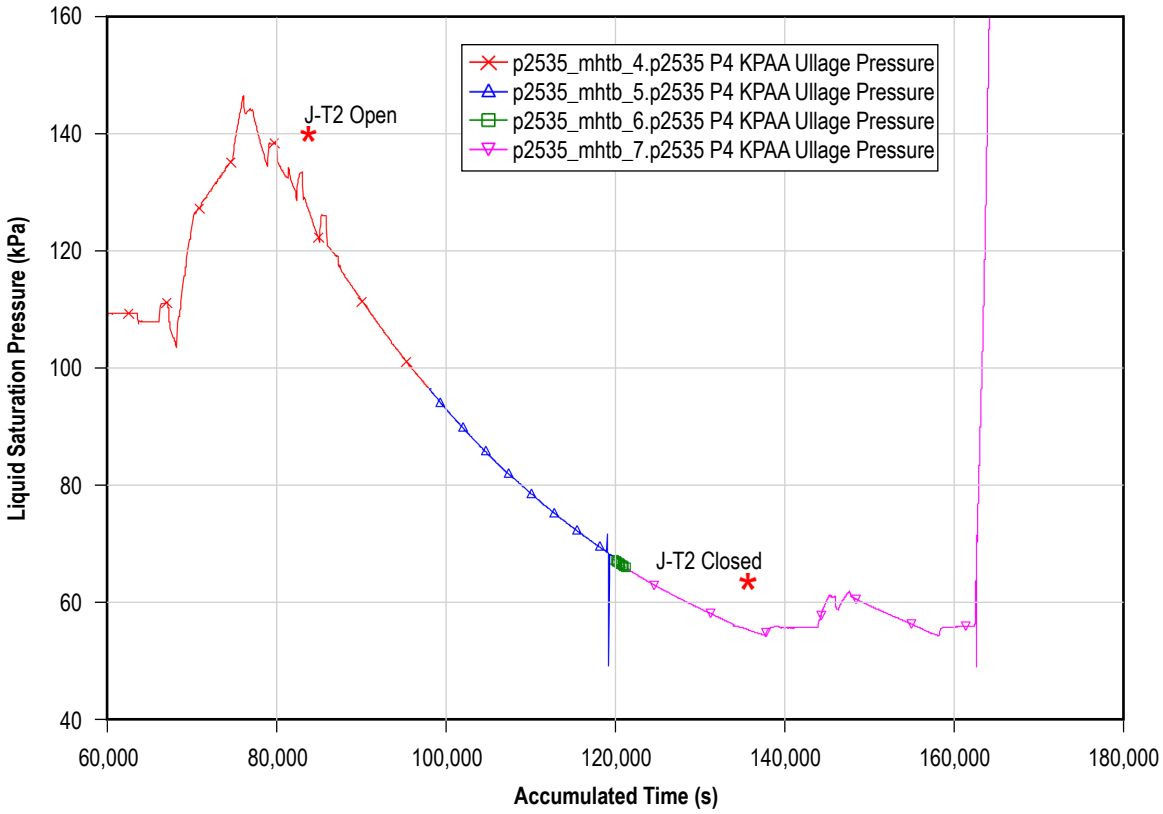

Figure 10. LCH_4 saturation pressure reduction—phase I testing.

4.2.2 Pressurization Conditioning

Following the saturation pressure reduction, the tank was locked up, two heaters were activated at 300 W each, and with the mixer on continuously, an expedited self-pressurization process was initiated. The measured temperature rise rates for the tank contents and wall are presented in figure 11. The tank contents and wall structure temperatures increased at a constant rate of 1.8×10^{-5} K/s throughout the expedited self-pressurization period, which resulted in average temperature increases of 2.38×10^{-5} K/s and 1.83×10^{-5} K/s for the ullage and liquid, respectively. A heat balance study indicated that not all of the heater power remained in the methane. The study indicated net thermal additions of 0.251 W (less than 1%) by the TVS pump operation, 440 W (61%) into the liquid, and 281 W (39%) to the tank structure for a gross energy input of 720 W.

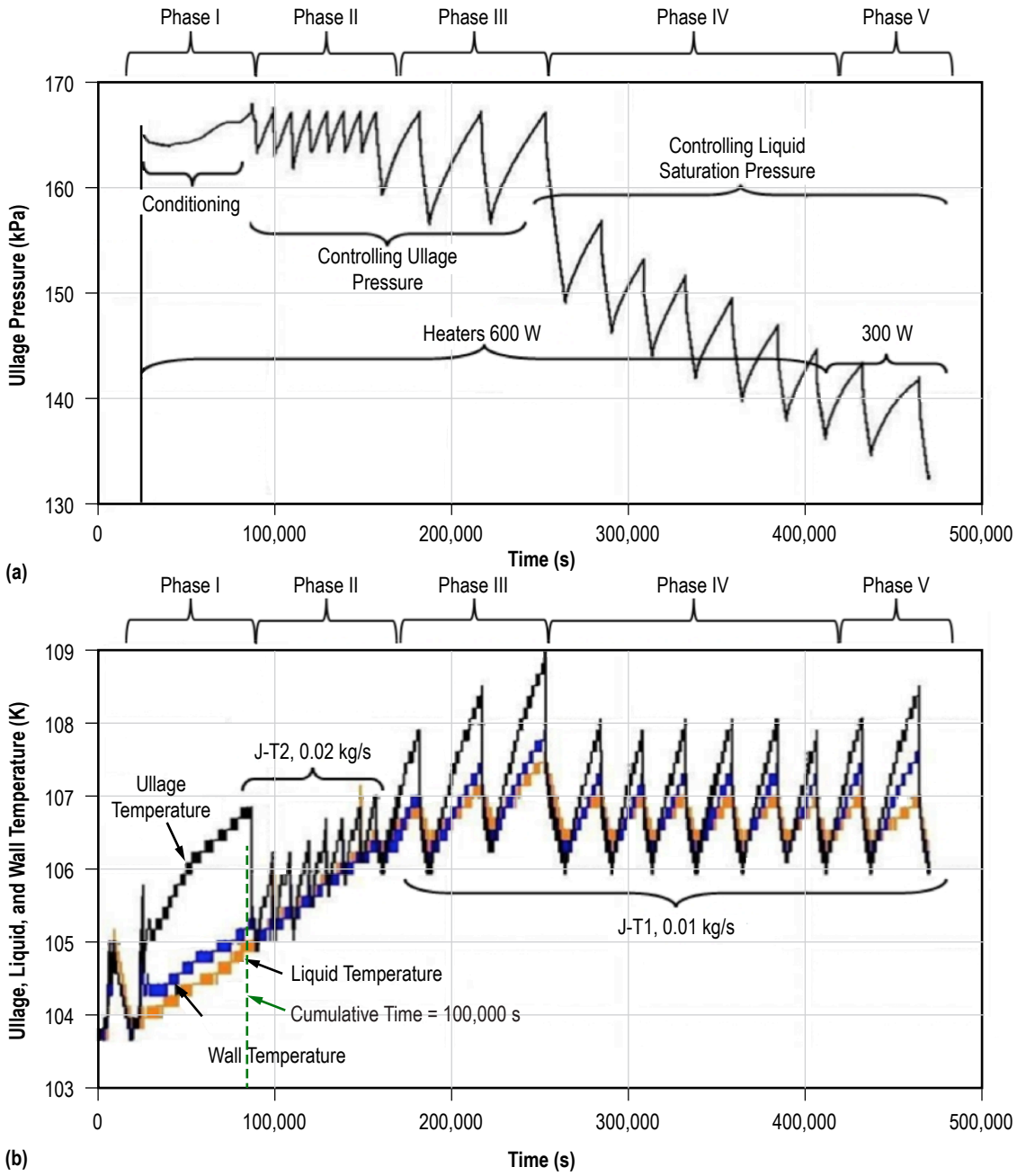

Figure 11. Measured (a) ullage pressure and (b) tank fluid and wall temperatures—phases I–V testing.

After tank topping to 90% was complete, with the pump and J-T valve still operating and the liquid saturated at 50 kPa (7.25 psia), GHe was injected into the ullage until the pressure reached 163.2 kPa (24 psia) (gaseous methane and GHe partial pressures were 50 kPa (7.25 psia) and 116 kPa (16.8 psia), respectively), the value selected for the ullage pressure control band minimum (P_{min}). Then the pump and J-T valve were turned off, and the ullage pressure was allowed to rise to 167.2 kPa (24.3 psia), the pressure control band maximum (P_{max}). As shown in figure 11, the preceding activities completed the phase I propellant conditioning in preparation for phase II of TVS testing.

4.3 Phase II—Initial Thermodynamic Vent System Pressure Control Testing

Completion of phase I established the following conditions for initiation of the TVS pressure control testing (phase II):

- Ullage pressure of 163 kPa (24 psia), the $P_{\min}$ set point.
- Two graphite heaters adjusted to 300 W each for a gross heat input from all sources of 720 W.
- The larger J-T valve, J-T2, with an expected flow rate of 0.02 kg/s, or 72 kg/hr, was selected based on the high thermal load into the propellant (440 W).

Eight mixing/vent cycles were conducted with the ullage pressure held within a ±1.725 kPa (±0.25 psia) control band for about 17 hr (fig. 11). Although the TVS maintained the tank ullage pressure within the prescribed control band, the liquid saturation pressure continued to rise throughout operation for a saturation pressure increase of 9 kPa (saturation temperature increased from 105 to 106.7 K). This result was somewhat unexpected because during previous MHTB tests with LH_2 and LN_2, the same spray bar TVS appeared to have controlled the ullage pressure while maintaining the liquid saturation pressure at a constant value.[2–4] However, since it was evident that the thermal energy removal capability was inadequate, it was reasoned that the flow rate had not allowed sufficient dwell time within the spray bar heat exchanger. That logic led to phase III testing with the smaller J-T valve, J-T1.

4.4 Phase III—Extended Vent Cycles With Reduced Flow Rate Joule-Thompson Valve

Phase III testing was initiated with the J-T1 valve with a predicted flow rate capability of 0.01 kg/s, which was one-half the flow rate capability of J-T2, with the heater setting remaining at 600 W. In addition to determining if tank pressure control would be improved, it was believed that the lower flow rate would reduce total propellant loss. It was immediately apparent that the reduced flow rate with J-T1 had significantly improved the ullage pressure control and therefore was used for the remainder of the testing (fig. 11).

On the second phase III test cycle, or the ninth total vent cycle, J-T1 was held open to establish a new liquid saturation pressure baseline pressure at 62 kPa (T_{sat}=106 K), which resulted in an ullage pressure decrease of 10.3 kPa. The ullage pressure was then allowed to increase 10.3 kPa; however, during this time, the liquid saturation pressure increased to a new maximum of about 69 kPa (T_{sat}=107 K). The conditions of the ninth TVS cycle were repeated during the tenth cycle to observe a trend, and the liquid saturation continued to rise in a sawtooth fashion. Since control of both ullage pressure and saturation level are often desired in an actual operation, the test team was faced with a decision on how the remaining test time could best be utilized in the next phase of testing, phase IV.

4.5 Phase IV—Thermodynamic Vent System Controls Keyed to Saturation Pressure

The test team elected to continue testing the existing fill level with the heater setting at 600 W, instead of proceeding to the planned 50% level. This decision was made for two reasons: (1) The higher fill case is the most difficult case to match analytically and (2) the team preferred to have extensive data at one test condition rather than sparse data at multiple test conditions. Therefore, phase IV testing was initiated with cycle 12 with the TVS controls keyed to saturation pressure instead of ullage pressure. The intent of this mode of operation was to keep the liquid temperature under control, thus demonstrating the capability of maintaining a prescribed propellant saturation level. The saturation level was successfully maintained at 62–68 kPa (T_{sat} between 106 and 107 K) during cycles 11–17 (fig. 11). However, the ullage pressure decreased in a sawtooth fashion by about 1.7 kPa per cycle for a total reduction of 13 kPa, or 7% during the six cycles, or about 42 hr. It was reasoned that large liquid losses associated with the long vent cycles in combination with an inefficient TVS were factors in the decreasing ullage pressure. The next logical step available to the test team was to reduce the thermal load, which led to the final TVS test phase, phase V.

4.6 Phase V—Controls Keyed to Saturation Pressure, Reduced Thermal Load

Although it was apparent that the heat load reduction was logical, the issue was that each TVS cycle duration increased inversely with decreasing thermal load, and the test time/budget limit was rapidly approaching. Therefore, the reasoning for the test conditions selected for the final test phase was as follows:

- Sufficient test time was not available to allow testing at a heat load closer to what could be expected on an actual mission, such as 25–50 W. Further, there was the concern that it could introduce a new thermal flow regime in the bulk liquid that would add confusion rather than clarification.

- The next TVS phase did not have to function perfectly to verify and anchor analytical modeling. It needed only to demonstrate that the reduced thermal load was a significant step in the correct direction.

Based on the preceding rationale, the test team elected to proceed with testing with the heater setting reduced by half to 300 W, with an estimated net input to the liquid of 256 W, during TVS cycles 18 and 19 (fig. 11). The ullage pressure decrease continued at a reduced rate.

5. PRELIMINARY DATA EVALUATION

5.1 Saturation Reduction

Examination of the J-T2 thermodynamic characteristics begins to reveal why there was limited energy removal. In figure 12, the liquid saturation reduction data are plotted in terms of liquid temperatures upstream and downstream of the J-T valve as opposed to the bulk liquid saturation pressure presented in figure 10. The data revealed that there was no temperature drop across the J-T valve, but instead there was a temperature rise of about 0.25 K. The pressure drop across the J-T valve was very slight, less than 0.2 kPa (0.03 psia). Based on J-T testing of subcooled methane by Jurns,[5] it is apparent the MHTB testing had been conducted with the methane in a 'metastable' state. The J-T expansion coefficient was negative; that is, the change in temperature, or delta temperature (ΔT), was negative relative to the positive change in pressure, or ΔP.

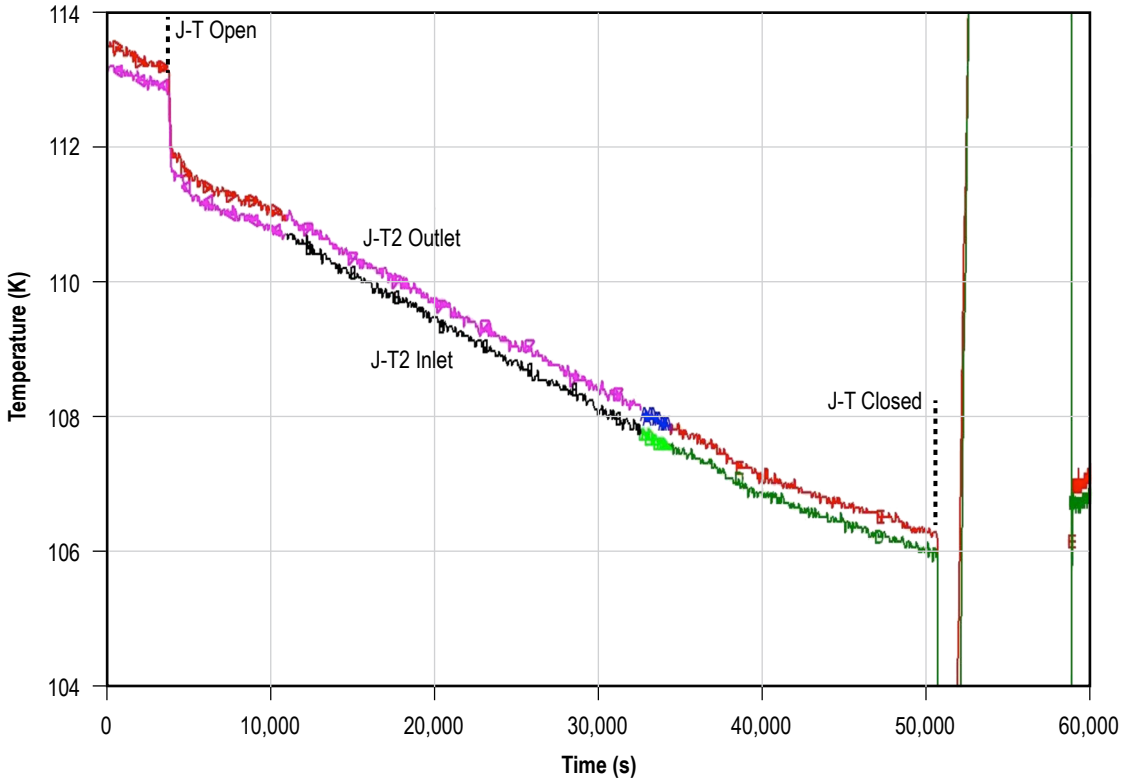

Figure 12. Joule-Thompson inlet and outlet temperature comparison during phase I saturation conditioning.

Although highly inefficient, the spray bar had managed to achieve the reduction in saturation conditions. The question is how does one quantify the effects of operating a TVS within the metastable regime of methane? The characteristics and implications of metastable conditions during TVS operations are briefly discussed in the following section.

5.2 Metastable Conditions

A common example of metastable conditions is demonstrated in the laboratory by gradually heating a glass tube of liquid (such as water) above its saturation level, superheating the liquid without boiling, or two-phase conditions. Similarly, as shown in figure 13, superheated conditions can be created by reducing pressure until the saturation line is crossed without boiling. In either case, the superheated liquid is in an unstable or metastable state, and the onset of boiling or two-phase liquid can erupt violently.

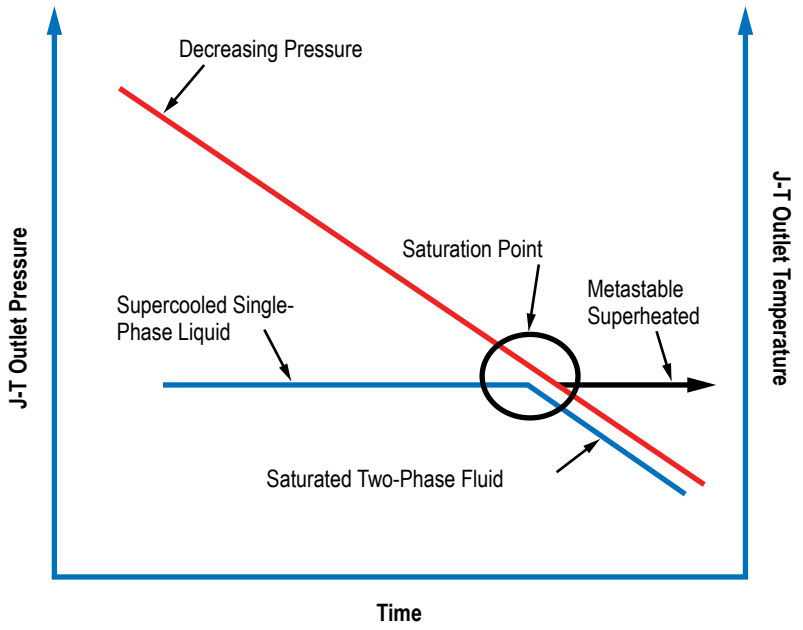

Figure 13. Recognizing presence of metastable liquid.

The same process can be visualized with a pressure-specific volume diagram for a pure fluid, as shown in figure 14. Again, pressure is reduced until the saturation line is crossed and the liquid becomes superheated. Also, operation within this region can lead to a negative J-T expansion coefficient wherein the temperature increases instead of decreasing with the pressure drop. Although the term 'metastable' conveys a lack of stability or predictability, helpful guidelines or techniques for estimating lower stability limits are described in reference 5.

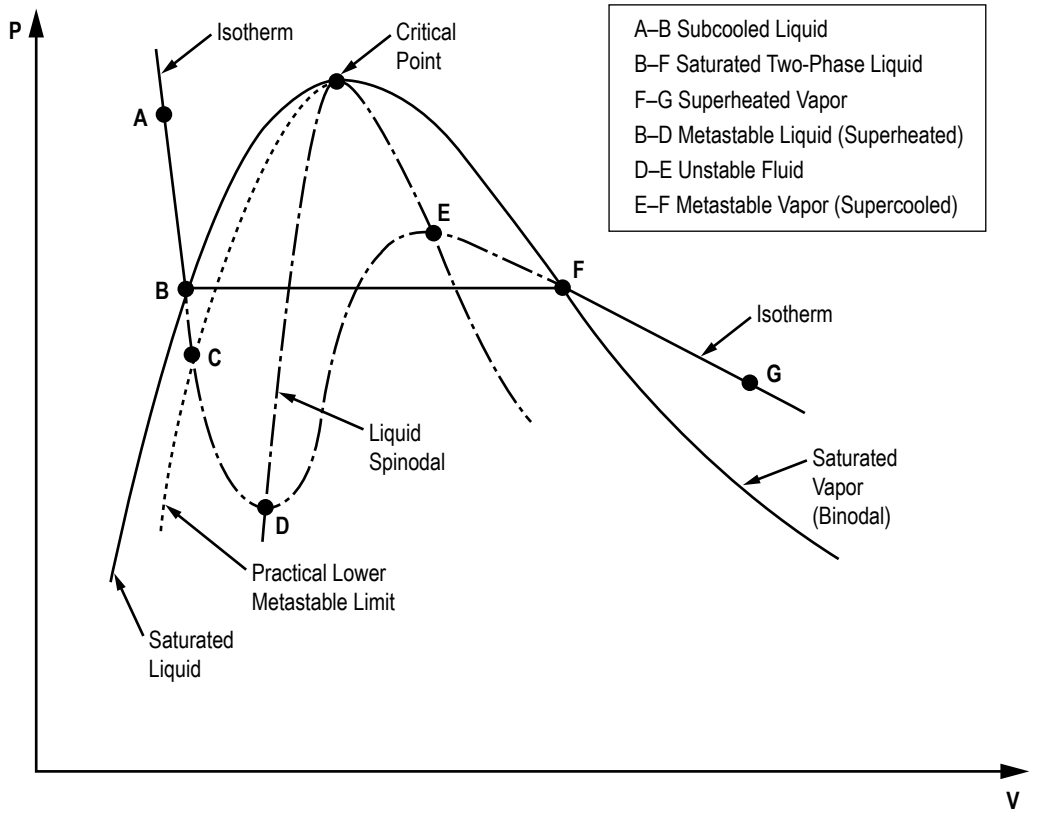

Figure 14. Schematic depicting saturation line and practical lower metastable limit.

The complexities introduced by metastable LCH_4 necessitated a component-by-component examination of the data to ensure that an equipment malfunction or instrumentation error had not contributed to the problem.

6. COMPONENT-BY-COMPONENT EVALUATION

A detailed examination of thermodynamic conditions throughout the TVS system was conducted on a component-by-component basis, beginning with the pump and recirculated liquid entrance and exit conditions on the warm side of the spray bar heat exchanger; then, the vented fluid entrance and exit conditions on the cold side of the spray bar.

6.1 Pump and Spray Bar Recirculation Flow

The recirculation flow rate measured by the flowmeter, F11 (positioned at the spray bar entrance), presented in figure 15, shows that the desired flow rate of 114 LPM (30 GPM) was consistently delivered by the pump throughout testing (with the exception of limited erratic behavior at about 540,000–550,000 test time interval). Additionally, the pump pressure rise or ΔP measured by DPP1, presented in figure 16, indicates an average of 28 kPa (4.1 psid). These data are consistent with the expected performance specifications in table 1.

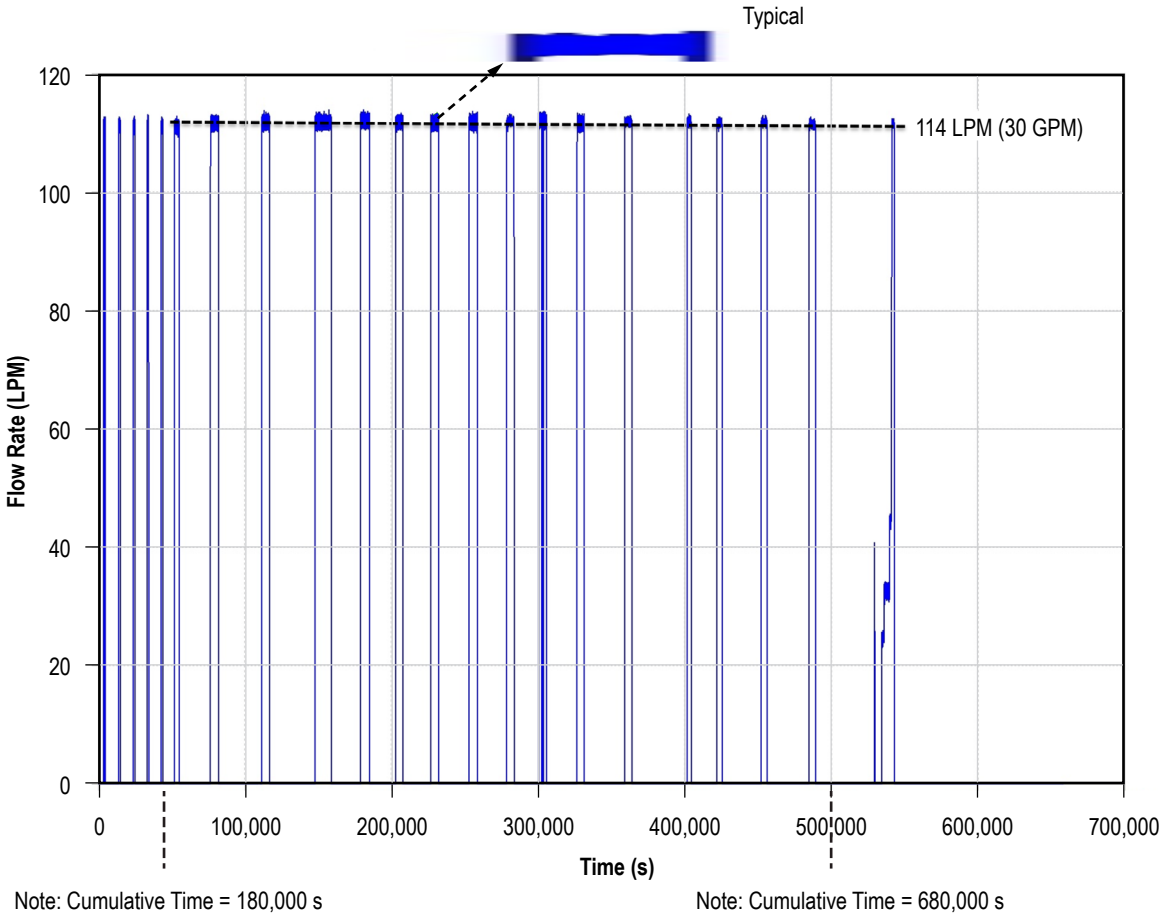

Figure 15. Spray bar recirculation flow rate (LPM).

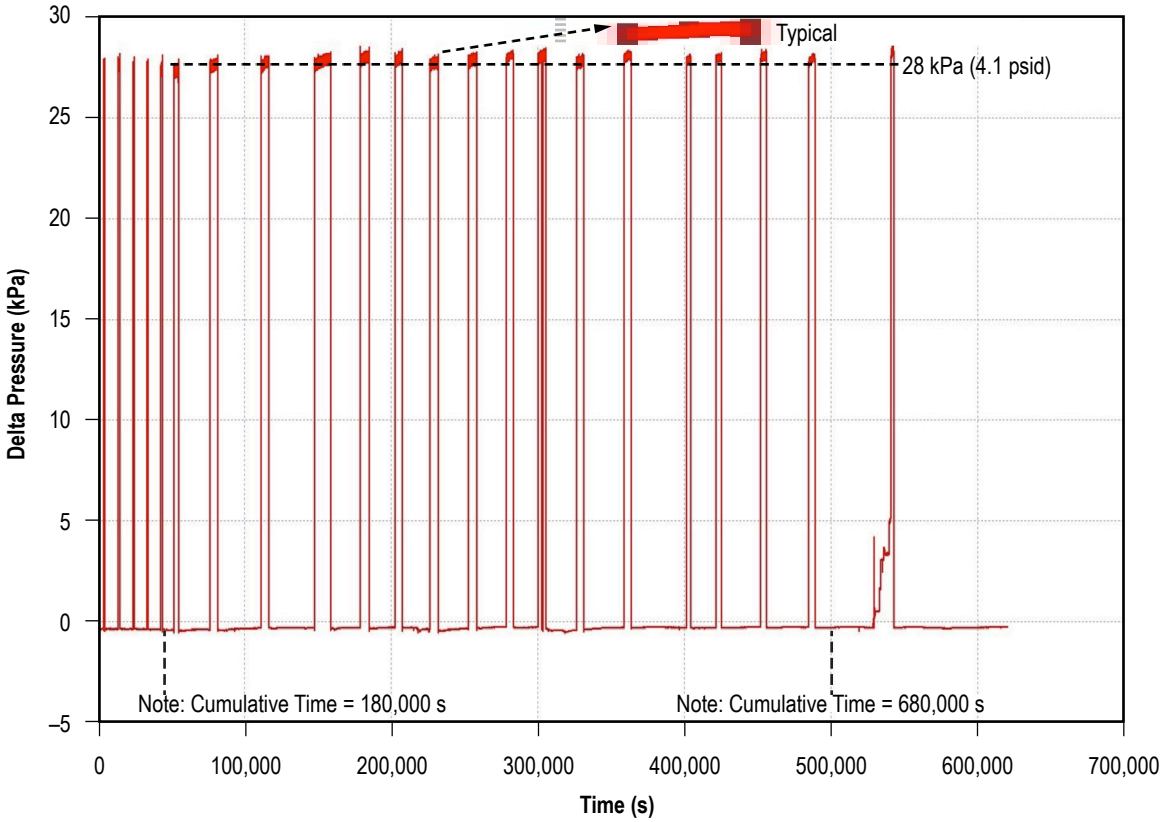

Figure 16. Spray bar pump delta pressure history.

The pump downstream pressure (PPA2) and spray bar entrance pressure (PSB1) measured data presented in figure 17 indicate patterns consistent with the ullage pressure trends observed during the various test phases previously described (sec. 4, fig. 11). Basically, the peak pressures observed during the active TVS periods decreased with each cycle when the saturation condition control began with phase IV testing. The rate of decrease averaged about 20 kPa over 12 cycles, or about 1.7 kPa per cycle. A representative expanded view of a data segment from figure 17 is presented in figure 18 to assist with data visualization.

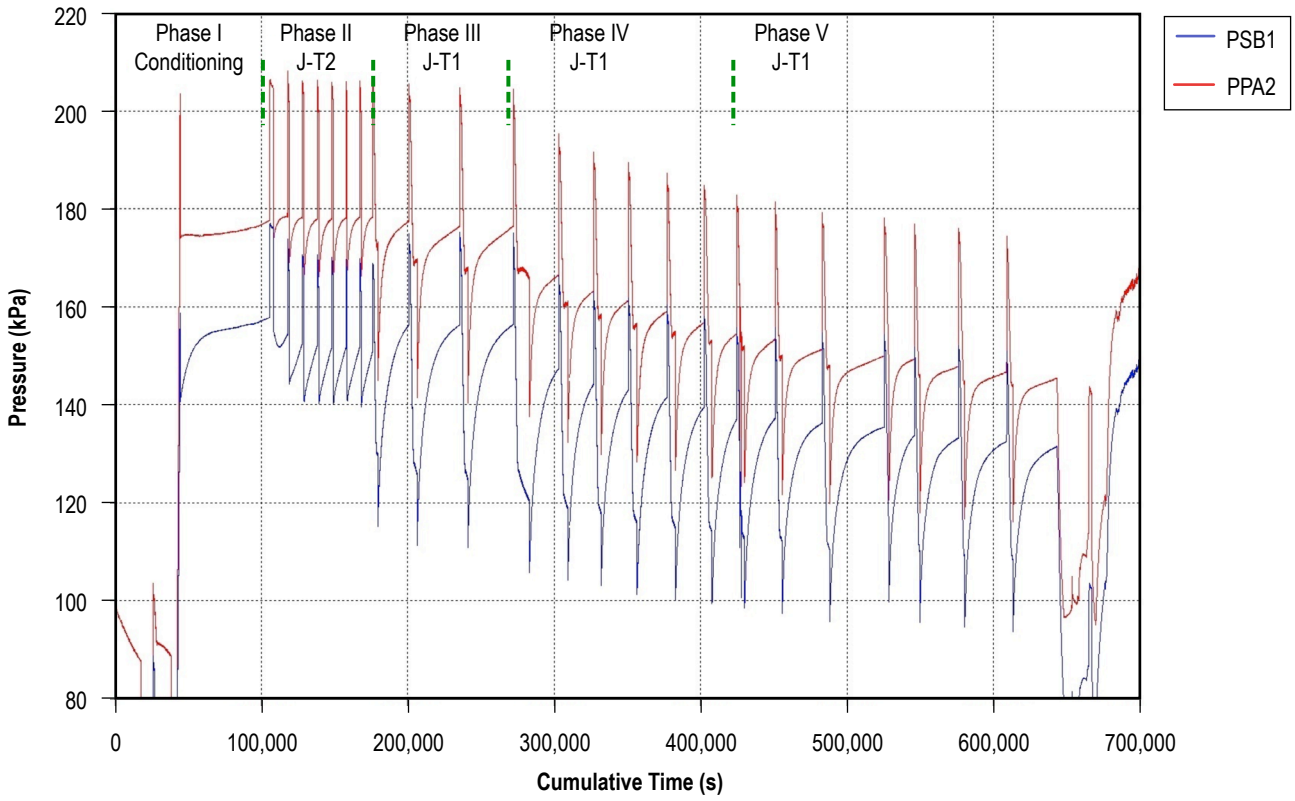

Figure 17. Pump outlet and spray bar inlet pressures.

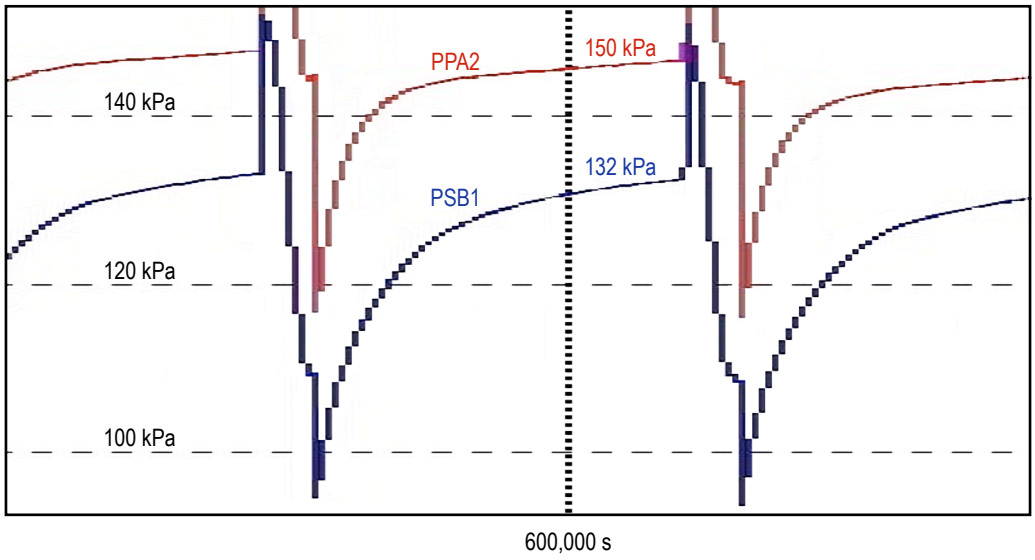

Figure 18. Expanded view of pump outlet and spray bar inlet pressures.

The measured and average ullage and spray exit temperatures (TSA1 and TSA2) presented in figures 19 and 20 demonstrate a strong correlation between the ullage and spray, as one would expect. Further, the trends presented throughout all the TVS test phases are consistent with those previously presented/discussed in section 4, figure 11. The expanded view of a representative data segment, presented in figure 20, is to assist with data visualization. Beginning with the phase IV testing, the ullage temperature was reduced by approximately 2–3 K during mixing periods to the spray temperature of ≈106 K. During the idle periods, the spray exit temperatures ranged from approximately 110 to 108 K and generally were about 1 K above the average ullage temperature.

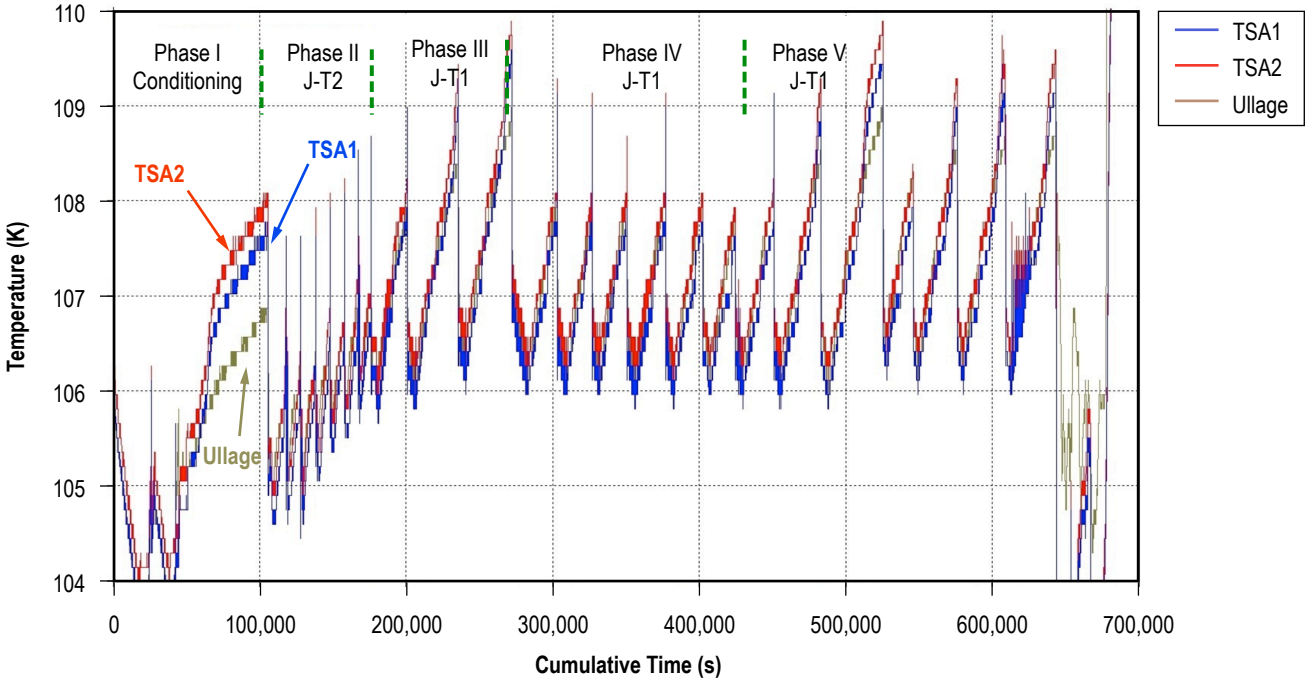

Figure 19. Measured spray exit and ullage temperatures.

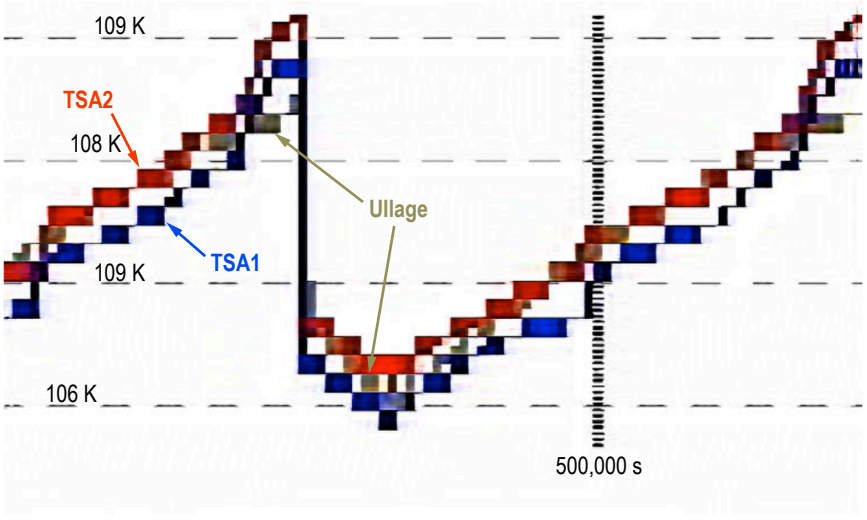

Figure 20. Expanded view of spray exit and ullage temperatures.

6.2 Joule-Thompson Valve Performance

6.2.1 Operation With J-T2

The phase II pressure and temperature data upstream and downstream of J-T2 are presented in figures 21 and 22. The pressure profile pattern at the J-T entrance follows that at the pump exit (PPA2) (fig. 21), which is consistent with expectations, and the downstream pressure generally ranged from 10 to 6 kPa below the inlet pressure (fig. 22). However, there was virtually no temperature change across the J-T valve. In fact, the downstream temperature (TJT2) was slightly, but consistently, warmer than the entrance temperature (TJT1). Therefore, as concluded earlier, the J-T expansion coefficient was negative and therefore did not contribute to an energy reduction within the tank contents. Referring again to figure 11, it was noted that the temperature rise rate of the tank and its contents actually increased after the TVS operation with J-T2 began. Therefore, although the ullage temperature and pressure was temporarily reduced during each mixer operation, thermal energy was added with each mixing cycle instead of reduced. Additionally, as described in more detail in section 7, the active cycle durations with the high flow rate were too abbreviated to allow any recirculation cooling. Consequently, the bulk liquid saturation level increased with each J-T2 cycle.

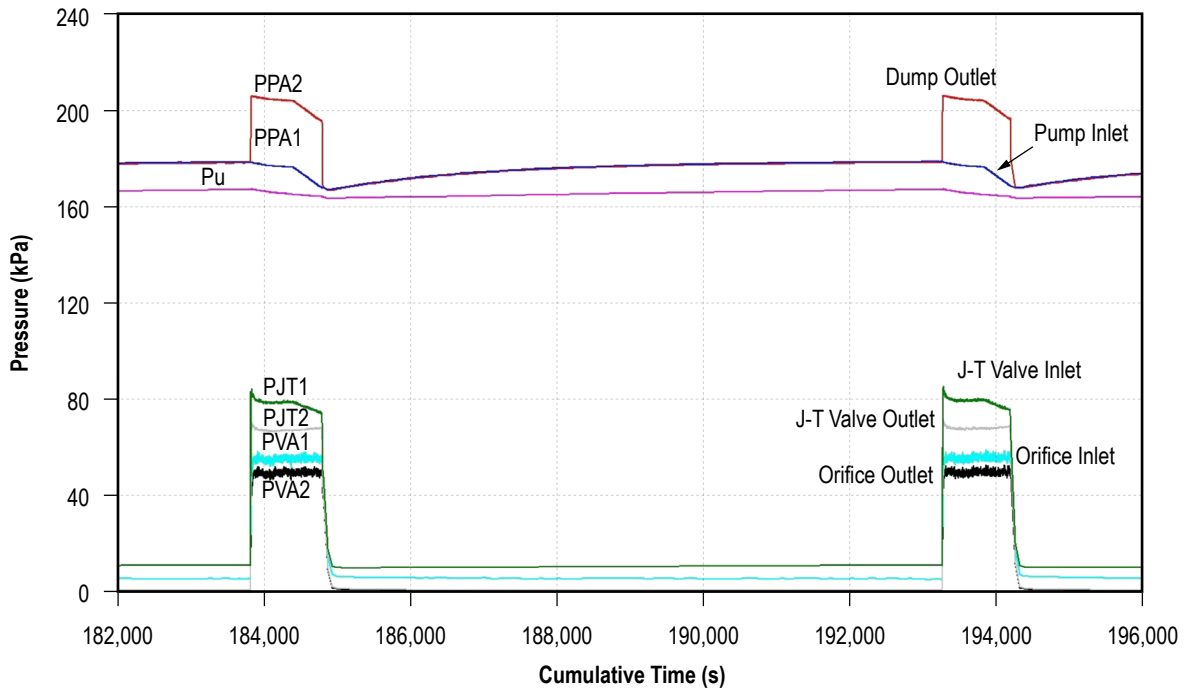

Figure 21. Measured pressure profiles at pump, J-T2 valve, and back pressure orifice.

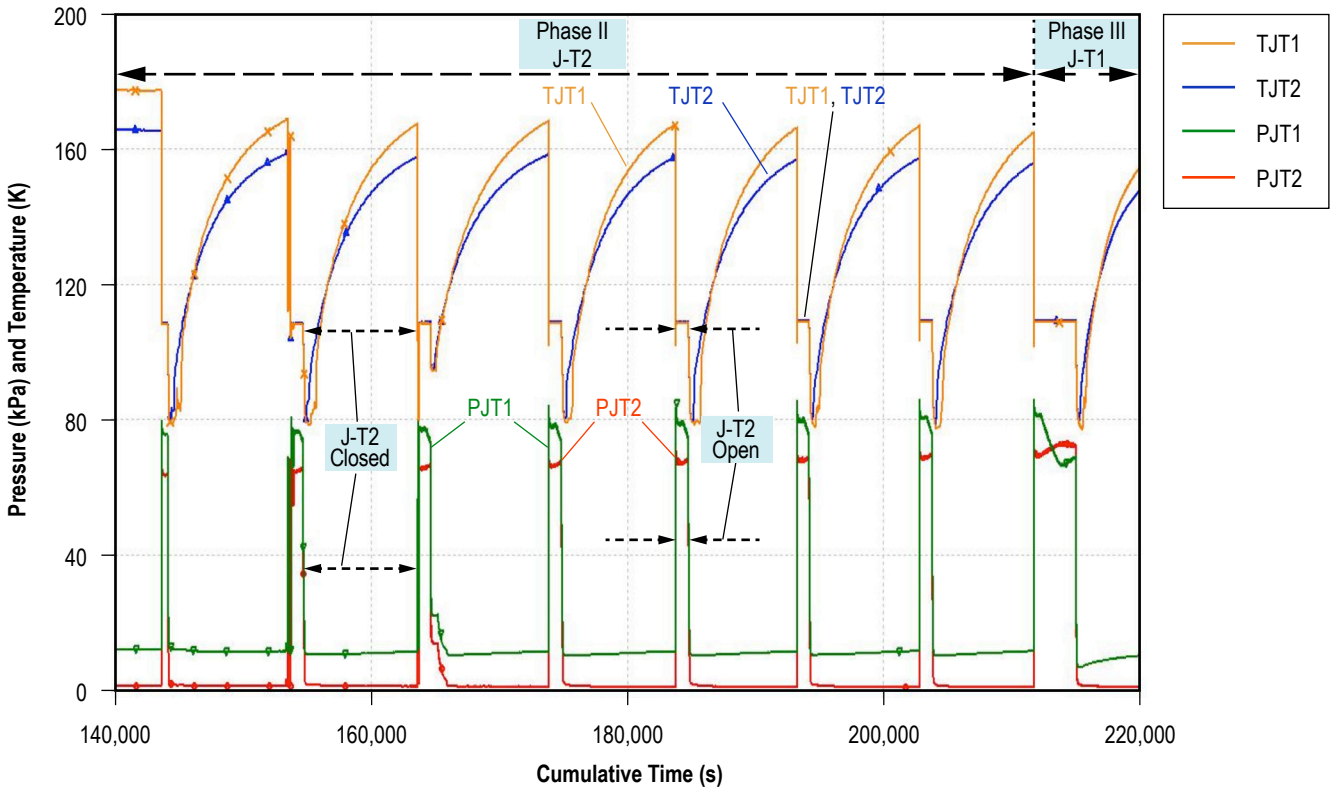

Figure 22. Measured pressure and temperature profiles at J-T2 in phase II testing, J-T1 initial phase III cycle.

6.2.2 Operation With J-T1

The fluid temperature behavior with the smaller J-T valve (J-T1) was virtually identical to that observed with the larger valve (J-T2); however, the inlet pressure patterns were different (figs. 23 and 24), and, as expected, the 'J-T valve open' durations were longer. The inlet pressure, PJT1, decreased until, about halfway through the cycle, it briefly dropped slightly below the outlet pressure, PJT2, and then increased until it equalized with the outlet pressure. Thus, flow across the J-T1 valve was possible during only a portion of the valve open cycle. This type of behavior difference between the two valves is clearer in the expanded view presented in figure 25. However, the J-T1 inlet pressure dwell time below that at the outlet began to moderate somewhat with the phase V heater input reduction, thereby allowing an increased flow duration during each valve open cycle. Although the tank pressure control was improved with the smaller J-T valve, it also is clear that the temperature increased across the J-T1 valve and that the J-T expansion coefficient remained negative.

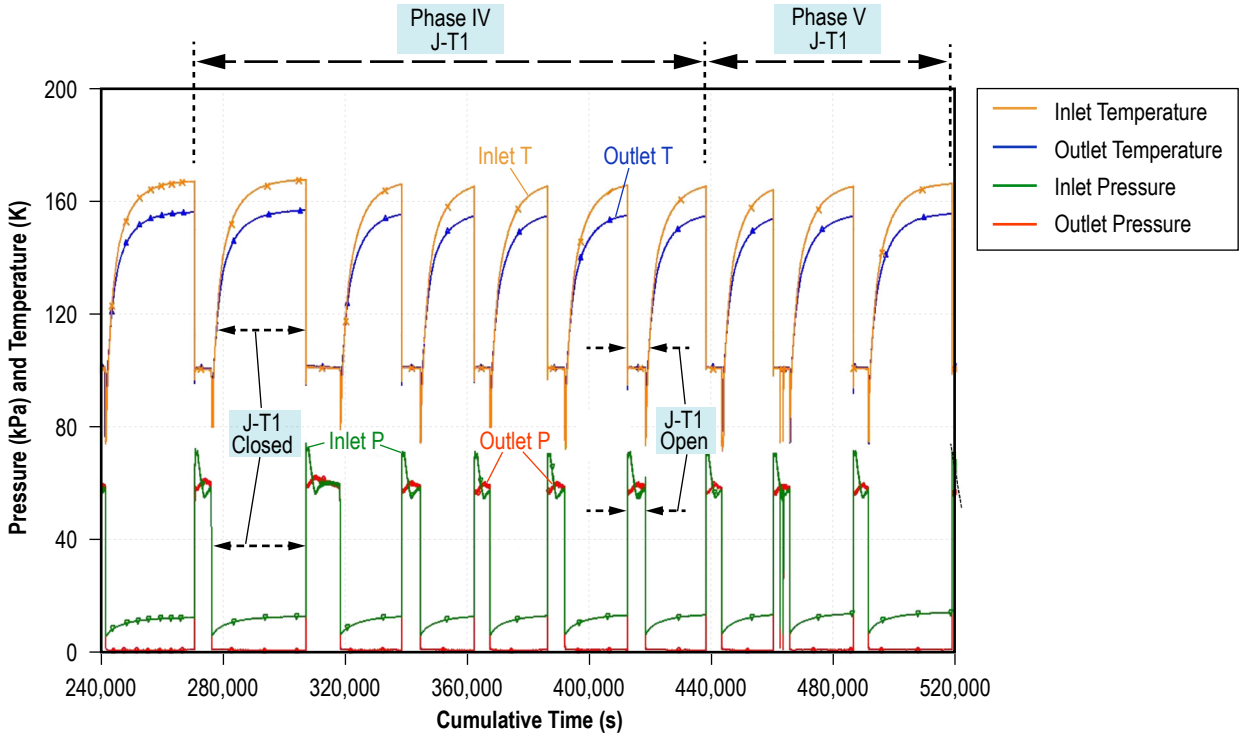

Figure 23. J-T1 pressure and temperature profiles during test phases IV and V.

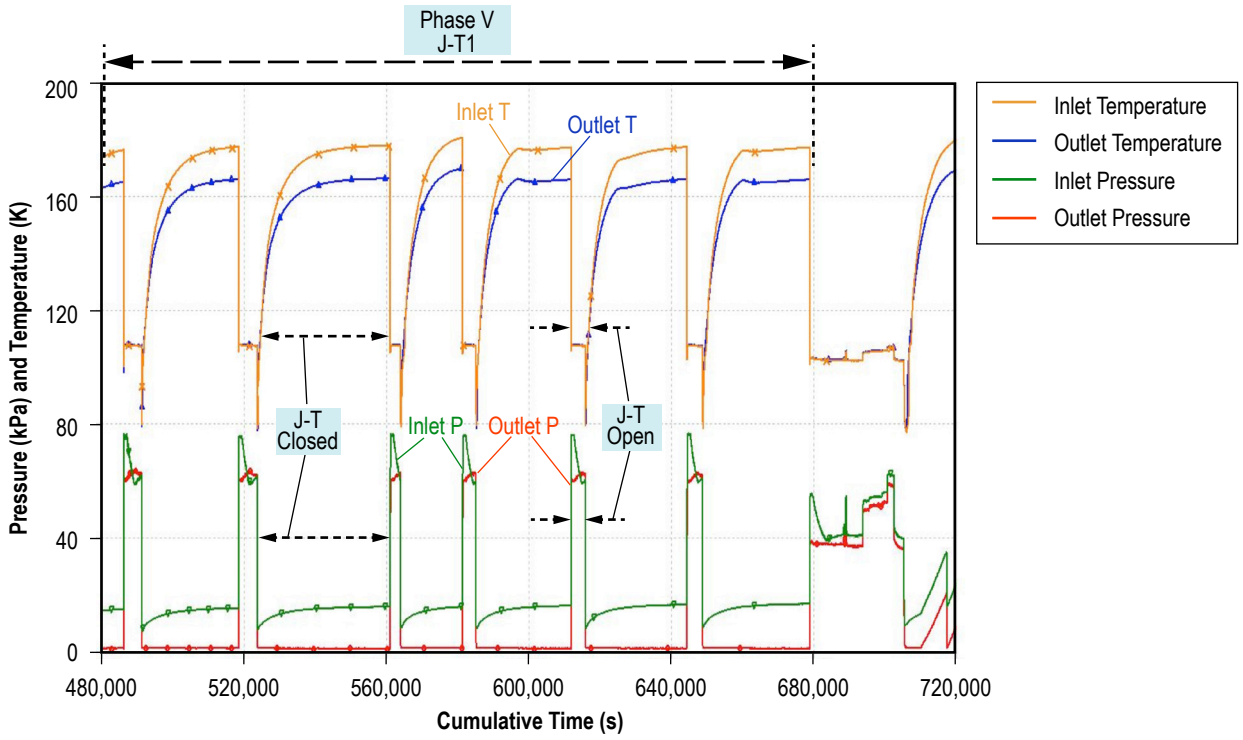

Figure 24. J-T1 pressure and temperature profiles during test phase V.

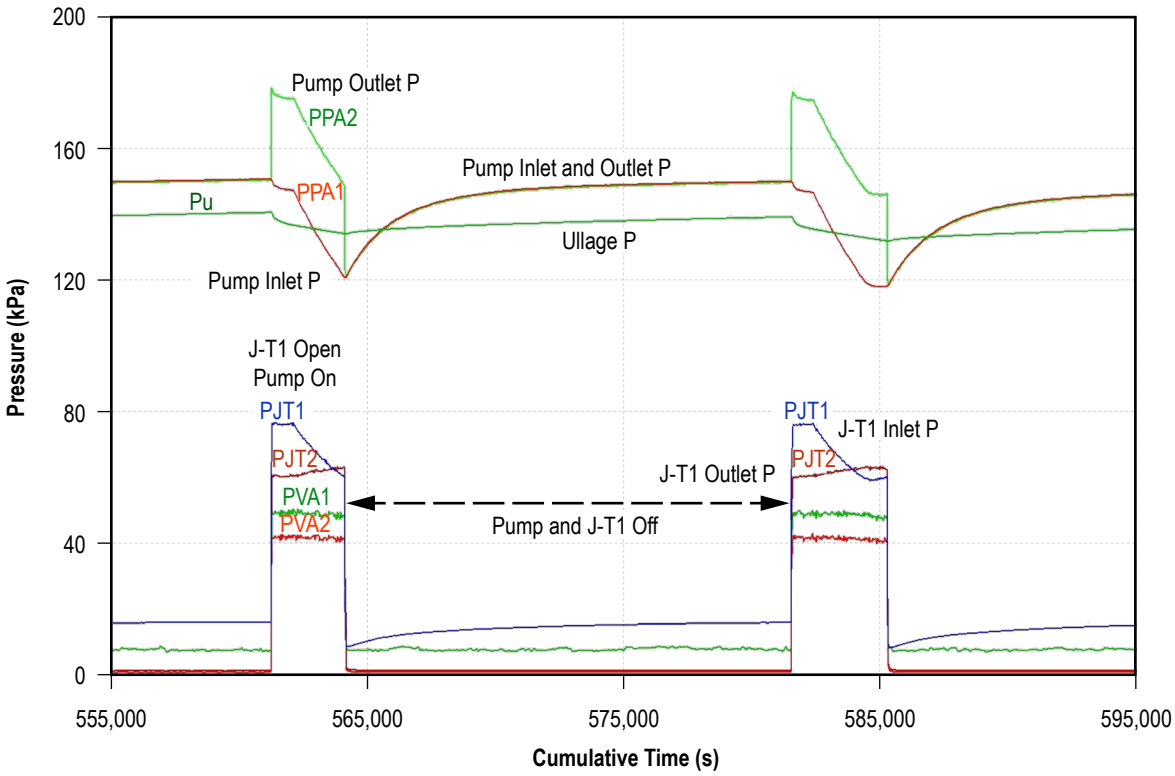

Figure 25. Measured pressure profiles at pump, J-T1 valve, and back pressure orifice.

As with J-T2, the J-T1 valve inlet pressure profile was driven by the pump outlet pressure profile during both the active and inactive periods (fig. 25). The pump data validity was initially questioned because the inlet pressure dropped 30 kPa below the total static pressure. However, the net positive suction pressure (NPSP) available to a pump is based primarily on total static pressure plus dynamic pressure minus vapor pressure plus friction loss. Since the dynamic pressure and friction loss terms are negligible, the NPSP equals total static pressure (150 kPa) minus the LCH_4 vapor pressure (65 kPa), or 85 kPa, which is more than adequate. Further, there is no evidence of cavitation, and the measured pressure difference (28 kPa) is consistent with that by DPP1 (sec. 6.1, fig. 16). Therefore, the measured inlet and outlet pressure data provided by PPA1 and PPA2 are considered valid.

Several significant observations can be made regarding the J-T valve data:

- During active TVS periods, a small temperature rise (≈0.25 K), as opposed to a temperature drop, occurred across both valves.
- The inlet and outlet fluid temperature magnitudes were unaffected by valve size or test conditions during the valve open periods and only slightly affected during the inactive periods.
- The reduced flow rates with J-T1 did improve pressure control performance.

Further details regarding effects of the J-T thermal interactions and effects on system performance are discussed in section 7.

6.3 Back Pressure Orifice

The measured back pressure orifice inlet and outlet temperatures, TVA1 and TVA2, presented in figure 26 along with the expanded view examples in figures 27 and 28, indicate trends consistent with those previously discussed except that, as shown in figure 27, the orifice temperatures were ≈2 K higher with the larger J-T2 than with J-T1. During active J-T1 periods, the orifice inlet and outlet temperatures were reduced to about 101 K, with the upstream temperature about 0.5 K warmer, except on selected occasions when a steep inlet temperature rise temporarily occurred upon J-T activation, followed by temperatures of ≈1 K above and below the outlet temperature (fig. 28). In fact, compared with the outlet, inlet temperature oscillations were generally more severe, especially during the inactive TVS periods. As opposed to data noise, this is believed to be due to LCH_4 residuals at and below triple-point pressures. The pressure profiles presented in figure 25 show that the orifice inlet and outlet pressures, PVA1 and PVA2, are about 48 kPa and 40 kPa, respectively, during active periods, but fall below the triple-point pressure of 12 kPa during the inactive periods. This issue is also discussed in more detail in section 7.

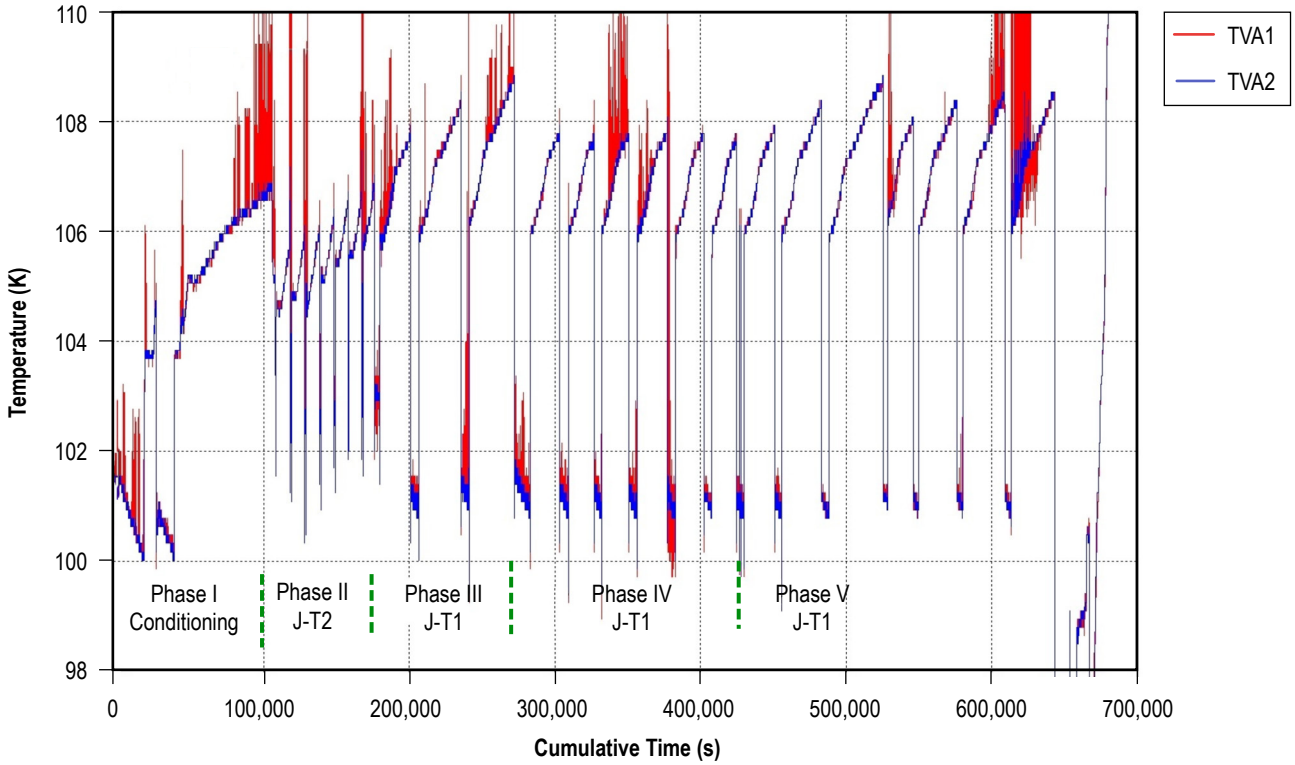

Figure 26. Measured temperatures at back pressure orifice inlet and outlet.

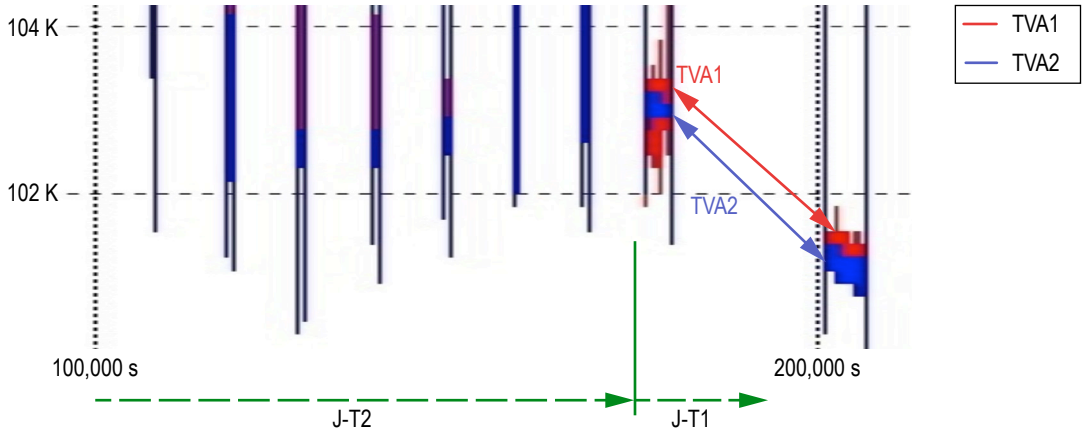

Figure 27. Expanded view of back pressure orifice temperatures with J-T1 and J-T2.

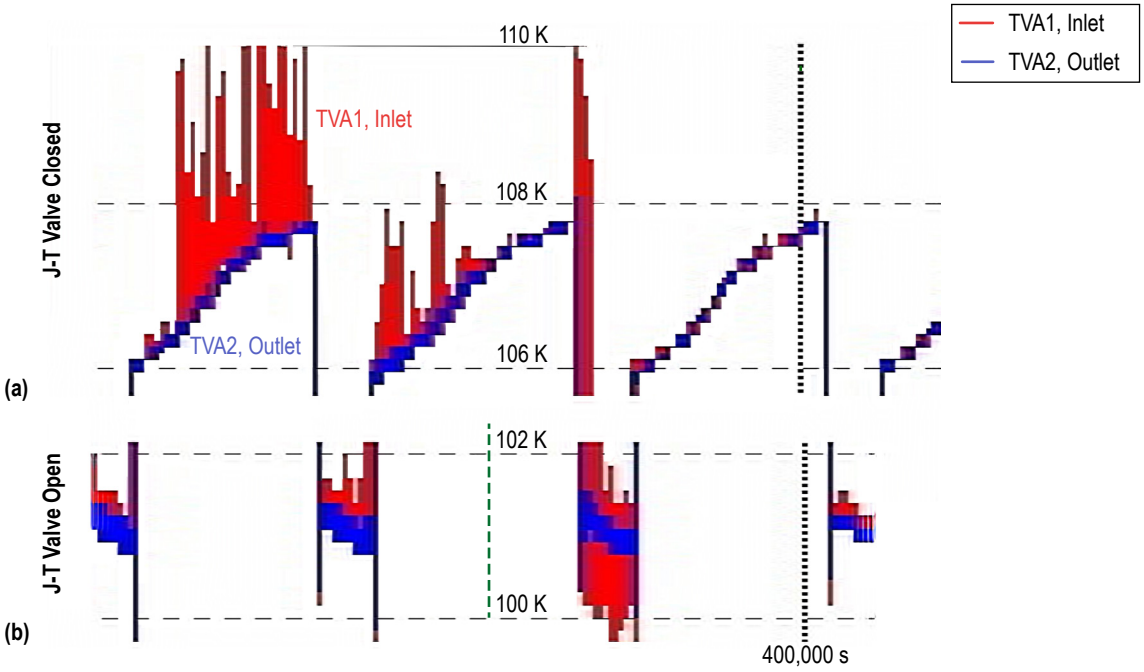

Figure 28. Expanded view of back pressure orifice temperatures: (a) J-T1 valve closed and (b) J-T1 valve open.

6.4 Fluid Vented Into 15-ft Vacuum Chamber

The temperature and pressure conditions (figs. 29 and 30, respectively) exiting the vent line back pressure orifice and entering the 15-ft vacuum chamber indicate trends consistent with those previously described and with the ≈8-m-long vacuum jacketed line between vacuum chambers. Referring to figure 29, the chamber entry temperatures (T3263) with the J-T2 orifice ranged from 150 to 140 K, or about 50 to 40 K above those at the back pressure orifice exit, TVA2; whereas with J-T1, the chamber entry temperatures averaged about 135 K during phase II and then became lower (≈123 K) beginning with phase IV (i.e., were about 23 K above the orifice exit temperatures). Referring to figure 30, the measured vent line pressures (VP3001) entering the vacuum chamber (VP3001) are compared with the back pressure orifice exit pressures, PVA2. The chamber entry pressures were about 300 kPa and 150 kPa with J-T2 and J-T1, respectively (i.e., were almost twice as high with J-T2), which is consistent with the relative flow rate capacities. Both the temperature and pressure entering the 15-ft vacuum chamber indicated downward trends as each vent cycle progressed, indicating that the cooling was still gradually increasing with venting duration.

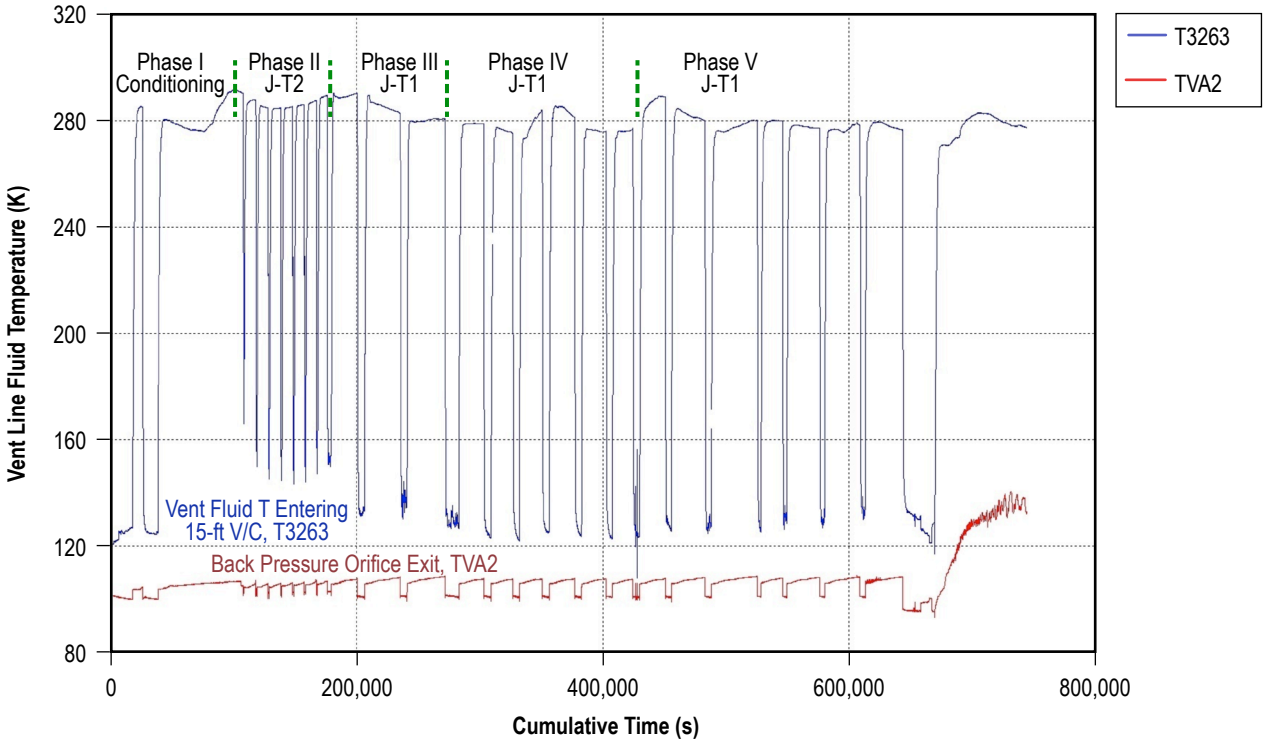

Figure 29. Vent line temperatures entering 15-ft vacuum chamber.

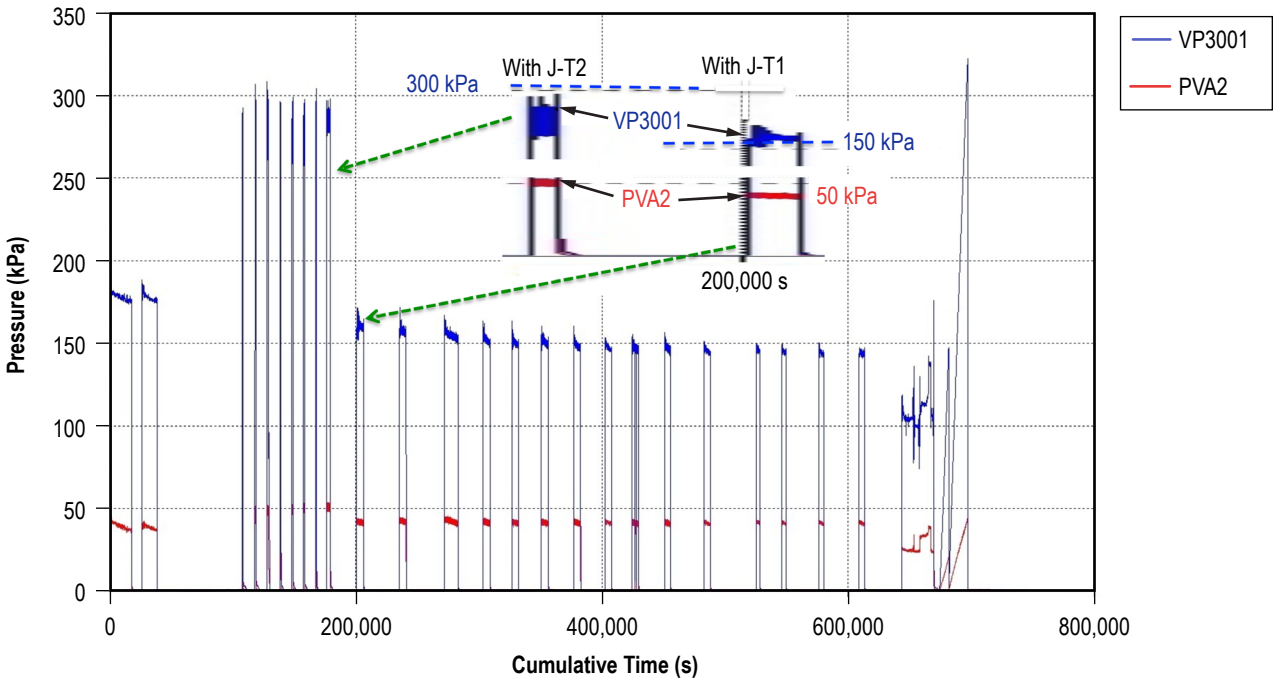

Figure 30. Vent line pressures entering 15-ft vacuum chamber.

7. SYSTEM EVALUATION

The component-by-component evaluations described in section 6 established the functionality of each TVS element or component and the consistency of measured performance trends throughout the system. Furthermore, regarding the valve open conditions measured at the J-T valve entrance and exit, it was noted that neither the temperature profile nor the magnitude varied substantially with test condition or valve size. However, small but consistent temperature and pressure variations were noted at the back pressure control orifice and elsewhere in the system that apparently had affected TVS performance. Therefore, a more detailed examination of these small temperature and pressure variations and interactions was conducted on selected, but representative, test segments. It is important to note the following whenever fluid conditions are discussed in the subsequent sections:

- Typically, the helium's purpose within a propellant tank is to ensure tank pressures are sufficient to prevent feed system cavitation, i.e., it ensures an 'effective degree of subcooling' within the feed system interior.

- The degree of 'actual subcooling' becomes applicable if a portion of the feed system liquid is recirculated and interacts with the ullage. In the TVS application, unless the spray exit temperature is below that of the ullage, a tank pressure reduction cannot be achieved.

- The TVS fluid conditions described herein are relative to the local pressure and temperature unless noted otherwise.

7.1 System Interactions

With these basic observations in mind, the expanded data views presented in figures 31 and 32 can be considered applicable to J-T1, other components and their interactions, and to conditions tested. The J-T1 temperature data presented in figure 31 and expanded in figure 32 enable the discernment of more data details that substantiate previous observations regarding J-T performance. Referring primarily to figures 31 and 32, the mixing period was initiated with pump inlet and outlet temperatures of 112 and 114 K, respectively, both of which were reduced to slightly above 110 K during mixing or the active TVS period. The J-T valve upstream and downstream temperatures were reduced from 180 and 170 K, respectively, to within the 108 to 107 K range, with the downstream about 0.25 K above the upstream temperature. The average liquid temperature was gradually reduced from 107 to 106 K, as the ullage was quickly reduced from 108 K to the liquid temperature and then slightly below (≈0.25 K) 106 K. Therefore, the expansion process at the J-T valve outlet definitely did not contribute to the liquid temperature reduction. The essentially equal inlet and outlet temperatures at the back pressure orifice, TVA1 and TVA2, were reduced from approximately 108 to 101 K. The 101 K consistently represented the lowest measured within the TVS during each active period. It was noted that the ullage temperature followed the downward trend at the back pressure orifice during mixing and was virtually equal to the orifice temperatures between

cycles, indicating a linkage between the vent exit and ullage temperatures. Recalling the strong linkage between the spray bar exit (TSA1 and TSA2) and ullage temperatures presented in figures 19 and 20, and that the spray temperatures at 106 K are second lowest within the TVS, it becomes clear that the temperature reduction between the J-T outlet and back pressure orifice did contribute some cooling of the recirculated liquid prior to exiting the spray bar vent.

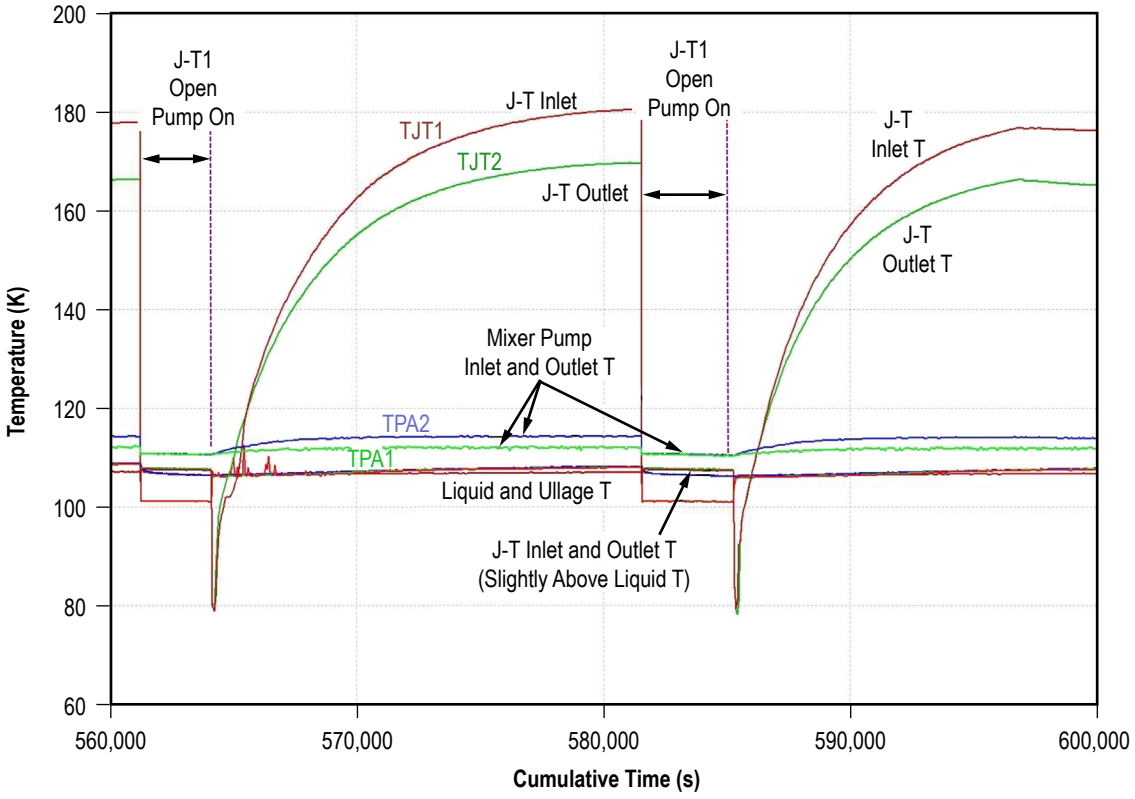

Figure 31. System temperatures with J-T1, test phase V.

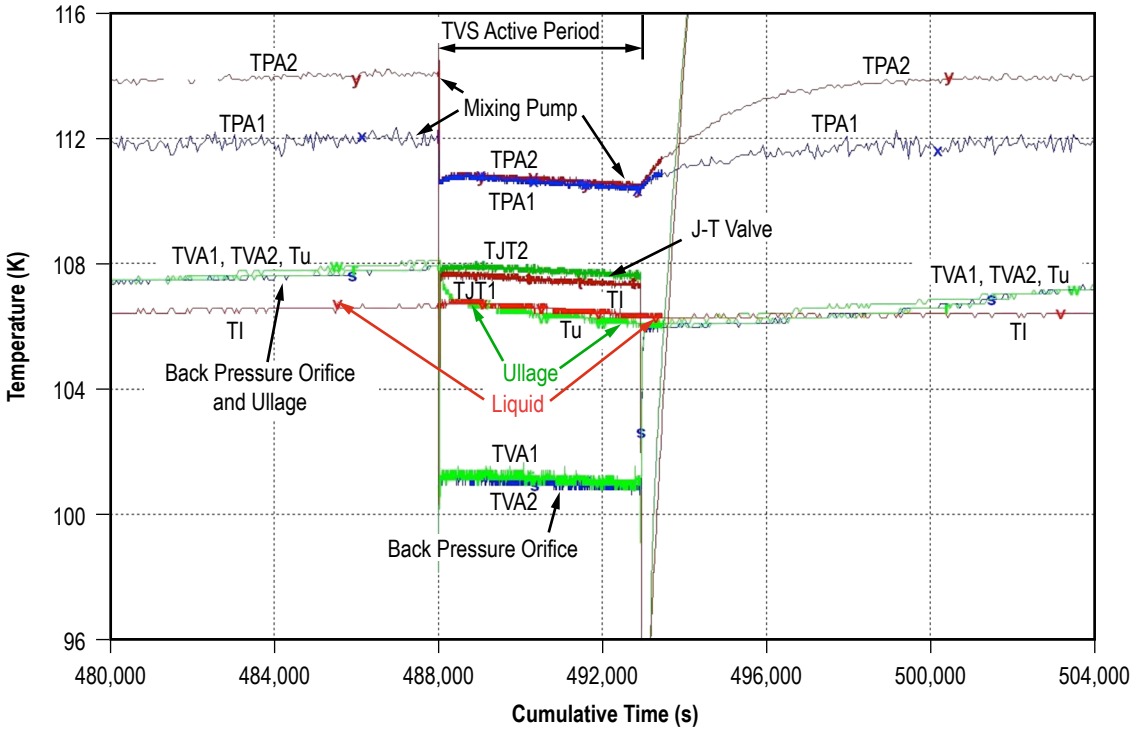

Figure 32. Expanded view of system temperatures with J-T1, test phase V.

7.2 Vented Fluid Conditions Versus Measurement Position

Based on those observations, an evaluation of the fluid conditions (liquid or vapor, degree of subcooling, at or near triple-point, etc.) versus vented fluid measurement position between the J-T1 orifice inlet and the back pressure orifice outlet during both active and inactive TVS periods was conducted, and results are summarized in tables 3 and 4, respectively. Observations regarding vented fluid conditions are discussed in the next section. Remember that the fluid conditions are relative to the local pressure and temperature unless noted otherwise.

Table 3. Vented fluid conditions during active TVS cycles. (Test data from a cumulative time interval of 440,000–504,000 s.)

Position	Measured Temperature (K)	Measured Pressure (kPa)	Saturation Temperature (K) at P_{meas}	Fluid State Comments
J-T1 inlet beginning to end of open cycle	107.2 to 106.6	76 to 60	108.3 to 105.7	Initially subcooled liquid (T_{meas}= 1.1 K below saturation); transitions to metastable liquid (T_{meas} = 0.9 K above saturation)
J-T1 outlet beginning to end of open cycle	107.7 to 107.4	60	105.7	Metastable liquid ($T_{meas} \approx 2$ K above saturation)
Back pressure inlet	101.4	48	103	Subcooled liquid (T_{meas} = 1.6 K below saturation)
Back pressure outlet	101	40	101	Saturated liquid ($T_{meas} = T_{sat}$)

Table 4. Vent line fluid conditions during inactive TVS cycles. (Test data from a cumulative time interval of 440,000–504,000 s.)

Position	Time After J-T Valve Closure (s)	Measured Temperature (K)	Measured Pressure (kPa)	Saturation Temperature (K) at P_{meas}	Fluid State Comments
J-T1 inlet	100	79.6	8.5	86	Below triple-point; slush likely
J-T1 outlet	150	78	≈2	78	Below triple-point; slush likely
J-T1 inlet	220	92.8	12	90.7	At triple-point; slush likely
J-T1 outlet	220	92.8	≈2	78	P_{meas} << triple-point; T_{meas} ≈1 K above triple-point; slush possible
Back pressure orifice inlet	Inactive duration	106–108	7–8.5	85–88	P_{meas} < triple-point; T_{meas} ≈17 K above triple-point; vapor likely
Back pressure orifice outlet	Inactive duration	106–108	≈1	74	P_{meas} << triple-point; T_{meas} ≈17 K above triple-point; vapor likely

7.2.1 Conditions During Venting

The measured J-T1 inlet pressure ranged from 76 to 60 kPa (fig. 25) during the open valve period (at the beginning and end of the open valve period, respectively), with a corresponding measured temperature range of 107.2 to 106.6 K (figs. 31 and 32). The saturation temperature corresponding to the inlet pressure range was 108.3 to 105.7 K. Thus, it can be concluded that the inlet fluid condition, which ranged from 1.1 K below saturation to 0.9 K above saturation, probably was metastable liquid. Similarly, the measured outlet temperature was slightly warmer than the inlet and was ≈2 K above saturation was representative of metastable liquid as well. The measured pressures at the back pressure orifice did not vary significantly during the J-T valve open periods. The orifice inlet pressure was 48 kPa and, as represented in figure 32, the temperature ranged from 101.4 to 101 K. The corresponding saturation level at 48 kPa was 103 K, indicating subcooled liquid at the inlet. However, as noted earlier with a more compressed timescale (sec. 6.3, fig. 28), temperature fluctuations became apparent at the orifice inlet, both prior to and after J-T valve cycling, which was most likely due to the presence of triple-point residuals. This trend was present at the back pressure orifice inlet throughout the testing. The orifice outlet pressure and temperature was 40 kPa and 101 K, respectively, indicating saturated liquid. Superheated vapor would be present at the orifice inlet in an optimized TVS system and was expected to be at least two-phase fluid with the nonoptimized setup. The presence of subcooled liquid at the orifice makes it obvious that the cooling was not even in the right regime. It is interesting to note that a small but persistent temperature decrease of about 0.4 K occurred with an 8 kPa pressure drop across the orifice, indicating a positive J-T expansion coefficient.

Observations regarding vent line conditions between vent cycles, or the inactive TVS periods, are described in the next section.

7.2.2 Conditions Between Vent Cycles

The period between vent cycles was briefly examined, primarily to determine whether or not conditions at or near the triple-point had compromised or affected the TVS operation. The

expanded temperature and pressure data presented in figures 33 and 34, in combination with previously presented data, indicate that 900 s after valve closure, the inlet and outlet temperature (fig. 33) and pressure (fig. 34) had decreased to below the triple-point (90.7 K, 12 kPa). The inlet temperature and pressure was 79.6 K and 8.5 kPa, respectively, whereas the outlet was at 78 K and ≈2 kPa. Even though the inlet and outlet pressures were at or below triple-point pressure after 2,600 s, the temperatures had increased to above 92.8 K, indicating that slush could have been present. This raised the question as to whether or not passage through the triple-point had resulted in the formation of solid particles and possible clogging of small flow passages, especially since this 'post-valve closure' pressure-temperature cycle was present throughout TVS testing with both J-T valves. Similar circumstances occurred at the back pressure orifice, where the inlet and outlet pressures dropped to and remained at about 8 and 1 kPa, respectively. Immediately following valve closure, the temperatures increased to 106 K, then subsequently to 108 K, indicating that vapor ultimately was present. However, as noted above, temperature fluctuations at the orifice inlet can be attributed to the presence of triple-point residuals. The conclusion, therefore, is that although the formation of triple-point solid particulates and/or slush probably was temporarily present at the J-T valve and back pressure orifice, it is not believed to have been a significant factor in system level performance.

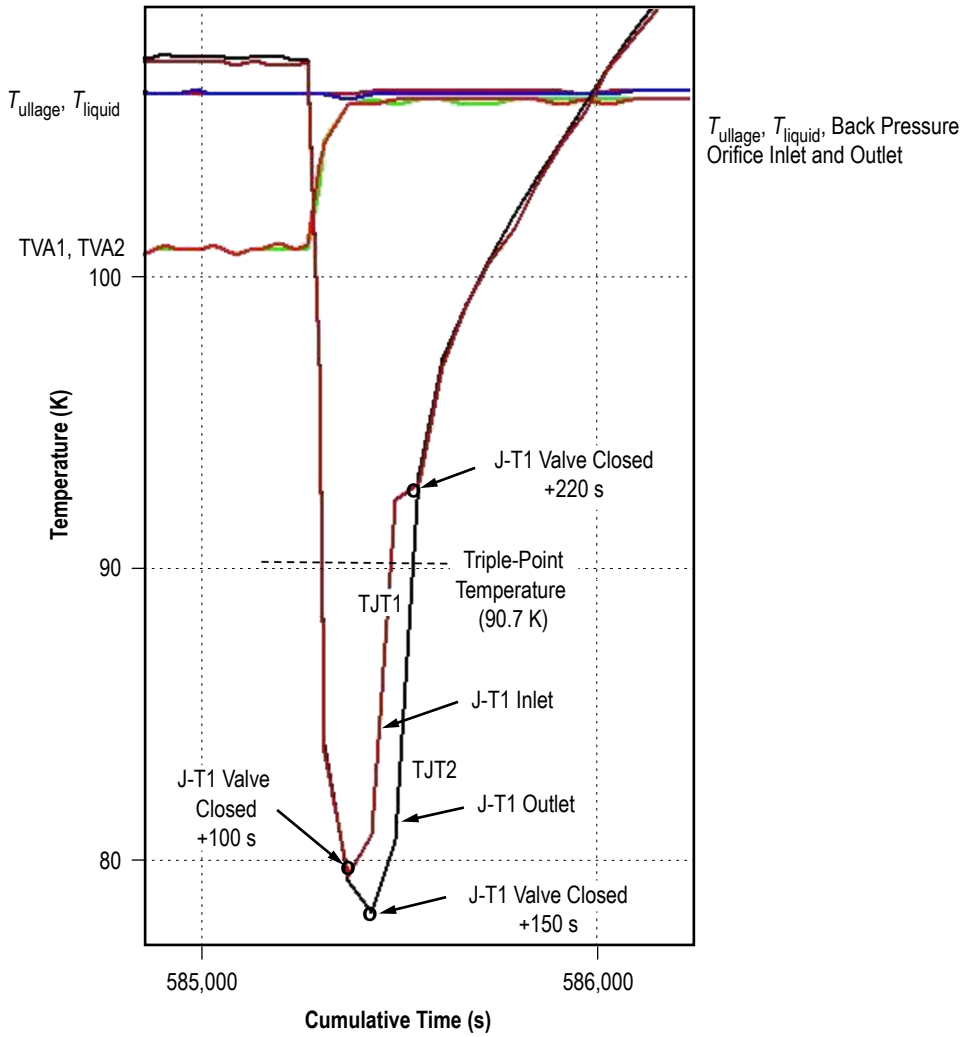

Figure 33. Expanded view of vent line temperatures between active TVS cycles.

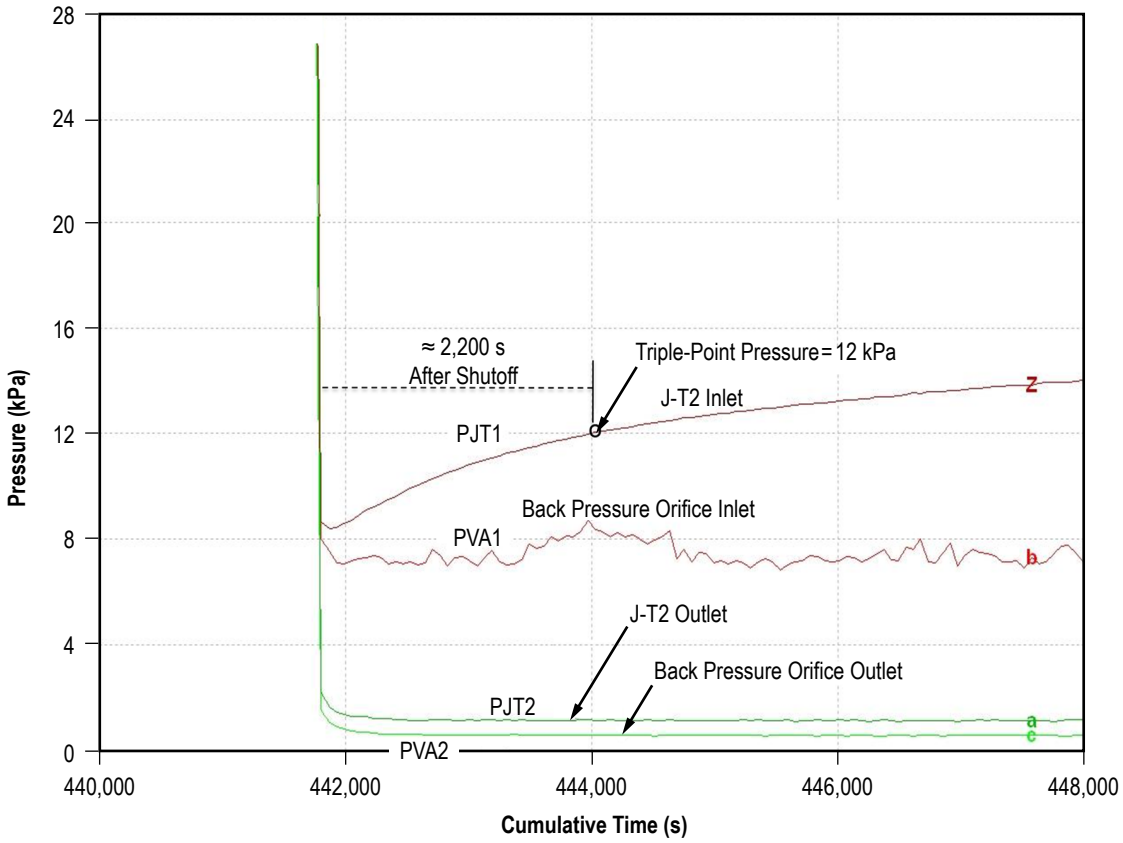

Figure 34. Expanded view of vent line pressures between active TVS cycles.

7.2.3 Fluid Conditions Summary

The graphical representation of the data presented in figure 35 assists with visualization of the data presented in tables 2 and 3. It is interesting to note that although there are small variations above and below the saturation line during the valve open or the active TVS periods, the data are consistently close to the saturation line, indicating liquid in either a subcooled or in a metastable state. The consistency of these conditions for all J-T1 testing becomes apparent when multiple test cycles are considered. Although the inactive TVS data are more scattered relative to the active period data for a particular cycle, they too have cycle-to-cycle consistency. Similar observations are applicable to the J-T2 data, except that the larger flow rate caused the cycle durations to become more compressed, and higher temperatures (approximately 1–2 K) resulted at the back pressure orifice. Once the relative commonality of temperatures for a given position and the J-T valve was established, it became convenient to group the vented fluid data for a particular measurement position onto a single graph. The inlet and outlet conditions for the J-T valve are presented in figures 36 and 37 and for the back pressure orifice in figures 38 and 39. These graphs illustrate the effects of the J-T valve size and flow rate duration. The J-T valve temperatures were not significantly affected by valve size during venting, but the longer periods between vent cycles led to higher temperatures between cycles with the smaller valve (figs. 36 and 37). Also evident is the higher, more compressed

duty cycle caused by the lack of cooling with the larger valve. Referring to the back pressure orifice data (figs. 38 and 39), the reduced flow rate with the smaller J-T1 valve enabled reduced temperatures at the back pressure orifice. Apparently, a slow expansion process occurred as the fluid traversed the 3-m distance between the J-T valve and back pressure orifice, which is substantiated by the close match between the measured pressure and temperature with saturation conditions (fig. 35).

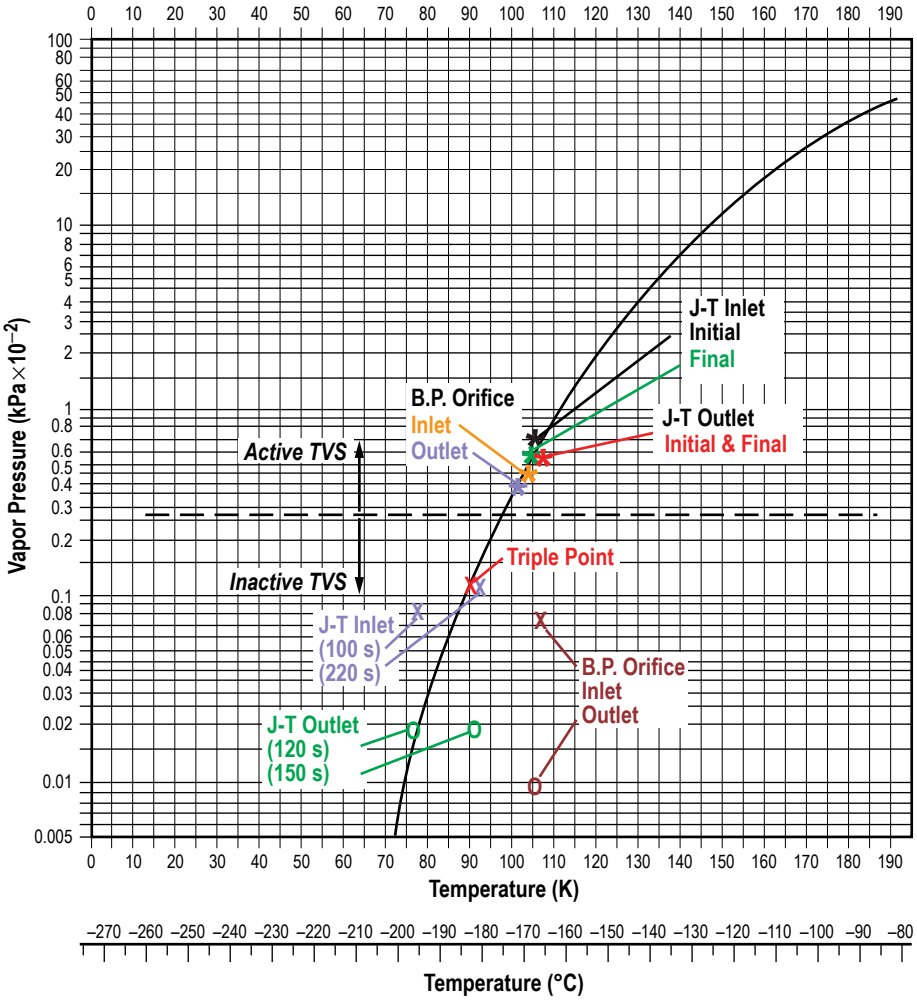

Figure 35. Vented fluid conditions versus saturation curve during active and inactive TVS cycles with J-T1.

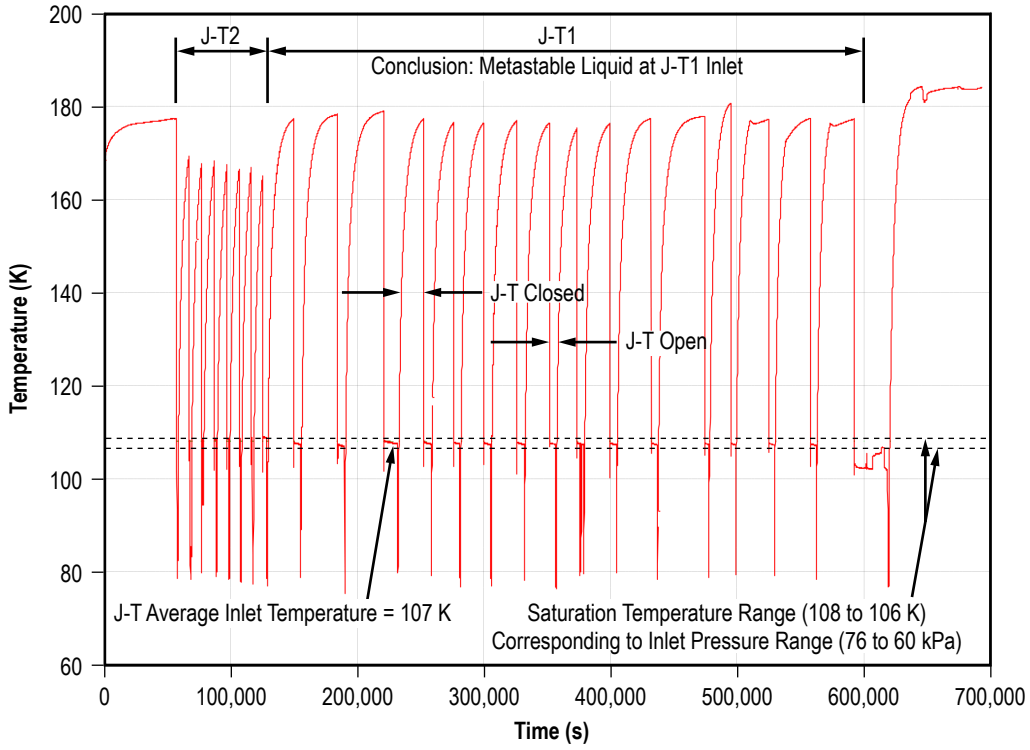

Figure 36. Joule-Thompson valve inlet temperature conditions.

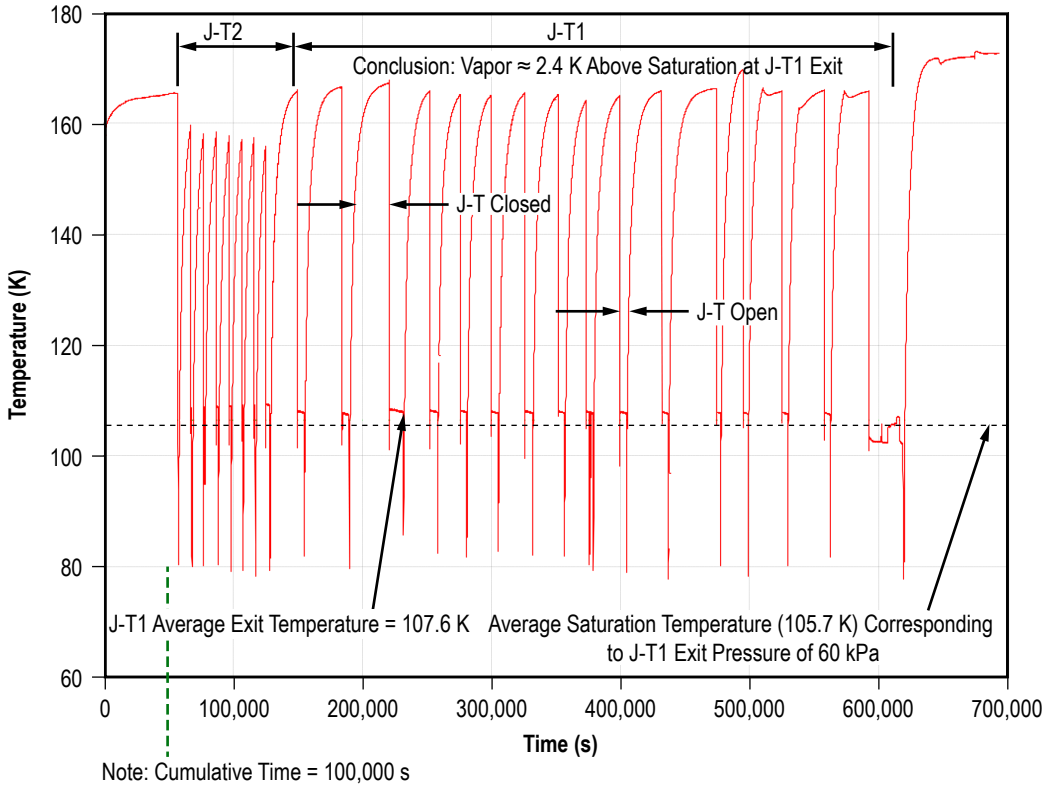

Figure 37. Joule-Thompson valve exit temperature conditions.

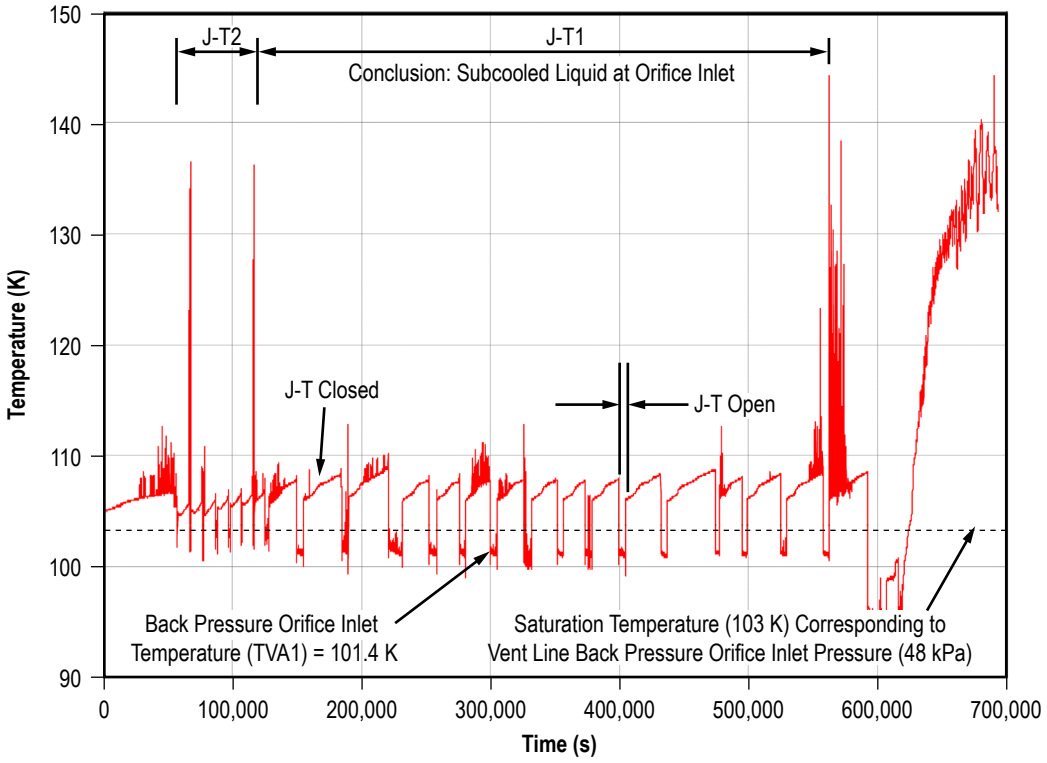

Figure 38. Back pressure orifice inlet temperature conditions.

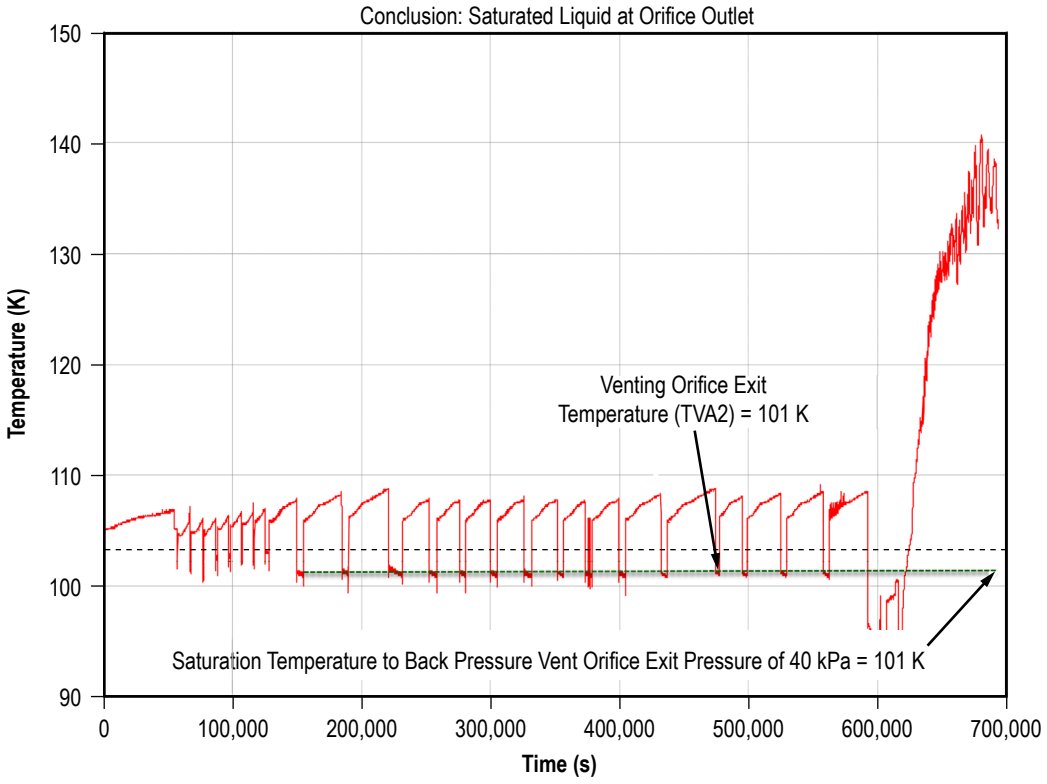

Figure 39. Back pressure orifice exit temperature conditions.

7.3 Analytical Comparison With Test Data

Although correlations of existing analytical models with the TVS instrumentation normally used were compromised, the helium presence did enable a means for computing the ullage volume increase for each test series with a reasonable degree of confidence. The quantification of measured liquid volume increases due to venting, combined with analytical computations based on a maximum theoretical TVS heat exchanger efficiency (100%), could then be used to provide a frame of reference. The vent losses derived from the test data and the analytical/measured comparisons, based on a 24-hr storage period, are discussed in the following sections.

7.3.1 Derived Vent Losses

Since the LCH_4 partial pressure equals the saturation pressure corresponding to the homogenous or destratified liquid-vapor temperature at the end of each mixing cycle, then the difference between the total measured ullage pressure and the LCH_4 saturation or partial pressure equals the GHe partial pressure. For example, beginning with the measured conditions during the helium injection process at the 90% fill level, the ullage volume was 1.81 m^3 (63.9 ft^3), the saturation temperature (at the end of the mixing cycle) was 103.7 K (187 R), and the ullage pressure was 166 kPa (24 psia). Then, the corresponding helium partial pressure was 116 kPa (16.8 psia), which equaled the total ullage pressure (166 kPa (24 psia)) minus the LCH_4 saturation pressure (50 kPa (7.25 psia)). Using the perfect gas law, $PV=mRT$, with the helium partial pressure, temperature, and 1.81 m^3 (63.9 ft^3) volume (90% fill level), the computed helium mass (m_{GHe}) was 0.965 kg (2.13 lb). Further, the helium mass can be considered constant throughout the testing because the ullage was never directly vented. Due to the small pressure and volume changes associated with individual vent cycles, the larger changes resulting from multiple vent cycles (i.e., during a particular test series) were preferred.

The measured tank pressure cycles identified in figures 40 and 41, in combination with the measured tank fluid temperatures (fig. 11), were used to derive the 'vented liquid volume and mass versus pressure control approach' data presented in table 5. The baseline conditions established during the helium injection process are represented by cycle 0 (test phase I). Condition differences between the end of the first mixing/vent cycle (cycle 1) and final mixing/vent cycle (cycle 7) were used to establish the ullage volume increase (conversely, the liquid volume decrease) during the six total cycles (mixing/venting plus self-pressurization) completed in the phase II testing with the larger J-T valve, J-T2. Similarly, test results with the smaller vent valve, J-T1, are represented by cycles 11–17 (test phase IV) and cycles 21–23 (test phase V) with high and low heat leak inputs of 440 W and 256 W, respectively. As previously noted, the phase II testing with J-T2 indicated that, although the ullage pressure was controlled, a negative TVS efficiency resulted (energy was added instead of removed). During the 15-hr period, beginning with the completion of the first mixing/vent event and ending with the completion of six complete cycles (self-pressurization plus mixing/venting, cycles 1–7), 82 kg (183 lb) of methane were vented with no heat removal benefits. During phase IV testing, the smaller vent valve (J-T1), working against the same heat load (440 W), provided adequate liquid saturation temperature control for 42 hr (cycles 11–17), with 183 kg (418 lb) vented during six cycles. The basic message is that the larger J-T2 flow rate combined with the brief vent periods (≈0.3 hr) rendered the TVS heat exchanger useless.

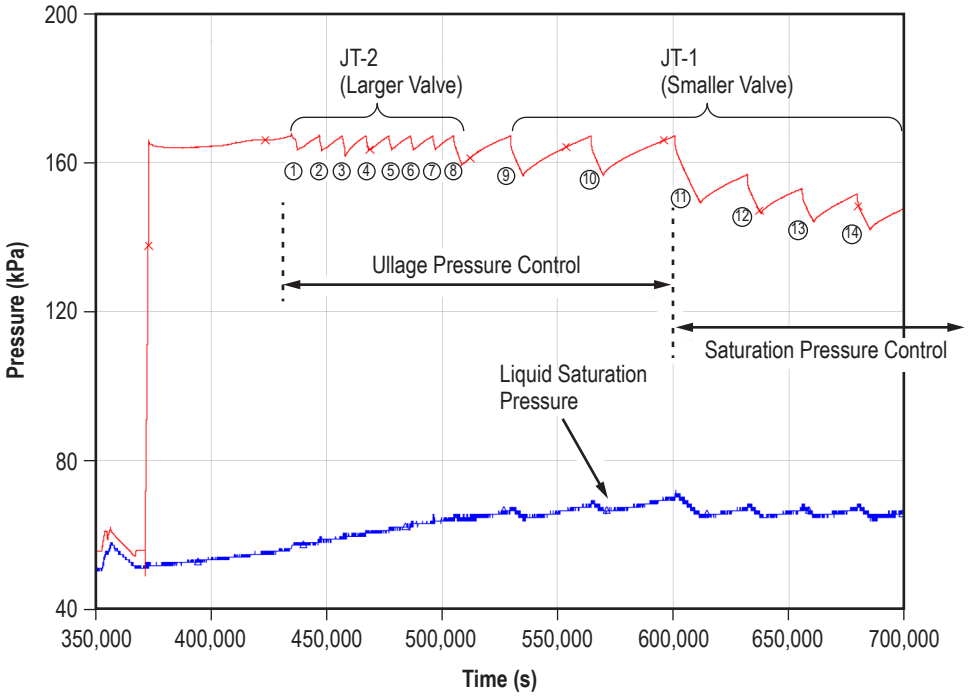

Figure 40. Ullage and liquid saturation pressures during cycles with ullage pressure control mode.

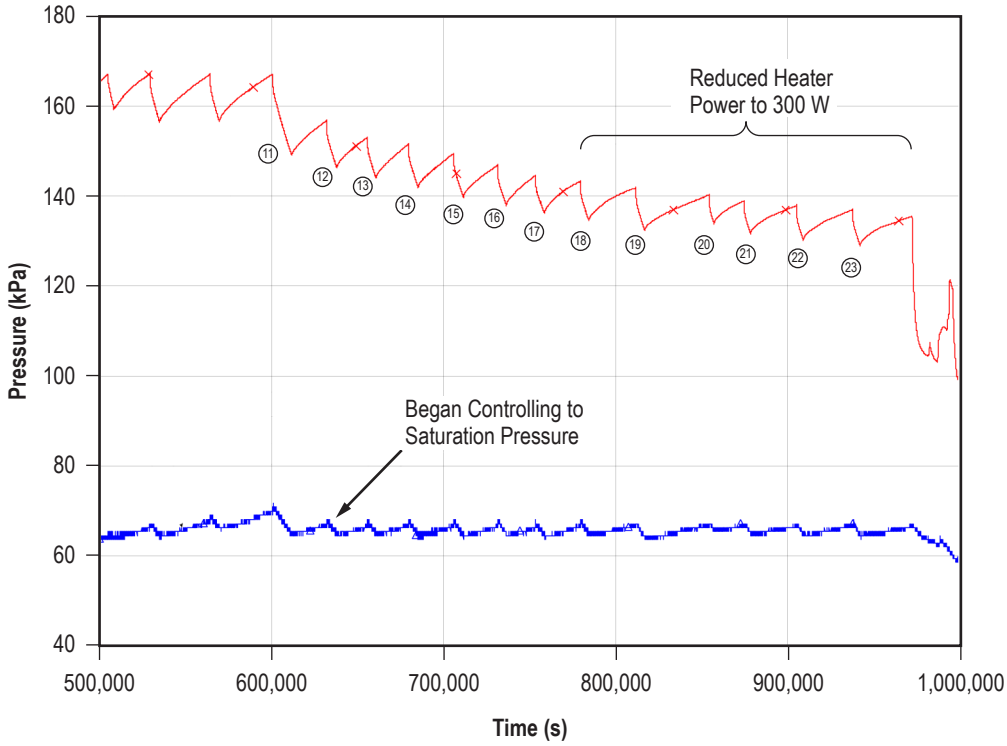

Figure 41. Ullage and liquid saturation pressure during cycles with saturation control mode.

Table 5. Vented mass versus pressure control test conditions.

Test Phase	Saturation Conditions		Helium Pressure*	Helium Volume	Vented Volume**	Vented LCH_4**	LCH_4/Vent	Time Between Vents (Each Vent Duration)
	Temperature	Pressure						
Propellant conditioning to establish initial condition (phase I)								
Cycle 0	103.7 K (187 R)	50 kPa (7.25 psia)	116 kPa (16.8 psia)	1.81 m^3 (63.9 ft^3)	NA	NA	NA	NA
Ullage pressure control with J-T2, 440 W input (phase II)								
Cycle 1	105 K (187 R)	56 kPa (8 psia)	107.6 kPa (15.5 psia)	1.958 m^3 (69.9 ft^3)	NA	NA	NA	NA
Cycle 7	106.7 K (192 R)	65 kPa (9.4 psia)	99.4 kPa (14.4 psia)	2.17 m^3 (76.7 ft^3)	0.19 m^3 (6.8 ft^3)	82 kg (183 lb)	13.5 kg (30.5 lb)	2.22 hr (0.28 hr)
Saturation control with J-T1, 440 W input (phase IV)								
Cycle 11	106 K (190.8 R)	62 kPa (9 psia)	87 kPa (12.6 psia)	2.46 m^3 (86.8 ft^3)	NA	NA	NA	NA
Cycle 17	106 K (190.8 R)	62 kPa (9 psia)	74 kPa (10.7 psia)	2.90 m^3 (102.3 ft^3)	0.44 m^3 (15.5 ft^3)	189 kg (417.5 lb)	31.5 kg (69.6 lb)	5.28 hr (1.67 hr)
Saturation control with J-T1, 256 W input (phase V)***								
Cycle 21	106.3 K (191.3 R)	64 kPa (9.3 psia)	69 kPa (10 psia)	3.10 m^3 (109.74 ft^3)	NA	NA	NA	NA
Cycle 23	106.3 K (191.3 R)	64 kPa (9.3 psia)	66 kPa (9.6 psia)	3.24 m^3 (114.3 ft^3)	0.133 m^3 (4.6 ft^3)	56.5 kg (124 lb)	28.0 kg (62 lb)	7.36 hr (1.25 hr)

* Constant helium mass of 0.635 kg (2.13 lb); based on initial ullage volume and helium partial pressure with no direct ullage vents.
** Helium volume increase = vented liquid volume for total number of cycles in the test interval evaluated.
*** Only two test cycles usable for derived data.

7.3.2 Analytical and Measured Vent Losses Per Day

The analytical model, Tank System Integrated Model (TankSIM), is currently baselined on an 'ullage pressure' control mode. Therefore, assuming a theoretical TVS performance limit of 100% efficiency, TankSIM was used to simulate the ullage pressure transients measured during the phase II testing, and the graphical results are presented in figure 42. Although the exercise is academic, the best test data available for comparison with analytical modeling are represented by the phase IV J-T1 data 'with the saturation' control mode. To improve visualization of the TVS performance level variations with test conditions, and in comparison with the maximum analytical performance limit, the table 5 vent losses were normalized to a common set of conditions, and the results are presented in table 6. The vented mass variations for a 24-hr storage period are presented for three heat input levels: the two tested (440 W and 256 W) and 44 W, a level more representative of on-orbit thermal conditions. It should be noted that no attempt was made to optimize the vent/mixing cycles presented in table 6. Therefore, the vented masses are simply scaled, either up or down, in direct proportion to the heat loads and storage periods.

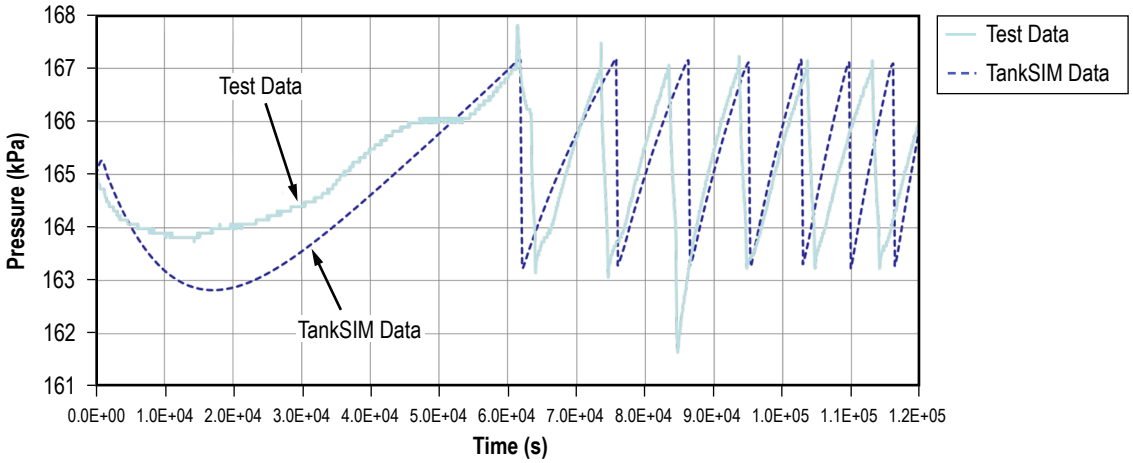

Figure 42. TVS analytical modeling of ullage pressure control with normal methane.

Table 6. Vented mass per day test versus 100% efficient TVS heat exchanger.

Data Source	Cycle Duration (hr)	LCH_4/Cycle	Cycles/Day (24 hr)	Vented LCH_4/Day	
Test data derived					
Ullage pressure control with J-T2, 440 W input	2.5	13.8 kg (30.5 lb)	9.6	123 kg (271 lb)	0.29 m^3 (10 ft^3)
Saturation control with J-T1, 440 W input	6.95	31.5 kg (69.6 lb)	3.5	111 kg (245 lb)	0.26 m^3 (9.1 ft^3)
Saturation control with J-T1, 256 W input	8.61	28 kg (62 lb)	2.8	79 kg (174 lb)	0.18 m^3 (6.4 ft^3)
Test data extrapolation: saturation control with 44-W heat leak	6.95	3.2 kg (7.2 lb)	3.5	11.1 kg (24.5 lb)	0.026 m^3 (0.90 ft^3)
Analytical data					
Analytical model with 440-W heat leak, 100% efficient TVS	6.3	4.8 kg (10.6 lb)	3.8	18.24 kg (40.2 lb)	0.042 m^3 (1.5 ft^3)
Analytical extrapolation with 44-W heat load, 100% efficient TVS	6.3	0.48 kg (1.06 lb)	3.8	1.83 kg (4.03 lb)	0.0042 m^3 (0.15 ft^3)

The ‘analytical modeling–measured data’ comparison based on the 440-W heat input with J-T1 indicated vent losses per day of 18 kg and 111 kg, respectively (i.e., the actual heat exchanger efficiency was less than 16%). As previously noted, the presence of a subcooled liquid at the vent outlet, as opposed to a slightly superheated vapor, was indicative of a poor measured TVS performance. With the heat input reduced by a factor of 10 W to 44 W and the cycle durations held constant, the extrapolated analytical and measured vent losses were 1.83 kg and 4.03 kg, respectively. It should be noted that the 44-W heat input has no basis other than it is a convenient representation that demonstrates the ‘order of magnitude’ losses one could expect in an actual on-orbit application.

Another important subject addressed during the TVS performance evaluation was the simultaneous control of ullage pressure and saturation level. Unless helium had been added to compensate for the ullage volume increase due to liquid removal, the total ullage pressure and propellant vapor pressure could not have been maintained constant simultaneously, i.e., the fixed helium mass dictated a partial pressure reduction with each liquid reduction increment. Therefore, volumetric losses alone became a significant factor with the exaggerated heat inputs used in the testing. For example, with the 440-W input, the volumetric reduction of 0.26 m^3 (9.1 ft^3) per day dictated an ullage pressure reduction of 7.4 kPa (1.1 psi) per day with the saturation control mode. Of course, the effect is much less noticeable with a smaller, more realistic heat input. With the heat input reduced by a factor of 10, the volumetric change, which is directly proportional, is reduced to 0.026 m^3 (0.9 ft^3) per day, and the corresponding total ullage pressure reduction becomes 0.74 kPa (0.11 psi) per day as the helium expands and its partial pressure is reduced. The 100% efficiency analytical pressure loss per day would be about 0.042 kPa (0.0064 psi) with the 'on-orbit-type' heat leak. Therefore, the 'volume loss effect' could easily be lost in short-term testing with realistic on-orbit heat leak inputs. Further, it is important to note that control of both the saturation and ullage pressure is achievable in cases where the ullage is a single component gas consisting of the stored cryogenic propellant vapor, i.e., self-pressurization compensates for ullage volume increases while the saturation level is controlled.

8. SUMMARY AND CONCLUSIONS

The primary objective of this program was to address TVS performance with densified LCH_4 pressurized with GHe. Although the MHTB spray bar TVS design was optimized for LH_2, the already-existing test hardware offered an expedient means for identifying any unusual or unique thermodynamic characteristics unique to TVS operations with densified LCH_4 propellant. Thirteen days of testing were performed with net heat inputs to the LCH_4 ranging from 440 to 256 W with high and low flow rate J-T valves (0.02 and 0.01 kg/hr) at a fill level of ≈90%. Observations as the testing progressed through the various stages or phases are as follows:

- Starting with a 90% tank fill level, the pump and the larger J-T valve remained on to reduce the liquid saturation pressure. After 14 hr and 40 min, the liquid saturation pressure was successfully reduced from 110 to 54.3 kPa.

- After tank refill back to 90% and with the methane saturated at 50 kPa (7.25 psia), GHe was injected into the ullage until the gaseous methane and helium partial pressures were 50 kPa and 116 kPa, respectively, thereby completing the propellant conditioning in preparation for the initial phase of TVS testing.

- Eight mixing/vent cycles were conducted, with the larger J-T valve maintaining the ullage pressure held within a ±3.45 kPa (±0.5 psia) control band for about 17 hr. However, the liquid saturation pressure continued to rise throughout operation from 56 to 66 kPa (saturation temperature increase of 1.6 K).

- Use of the smaller J-T valve was implemented and did improve the pressure control; however, the liquid saturation level continued to rise in a sawtooth fashion.

- Testing was initiated with the TVS controls keyed to saturation pressure instead of ullage pressure. The intent of this mode was to demonstrate the pressure control capability while maintaining a prescribed propellant saturation level. The saturation level was successfully maintained at 65–68 kPa. However, the ullage pressure decreased in a sawtooth fashion by about 1.7 kPa per cycle for a total reduction of 10 kPa during the six cycles, or about 36 hr. With the heater setting reduced by half, the ullage pressure decrease continued at a reduced rate.

Subsequent to the above testing, a detailed examination of the data revealed that the J-T cooling with either of the two valves had been seriously compromised. In both cases, the downstream temperature was higher than the upstream or inlet temperature, even though the downstream pressure was lower. In other words, the J-T expansion coefficient was negative (negative ΔT over positive ΔP), a characteristic of metastability. Therefore, a component-by-component examination of the data was conducted to assure that an equipment malfunction or instrumentation error had not contributed to the metastable condition. The component-by-component evaluations validated the

functionality of each TVS element or component and the consistency of measured performance data trends throughout the system. Furthermore, regarding the valve open conditions measured at the J-T valve entrance and exit, it was noted that neither the temperature profile nor the magnitude varied substantially with test condition or valve size.

However, the reduced flow rate with the smaller J-T valve did enable reduced temperatures at the back pressure orifice, which in turn provided some degree of cooling of the recirculated or sprayed liquid. Apparently, a slow expansion process occurred as the fluid traversed the 3-m distance between the J-T valve and back pressure orifice, which is substantiated by the close match between the measured pressure and temperature with saturation conditions. The larger flow rate J-T valve led to more compressed TVS cycles and higher temperatures (approximately 1–2 K) at the back pressure orifice, which evidently negated the chance for any cooling of the recirculated liquid. Other observations are as follows:

- The presence of subcooled 101 K liquid at the back pressure orifice made it obvious that the TVS cooling obtained with the smaller J-T valve was not even in the right regime. Superheated vapor should be present at the orifice inlet in an optimized TVS system and was expected to be at least two-phase fluid, even with the nonoptimized TVS setup.

- Although the formation of triple-point solid particulates and/or slush probably was temporarily present at the J-T valve and back pressure orifice, it is not believed to have been a significant factor in system level performance.

- The pervasive presence of metastable conditions and resultant negative expansion coefficients across the J-T valve severely compromised analytical correlations with existing computational modeling since the thermodynamic venting concept is dependent on J-T cooling.

- In the MHTB test setup, the total ullage pressure and propellant vapor pressure could not be maintained constant simultaneously. The propellant supply to the TVS was drained from the tank bottom with a fixed helium mass within the ullage, thereby dictating a helium partial pressure reduction with each liquid reduction increment. The 'volume loss effect' would be much less noticeable in short-term testing with more realistic on-orbit heat leak inputs.

- Control of both the saturation and ullage pressure is achievable wherein the ullage is a single component gas consisting of the stored cryogenic propellant vapor, i.e., self-pressurization can compensate for ullage volume increases while the saturation level is controlled.

Recommendations for future space applications of LCH_4 are as follows:

- Although testing discussed herein was conducted with a spray bar TVS, it is believed that the metastable methane condition is primarily a function of the degree of densification and the level of helium pressurization. Until further testing demonstrates otherwise, it is recommended that it be assumed that the metastable methane conditions observed herein are also applicable to other TVS concepts. Similarly, the application of TVSs to concepts with high partial pressure helium should be constrained (because liquid below the liquid-vapor interface behaves as though it is subcooled).

- In future applications of J-T cooling to methane storage, assurance must be provided that metastable effects have either been mitigated or circumvented. A strong bench test program is recommended for any and all TVS applications to space-based LCH_4 storage.

- Propellant settling to support venting during reduced gravity methane storage now seems more probable. This may prove to be a modest constraint because the relatively high heat capacity of liquid methane can, in many cases, be effectively used to limit the vent frequency.

- Ground-based testing of pressure control concepts for reduced gravity storage of high-density cryogens (such as LCH_4, oxygen, and nitrogen) often necessitates heaters to expedite pressure control cycle rates. However, experience with the subject methane testing demonstrated the need for thermal modeling sufficient to determine the energy distribution to the tank contents versus the tank walls and other heat leak sources.

- To avoid obscuring heat transfer and thermodynamic regimes that can be expected in operational scenarios, it is strongly recommended that future testing include at least a partial test cycle with the actual anticipated heat load.

APPENDIX A—MULTIPURPOSE HYDROGEN TEST BED TANKING TABLE

A tanking table (table 7) has been calculated based on the design geometry of the MHTB test tank. This table provides volume, ullage, and mass estimates based on the fluid level as referenced to the tank bottom.

Table 7. MHTB tanking table.

Total Tank Volume = 639.34 ft^3 18.10 m^3
LH_2 Density = 4.419 lbm/ft^3 70.786 kg/m^3
Note: Height is measured from the bottom of the tank.

Height (in)	Height (cm)	Volume (ft^3)	Volume (m^3)	Ullage (%)	Liquid (%)	Liquid Mass (lbm)	Liquid Mass (kg)
0.00	0.00	0.00	0.0000	100.00	0.00	0.00	0.0000
0.50	1.27	0.05	0.0015	99.99	0.01	0.24	0.1087
1.00	2.54	0.22	0.0061	99.97	0.03	0.95	0.4324
1.50	3.81	0.48	0.0137	99.92	0.08	2.13	0.9673
2.00	5.08	0.85	0.0242	99.87	0.13	3.77	1.7098
2.50	6.35	1.33	0.0375	99.79	0.21	5.86	2.6560
3.00	7.62	1.90	0.0537	99.70	0.30	8.38	3.8025
3.50	8.89	2.57	0.0727	99.60	0.40	11.34	5.1453
4.00	10.16	3.33	0.0944	99.48	0.52	14.73	6.6809
4.50	11.43	4.19	0.1187	99.34	0.66	18.53	8.4055
5.00	12.70	5.15	0.1457	99.20	0.80	22.74	10.3154
5.50	13.97	6.19	0.1753	99.03	0.97	27.35	12.4068
6.00	15.24	7.32	0.2073	98.85	1.15	32.36	14.6762
6.50	16.51	8.54	0.2419	98.66	1.34	37.74	17.1198
7.00	17.78	9.85	0.2788	98.46	1.54	43.51	19.7338
7.50	19.05	11.23	0.3181	98.24	1.76	49.64	22.5146
8.00	20.32	12.70	0.3597	98.01	1.99	56.13	25.4585
8.50	21.59	14.25	0.4035	97.77	2.23	62.97	28.5618
9.00	22.86	15.88	0.4495	97.52	2.48	70.15	31.8207
9.50	24.13	17.58	0.4977	97.25	2.75	77.67	35.2316
10.00	25.40	19.35	0.5480	96.97	3.03	85.52	38.7907
10.50	26.67	21.20	0.6003	96.68	3.32	93.68	42.4943
11.00	27.94	23.12	0.6546	96.38	3.62	102.16	46.3388
11.50	29.21	25.10	0.7109	96.07	3.93	110.94	50.3204
12.00	30.48	27.16	0.7690	95.75	4.25	120.01	54.4354
12.50	31.75	29.28	0.8290	95.42	4.58	129.37	58.6801
13.00	33.02	31.46	0.8907	95.08	4.92	139.00	63.0509
13.50	34.29	33.70	0.9542	94.73	5.27	148.91	67.5439
14.00	35.56	36.00	1.0193	94.37	5.63	159.08	72.1556
14.50	36.83	38.36	1.0861	94.00	6.00	169.50	76.8821
15.00	38.10	40.77	1.1545	93.62	6.38	180.16	81.7198
15.50	39.37	43.24	1.2243	93.24	6.76	191.06	86.6650

Table 7. MHTB tanking table (Continued).

Height (in)	Height (cm)	Volume (ft^3)	Volume (m^3)	Ullage (%)	Liquid (%)	Liquid Mass (lbm)	Liquid Mass (kg)
16.00	40.64	45.76	1.2957	92.84	7.16	202.19	91.7140
16.50	41.91	48.32	1.3684	92.44	7.56	213.55	96.8630
17.00	43.18	50.94	1.4425	92.03	7.97	225.11	102.1084
17.50	44.45	53.60	1.5179	91.62	8.38	236.88	107.4464
18.00	45.72	56.31	1.5946	91.19	8.81	248.84	112.8734
18.50	46.99	59.06	1.6724	90.76	9.24	261.00	118.3856
19.00	48.26	61.85	1.7515	90.33	9.67	273.33	123.9794
19.50	49.53	64.68	1.8316	89.88	10.12	285.83	129.6510
20.00	50.80	67.55	1.9128	89.43	10.57	298.50	135.3967
20.50	52.07	70.45	1.9949	88.98	11.02	311.32	141.2128
21.00	53.34	73.39	2.0780	88.52	11.48	324.29	147.0957
21.50	54.61	76.35	2.1620	88.06	11.94	337.40	153.0415
22.00	55.88	79.35	2.2469	87.59	12.41	350.64	159.0467
22.50	57.15	82.37	2.3325	87.12	12.88	364.00	165.1074
23.00	58.42	85.42	2.4188	86.64	13.36	377.48	171.2200
23.50	59.69	88.49	2.5059	86.16	13.84	391.06	177.3808
24.00	60.96	91.59	2.5935	85.67	14.33	404.74	183.5861
24.50	62.23	94.71	2.6818	85.19	14.81	418.51	189.8321
25.00	63.50	97.84	2.7705	84.70	15.30	432.36	196.1152
25.50	64.77	100.99	2.8598	84.20	15.80	446.29	202.4317
26.00	66.04	104.16	2.9494	83.71	16.29	460.28	208.7778
26.50	67.31	107.34	3.0394	83.21	16.79	474.32	215.1498
27.00	68.58	110.53	3.1298	82.71	17.29	488.42	221.5441
27.50	69.85	113.73	3.2204	82.21	17.79	502.56	227.9569
28.00	71.12	116.93	3.3112	81.71	18.29	516.73	234.3845
28.50	72.39	120.15	3.4021	81.21	18.79	530.92	240.8233
29.00	73.66	123.36	3.4932	80.70	19.30	545.14	247.2695
29.50	74.93	126.58	3.5843	80.20	19.80	559.36	253.7193
30.00	76.20	129.80	3.6755	79.70	20.30	573.58	260.1718
30.50	77.47	133.02	3.7666	79.19	20.81	587.80	266.6225
31.00	78.74	136.23	3.8577	78.69	21.31	602.02	273.0731
31.50	80.01	139.45	3.9489	78.19	21.81	616.24	279.5237
32.00	81.28	142.67	4.0400	77.68	22.32	630.47	285.9743
32.50	82.55	145.89	4.1311	77.18	22.82	644.69	292.4250
33.00	83.82	149.11	4.2222	76.68	23.32	658.91	298.8756
33.50	85.09	152.33	4.3134	76.17	23.83	673.13	305.3262
34.00	86.36	155.54	4.4045	75.67	24.33	687.35	311.7768
34.50	87.63	158.76	4.4956	75.17	24.83	701.57	318.2275
35.00	88.90	161.98	4.5868	74.66	25.34	715.79	324.6781
35.50	90.17	165.20	4.6779	74.16	25.84	730.01	331.1287

Table 7. MHTB tanking table (Continued).

Height (in)	Height (cm)	Volume (ft^3)	Volume (m^3)	Ullage (%)	Liquid (%)	Liquid Mass (lbm)	Liquid Mass (kg)
36.00	91.44	168.42	4.7690	73.66	26.34	744.24	337.5793
36.50	92.71	171.63	4.8601	73.15	26.85	758.46	344.0300
37.00	93.98	174.85	4.9513	72.65	27.35	772.68	350.4806
37.50	95.25	178.07	5.0424	72.15	27.85	786.90	356.9312
38.00	96.52	181.29	5.1335	71.64	28.36	801.12	363.3818
38.50	97.79	184.51	5.2247	71.14	28.86	815.34	369.8325
39.00	99.06	187.73	5.3158	70.64	29.36	829.56	376.2831
39.50	100.33	190.94	5.4069	70.13	29.87	843.78	382.7337
40.00	101.60	194.16	5.4980	69.63	30.37	858.00	389.1843
40.50	102.87	197.38	5.5892	69.13	30.87	872.23	395.6350
41.00	104.14	200.60	5.6803	68.62	31.38	886.45	402.0856
41.50	105.41	203.82	5.7714	68.12	31.88	900.67	408.5362
42.00	106.68	207.03	5.8626	67.62	32.38	914.89	414.9868
42.50	107.95	210.25	5.9537	67.11	32.89	929.11	421.4375
43.00	109.22	213.47	6.0448	66.61	33.39	943.33	427.8881
43.50	110.49	216.69	6.1359	66.11	33.89	957.55	434.3387
44.00	111.76	219.91	6.2271	65.60	34.40	971.77	440.7893
44.50	113.03	223.13	6.3182	65.10	34.90	986.00	447.2400
45.00	114.30	226.34	6.4093	64.60	35.40	1000.22	453.6906
45.50	115.57	229.56	6.5005	64.09	35.91	1014.44	460.1412
46.00	116.84	232.78	6.5916	63.59	36.41	1028.66	466.5918
46.50	118.11	236.00	6.6827	63.09	36.91	1042.88	473.0425
47.00	119.38	239.22	6.7738	62.58	37.42	1057.10	479.4931
47.50	120.65	242.43	6.8650	62.08	37.92	1071.32	485.9437
48.00	121.92	245.65	6.9561	61.58	38.42	1085.54	492.3943
48.50	123.19	248.87	7.0472	61.07	38.93	1099.76	498.8450
49.00	124.46	252.09	7.1384	60.57	39.43	1113.99	505.2956
49.50	125.73	255.31	7.2295	60.07	39.93	1128.21	511.7462
50.00	127.00	258.53	7.3206	59.56	40.44	1142.43	518.1968
50.50	128.27	261.74	7.4117	59.06	40.94	1156.65	524.6475
51.00	129.54	264.96	7.5029	58.56	41.44	1170.87	531.0981
51.50	130.81	268.18	7.5940	58.05	41.95	1185.09	537.5487
52.00	132.08	271.40	7.6851	57.55	42.45	1199.31	543.9993
52.50	133.35	274.62	7.7763	57.05	42.95	1213.53	550.4500
53.00	134.62	277.83	7.8674	56.54	43.46	1227.76	556.9006
53.50	135.89	281.05	7.9585	56.04	43.96	1241.98	563.3512
54.00	137.16	284.27	8.0496	55.54	44.46	1256.20	569.8018
54.50	138.43	287.49	8.1408	55.03	44.97	1270.42	576.2525
55.00	139.70	290.71	8.2319	54.53	45.47	1284.64	582.7031
55.50	140.97	293.93	8.3230	54.03	45.97	1298.86	589.1537

Table 7. MHTB tanking table (Continued).

Height (in)	Height (cm)	Volume (ft^3)	Volume (m^3)	Ullage (%)	Liquid (%)	Liquid Mass (lbm)	Liquid Mass (kg)
56.00	142.24	297.14	8.4142	53.52	46.48	1313.08	595.6043
56.50	143.51	300.36	8.5053	53.02	46.98	1327.30	602.0550
57.00	144.78	303.58	8.5964	52.52	47.48	1341.53	608.5056
57.50	146.05	306.80	8.6875	52.01	47.99	1355.75	614.9562
58.00	147.32	310.02	8.7787	51.51	48.49	1369.97	621.4068
58.50	148.59	313.23	8.8698	51.01	48.99	1384.19	627.8575
59.00	149.86	316.45	8.9609	50.50	49.50	1398.41	634.3081
59.50	151.13	319.67	9.0521	50.00	50.00	1412.63	640.7587
60.00	152.40	322.89	9.1432	49.50	50.50	1426.85	647.2093
60.50	153.67	326.11	9.2343	48.99	51.01	1441.07	653.6600
61.00	154.94	329.33	9.3254	48.49	51.51	1455.29	660.1106
61.50	156.21	332.54	9.4166	47.99	52.01	1469.52	666.5612
62.00	157.48	335.76	9.5077	47.48	52.52	1483.74	673.0118
62.50	158.75	338.98	9.5988	46.98	53.02	1497.96	679.4625
63.00	160.02	342.20	9.6900	46.48	53.52	1512.18	685.9131
63.50	161.29	345.42	9.7811	45.97	54.03	1526.40	692.3637
64.00	162.56	348.63	9.8722	45.47	54.53	1540.62	698.8143
64.50	163.83	351.85	9.9633	44.97	55.03	1554.84	705.2650
65.00	165.10	355.07	10.0545	44.46	55.54	1569.06	711.7156
65.50	166.37	358.29	10.1456	43.96	56.04	1583.29	718.1662
66.00	167.64	361.51	10.2367	43.46	56.54	1597.51	724.6168
66.50	168.91	364.73	10.3278	42.95	57.05	1611.73	731.0675
67.00	170.18	367.94	10.4190	42.45	57.55	1625.95	737.5181
67.50	171.45	371.16	10.5101	41.95	58.05	1640.17	743.9687
68.00	172.72	374.38	10.6012	41.44	58.56	1654.39	750.4193
68.50	173.99	377.60	10.6924	40.94	59.06	1668.61	756.8700
69.00	175.26	380.82	10.7835	40.44	59.56	1682.83	763.3206
69.50	176.53	384.03	10.8746	39.93	60.07	1697.06	769.7712
70.00	177.80	387.25	10.9657	39.43	60.57	1711.28	776.2218
70.50	179.07	390.47	11.0569	38.93	61.07	1725.50	782.6725
71.00	180.34	393.69	11.1480	38.42	61.58	1739.72	789.1231
71.50	181.61	396.91	11.2391	37.92	62.08	1753.94	795.5737
72.00	182.88	400.13	11.3303	37.42	62.58	1768.16	802.0243
72.50	184.15	403.34	11.4214	36.91	63.09	1782.38	808.4750
73.00	185.42	406.56	11.5125	36.41	63.59	1796.60	814.9256
73.50	186.69	409.78	11.6036	35.91	64.09	1810.82	821.3762
74.00	187.96	413.00	11.6948	35.40	64.60	1825.05	827.8268
74.50	189.23	416.22	11.7859	34.90	65.10	1839.27	834.2775
75.00	190.50	419.43	11.8770	34.40	65.60	1853.49	840.7281
75.50	191.77	422.65	11.9682	33.89	66.11	1867.71	847.1787

Table 7. MHTB tanking table (Continued).

Height (in)	Height (cm)	Volume (ft^3)	Volume (m^3)	Ullage (%)	Liquid (%)	Liquid Mass (lbm)	Liquid Mass (kg)
76.00	193.04	425.87	12.0593	33.39	66.61	1881.93	853.6293
76.50	194.31	429.09	12.1504	32.89	67.11	1896.15	860.0800
77.00	195.58	432.31	12.2415	32.38	67.62	1910.37	866.5306
77.50	196.85	435.53	12.3327	31.88	68.12	1924.59	872.9812
78.00	198.12	438.74	12.4238	31.38	68.62	1938.82	879.4318
78.50	199.39	441.96	12.5149	30.87	69.13	1953.04	885.8824
79.00	200.66	445.18	12.6061	30.37	69.63	1967.26	892.3331
79.50	201.93	448.40	12.6972	29.87	70.13	1981.48	898.7837
80.00	203.20	451.62	12.7883	29.36	70.64	1995.70	905.2343
80.50	204.47	454.83	12.8794	28.86	71.14	2009.92	911.6849
81.00	205.74	458.05	12.9706	28.36	71.64	2024.14	918.1356
81.50	207.01	461.27	13.0617	27.85	72.15	2038.36	924.5862
82.00	208.28	464.49	13.1528	27.35	72.65	2052.58	931.0368
82.50	209.55	467.71	13.2440	26.85	73.15	2066.81	937.4874
83.00	210.82	470.93	13.3351	26.34	73.66	2081.03	943.9381
83.50	212.09	474.14	13.4262	25.84	74.16	2095.25	950.3887
84.00	213.36	477.36	13.5173	25.34	74.66	2109.47	956.8393
84.50	214.63	480.58	13.6085	24.83	75.17	2123.69	963.2899
85.00	215.90	483.80	13.6996	24.33	75.67	2137.91	969.7406
85.50	217.17	487.02	13.7907	23.83	76.17	2152.13	976.1912
86.00	218.44	490.23	13.8819	23.32	76.68	2166.35	982.6418
86.50	219.71	493.45	13.9730	22.82	77.18	2180.58	989.0924
87.00	220.98	496.67	14.0641	22.32	77.68	2194.80	995.5431
87.50	222.25	499.89	14.1552	21.81	78.19	2209.02	1001.9937
88.00	223.52	503.11	14.2464	21.31	78.69	2223.24	1008.4443
88.50	224.79	506.33	14.3375	20.80	79.20	2237.46	1014.8949
89.00	226.06	509.54	14.4286	20.30	79.70	2251.68	1021.3456
89.50	227.33	512.76	14.5198	19.80	80.20	2265.90	1027.7962
90.00	228.60	515.98	14.6108	19.30	80.70	2280.12	1034.2433
90.50	229.87	519.19	14.7019	18.79	81.21	2294.33	1040.6895
91.00	231.14	522.41	14.7929	18.29	81.71	2308.52	1047.1282
91.50	232.41	525.61	14.8837	17.79	82.21	2322.69	1053.5559
92.00	233.68	528.81	14.9743	17.29	82.71	2336.83	1059.9687
92.50	234.95	532.00	15.0646	16.79	83.21	2350.93	1066.3630
93.00	236.22	535.18	15.1546	16.29	83.71	2364.98	1072.7350
93.50	237.49	538.35	15.2443	15.80	84.20	2378.97	1079.0811
94.00	238.76	541.50	15.3335	15.30	84.70	2392.89	1085.3976
94.50	240.03	544.63	15.4223	14.81	85.19	2406.74	1091.6807
95.00	241.30	547.75	15.5105	14.33	85.67	2420.51	1097.9267
95.50	242.57	550.84	15.5982	13.84	86.16	2434.19	1104.1320

Table 7. MHTB tanking table (Continued).

Height (in)	Height (cm)	Volume (ft^3)	Volume (m^3)	Ullage (%)	Liquid (%)	Liquid Mass (lbm)	Liquid Mass (kg)
96.00	243.84	553.92	15.6852	13.36	86.64	2447.78	1110.2928
96.50	245.11	556.97	15.7716	12.88	87.12	2461.25	1116.4054
97.00	246.38	559.99	15.8572	12.41	87.59	2474.61	1122.4661
97.50	247.65	562.99	15.9420	11.94	88.06	2487.85	1128.4713
98.00	248.92	565.95	16.0260	11.48	88.52	2500.96	1134.4171
98.50	250.19	568.89	16.1091	11.02	88.98	2513.93	1140.3000
99.00	251.46	571.79	16.1913	10.57	89.43	2526.75	1146.1161
99.50	252.73	574.66	16.2724	10.12	89.88	2539.42	1151.8618
100.00	254.00	577.49	16.3526	9.67	90.33	2551.92	1157.5334
100.50	255.27	580.28	16.4316	9.24	90.76	2564.26	1163.1272
101.00	256.54	583.03	16.5095	8.81	91.19	2576.41	1168.6394
101.50	257.81	585.73	16.5861	8.38	91.62	2588.37	1174.0664
102.00	259.08	588.40	16.6615	7.97	92.03	2600.14	1179.4044
102.50	260.35	591.01	16.7356	7.56	92.44	2611.71	1184.6498
103.00	261.62	593.58	16.8084	7.16	92.84	2623.06	1189.7988
103.50	262.89	596.10	16.8797	6.76	93.24	2634.19	1194.8478
104.00	264.16	598.57	16.9496	6.38	93.62	2645.09	1199.7930
104.50	265.43	600.98	17.0179	6.00	94.00	2655.76	1204.6307
105.00	266.70	603.34	17.0847	5.63	94.37	2666.18	1209.3572
105.50	267.97	605.64	17.1498	5.27	94.73	2676.34	1213.9689
106.00	269.24	607.88	17.2133	4.92	95.08	2686.25	1218.4619
106.50	270.51	610.06	17.2751	4.58	95.42	2695.88	1222.8327
107.00	271.78	612.18	17.3350	4.25	95.75	2705.24	1227.0774
107.50	273.05	614.23	17.3932	3.93	96.07	2714.31	1231.1924
108.00	274.32	616.22	17.4494	3.62	96.38	2723.09	1235.1740
108.50	275.59	618.14	17.5037	3.32	96.68	2731.57	1239.0185
109.00	276.86	619.99	17.5560	3.03	96.97	2739.73	1242.7221
109.50	278.13	621.76	17.6063	2.75	97.25	2747.58	1246.2812
110.00	279.40	623.46	17.6545	2.48	97.52	2755.10	1249.6921
110.50	280.67	625.09	17.7005	2.23	97.77	2762.28	1252.9510
111.00	281.94	626.64	17.7444	1.99	98.01	2769.13	1256.0543
111.50	283.21	628.11	17.7860	1.76	98.24	2775.62	1258.9981
112.00	284.48	629.49	17.8253	1.54	98.46	2781.75	1261.7790
112.50	285.75	630.80	17.8622	1.34	98.66	2787.51	1264.3930
113.00	287.02	632.02	17.8967	1.15	98.85	2792.90	1266.8366
113.50	288.29	633.15	17.9288	0.97	99.03	2797.90	1269.1060
114.00	289.56	634.19	17.9583	0.80	99.20	2802.51	1271.1974
114.50	290.83	635.15	17.9853	0.66	99.34	2806.72	1273.1073
115.00	292.10	636.01	18.0097	0.52	99.48	2810.52	1274.8319
115.50	293.37	636.77	18.0313	0.40	99.60	2813.91	1276.3675

Table 7. MHTB tanking table (Continued).

Height (in)	Height (cm)	Volume (ft^3)	Volume (m^3)	Ullage (%)	Liquid (%)	Liquid Mass (lbm)	Liquid Mass (kg)
116.00	294.64	637.44	18.0503	0.30	99.70	2816.87	1277.7103
116.50	295.91	638.01	18.0665	0.21	99.79	2819.40	1278.8567
117.00	297.18	638.49	18.0799	0.13	99.87	2821.48	1279.8030
117.50	298.45	638.86	18.0904	0.08	99.92	2823.12	1280.5455
118.00	299.72	639.12	18.0979	0.03	99.97	2824.30	1281.0804
118.50	300.99	639.28	18.1025	0.01	99.99	2825.01	1281.4041
119.00	302.26	639.34	18.1040	0.00	100.00	2825.25	1281.5128

APPENDIX B—PUMP OPERATING MANUAL

Appendix B contains the installation, operating, and maintenance manual for the Barber-Nichols, Inc., BNHP-08B-000 centrifugal cryogenic pump used in the recirculation process.

NASA – MARSHALL SPACE FLIGHT CENTER

LIQUID NITROGEN/ LIQUID HYDROGENPUMP BNHP-08B-000

Installation, Operating, and Maintenance Manual

November 2003

Prepared for: **NASA – Marshall Space Flight Center**
Huntsville, AL 35812

Prepared by: **Barber-Nichols Inc.**
6325 W. 55th Avenue
Arvada, CO 80002

Barber Nichols

Manual #BNHP-08B-1-A

NASA – MARSHALL SPACE FLIGHT CENTER

LIQUID NITROGEN/ LIQUID HYDROGENPUMP BNHP-08B-000

Installation, Operating, and Maintenance Manual

November 2003

Prepared for: **NASA – Marshall Space Flight Center**
Huntsville, AL 35812

Prepared by: **Barber-Nichols Inc.**
6325 W. 55th Avenue
Arvada, CO 80002

_____ _____
Robert A. Stannard — Date
Quality Assurance Manager

_____ _____
Kevin Hotton — Date
Project Manager

Barber Nichols

Manual #BNHP-08B-1-A

TABLE OF CONTENTS

INSTALLATION, OPERATING, AND MAINTENANCE MANUAL

1.0 INTRODUCTION

The BNHP-08B is a full emission, cryogenic pump. The pump is designed to circulate liquid nitrogen, but can also be used with liquid hydrogen. The pump is a hermitic design with motor cooling and bearing lubrication provided by the pumped cryogen. This pump is for use in the Zero Boil-Off Demonstration system.

The motor in the pump is controlled by a variable frequency drive. The VFD is 208 VAC, 3-phase 60 hertz input and up to 200 VAC, 3-phase, 400 hertz output. The VFD allows adjustment of the pump speed to produce any desired head and flow within the available power range of the pump motor.

This manual describes the installation, electrical hook-up, operation, replacement and maintenance of the BNHP-08B.

2.0 INSTALLATION

2.1 GENERAL INSTALLATION GUIDELINES

The pump contain precision mechanical components and must be handled with care during installation. Excessive bumping, jolting or mishandling may result in damage to the pump. Avoid putting any loads or moments on the pump inlet and discharge connections.

The inlet and outlet piping must be sufficiently flexible to transfer minimal piping loads or moments into the housing.

It is recommended that the pump run in a vertical position with the inlet pointing vertically upward. Alternatively, the pump can be installed horizontally.

The motor is cooled by the liquid nitrogen (liquid hydrogen). Circulation of the pumped cryogen, when running, is used to insure adequate cooling and bearing lubrication. The pump should not be run dry.

2.2 MECHANICAL INSTALLATION

The BNHP-08B pump uses welded connections at both inlet and discharge ports. Hence, it is recommended that the electrical installation is completed first (see Section 2.3) so that pump rotation can be visually verified; then proceed with mechanical installation.

Before installing the pump, ensure that the inlet and discharge ports for are clean, dry, and free of any substance that could be

detrimental to the seal weld quality. When welding the inlet/outlet of the pump into the system piping, wrap the central body of the pump with a towel soaked in cool water to prevent overheating the pump motor.

2.3 ELECTRICAL INSTALLATION

- W A R N I N G -

NATIONAL OR LOCAL ELECTRICAL CODES OUTLINE PROVISIONS FOR SAFELY INSTALLING ELECTRICAL EQUIPMENT. INSTALLATION MUST COMPLY WITH SPECIFICATIONS REGARDING WIRE SIZE, TYPE, CONDUCTOR SIZE, BRANCH CIRCUIT PROTECTION AND DISCONNECT DEVICES. FAILURE TO DO SO MAY RESULT IN PERSONAL INJURY AND/OR EQUIPMENT DAMAGE.

The electrical installation is to be accomplished using relevant electrical codes (NEC-2002) and VFD manufacturer furnished technical manuals as a guideline. Basic wiring is per section 430-22 and table 310-16 of the US NEC-2002. Installation of the motor and controls is per section 430-2 and diagram 430-1 of NEC-2002.

1. Remove the VFD cover by removing the cover screw at the bottom of the VFD. See Figure 1 for the location of the Main and Motor terminal blocks.

2. Wire the VFD to the motor as shown in Figure 2. Refer to the VFD manual for additional information on wiring the VFD to the motor.

3. After wiring the VFD to the motor, the unit is ready for operation. However, the direction of motor rotation must be checked prior to functional operation. To check motor rotation, apply electrical power to the VFD. Set the operating frequency to a low value, 10-15 hertz. Depress the START/STOP button on the VFD digital keypad and visually observe the direction of shaft rotation by viewing the direction of inducer rotation. Rotation should be counter clockwise when viewed from the pump inlet. If pump rotation is incorrect, interchange any two of the three wires between the pump and the VFD. DO NOT interchange any of the wires between the VFD and the power source. This will have no affect on motor rotational direction. Stop the pump, and set the VFD to the desired operating frequency (design frequency is 110 Hz).

4. Install the VFD terminal cover on the VFD.

Front cover removed

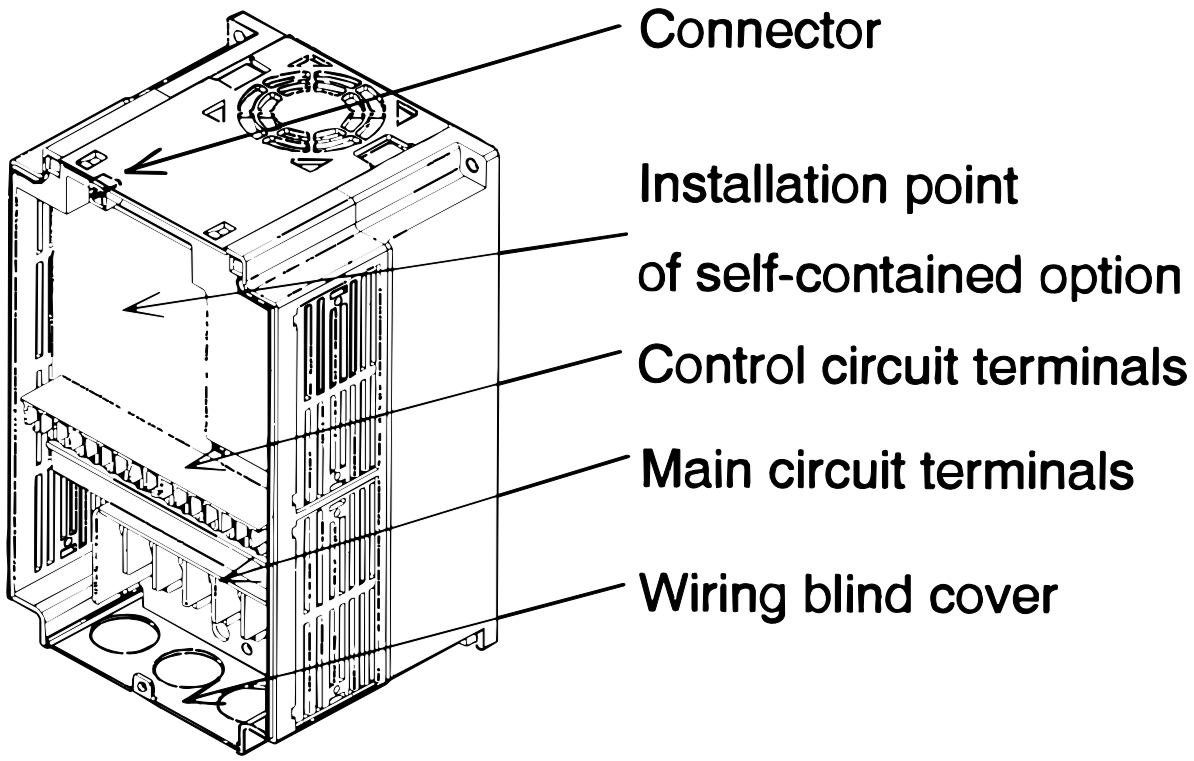

Figure 1.0

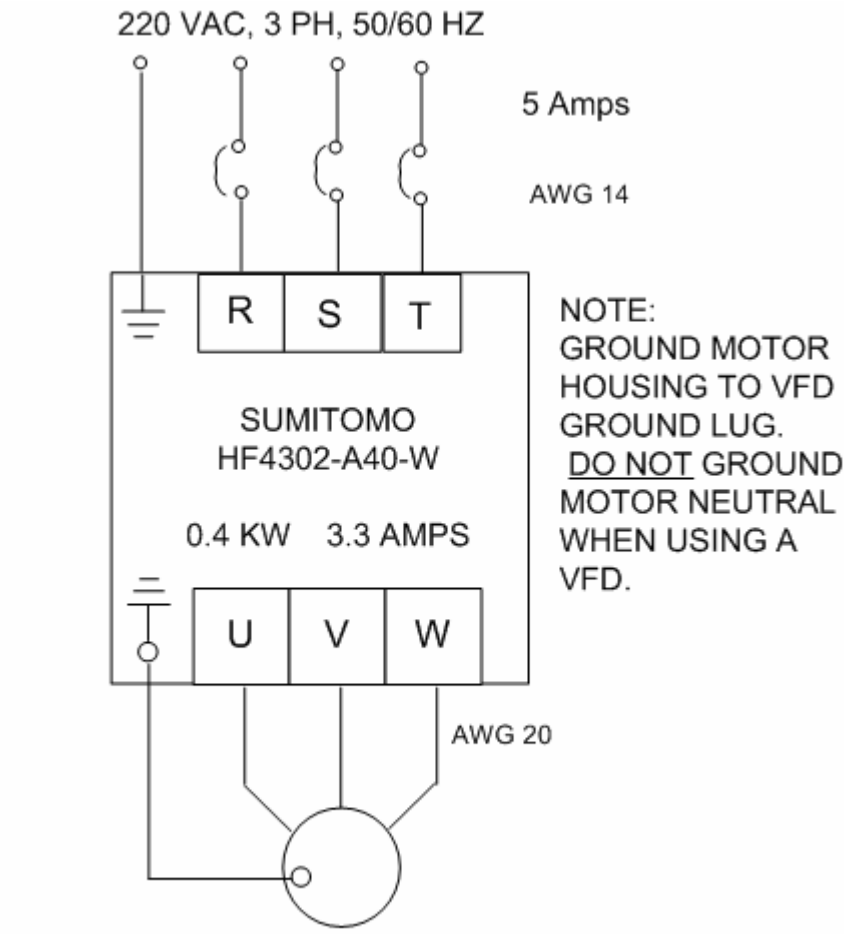

Figure 2: VFD WIRING DIAGRAM

3.0 OPERATION

3.1 PUMP DESIGN POINT OPERATION

The pump design point operating conditions are:

Fluid	Liquid Nitrogen
Alternate Fluid	Liquid Hydrogen
Inlet pressure	23.0 psia
Inlet temperature	-313°F (81 K)
Flow rate	30 gpm
Differential pressure	4.8 psid (14-ft head-rise)
Approx. operating speed	3100 rpm

Figure 3 shows the head-flow curve for the BNHP-08B pump at its operating speeds of 3100 rpm.

3.2 MOTOR NAMEPLATE DATA

The pump motor is a 3-phase, inverter duty motor. In this application it is running at a fraction of the 200 VAC (400 Hz) design speed. The nameplate data for the motor as used in the BNHP-08B liquid nitrogen pump is as follows:

Manufacturer	Lucas Western
Motor Series	181RA50
Volts, AC	57
Amps	1.1
Phase	3
Hertz	110
Poles	4
Horsepower	.07*
Speed	3100 rpm
Ambient temp.	40°C
Duty	Continuous
Insulation class	H
Enclosure	TELC Submerged

* Motor power is 0.15 hp at cryogenic temperatures

3.3 PUMP CHECKS AND OPERATION

Before operating the pump, perform the following checks and operations:

1. The pump should always be evacuated before charging with nitrogen (hydrogen) to prevent the formation of solid crystals (ice or other foreign materia) which could damage the bearings.

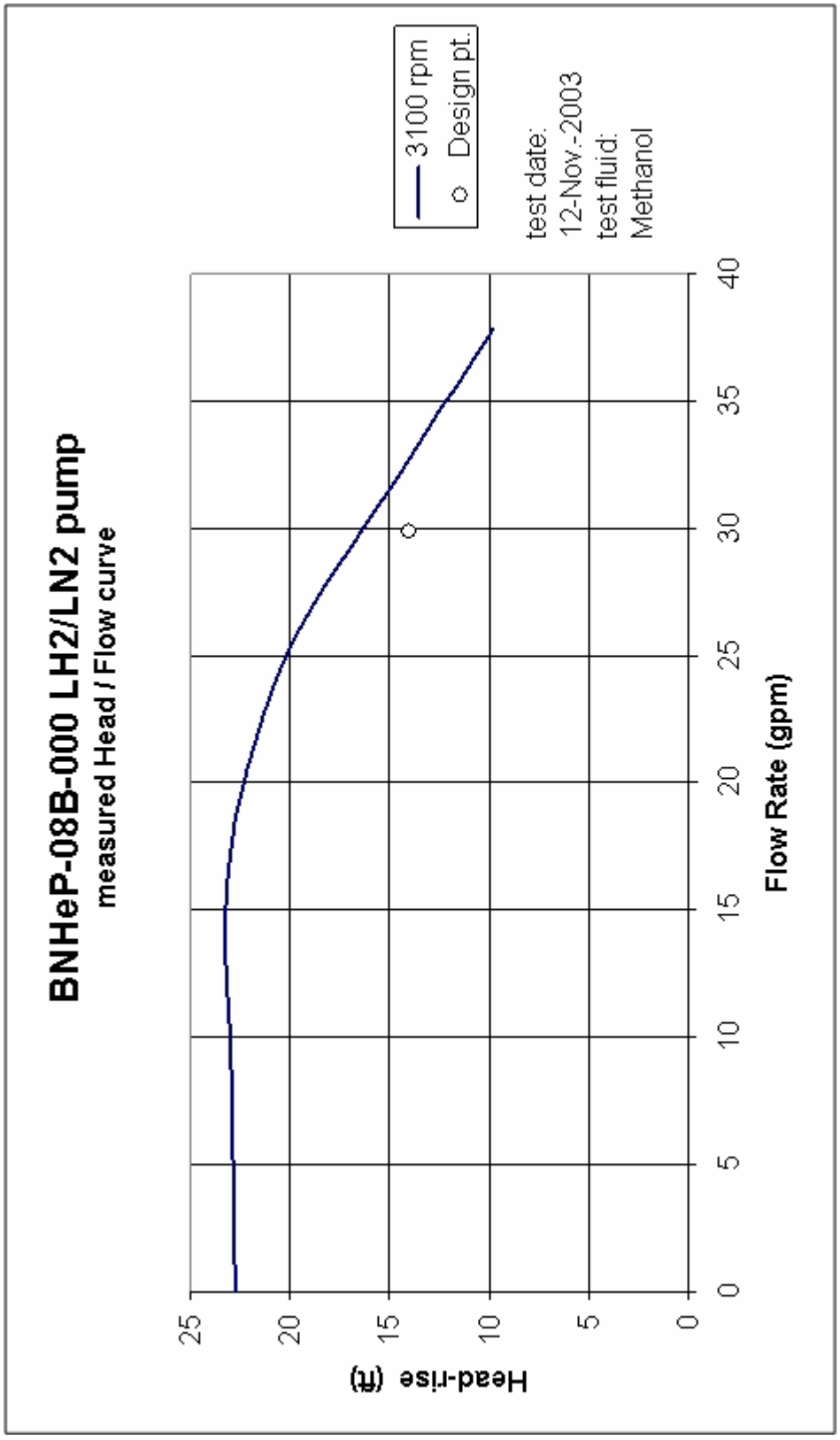
BNHeP-08B-000 LH2/LN2 pump
measured Head / Flow curve
3100 rpm
Design pt.
test date:
12-Nov.-2003
test fluid:
Methanol
Head-rise (ft)
Flow Rate (gpm)
0
5
10
15
20
25
30
35
40

Figure 3

2. Be sure there are no loose objects or large particles in the dewar which could get caught in the impeller clearances and cause damage to the pump.

3. The pump was not designed to operate under shock loading. Ensure that heavy shock loads are not encountered in service.

4. The motor maximum speed is 125 Hz. Exceeding this speed could overload or damage the motor. Ensure that the VFD is set up to limit motor speed at or below 125 Hz. Setting the speed limit on the VFD will ensure overspeed protection of the pump. The pump speed cannot exceed the speed of the VFD even if the impeller is suddenly unloaded. Normal operating speed for the pump is 3100 rpm (110 Hertz).

The pump is operated by controlling the frequency of the variable frequency drive (VFD). The motor is 4 pole induction type. Consequently, the synchronous speed of the rotor and shaft are related to the frequency of the VFD (60 Hz = 1800 rpm synchronous). The true speed of the rotor and shaft will be slightly less than the synchronous speed due to rotor slip. Under normal operation, the difference between the synchronous speed and true shaft speed depends on the load, but for the pump motor is typically about 8%.

The VFD has been programmed to run the pump motor at its normal operating speed of 110 Hz (3100 rpm) using three-phase power at 200 VAC. The pump was tested at Barber-Nichols and meets the design performance requirements. Operating at speeds in excess of design speed will reduce bearing life and is not recommended. Operating at speeds less than 3100 rpm will extend the life of the bearings.

Basic operation of the VFD is described below. For further information, refer to the Sumitomo HF-430 VFD manual sections 3 and 4.

Figure 4 shows the VFD digital operator panel. The RUN and STOP keys are used to start and stop the motor. The LED digits display set frequency, running frequency, current, volts, etc. The FUNC key is used to sequence the display through various functions and parameters. The STR key is used to display data in memory and to enter new data to memory. The RESET key is used to reset operation after a fault. The STOP key is used to stop the motor. The UP/DOWN keys change extension function mode, function mode and set value.

Chapter 4 Explanation of function

4.1 About Digital Operator

Explanation of operating the digital operator

HF430 series operates by using the digital operator, which is fitted as standard.

1. Name and contents of each part of the digital operator

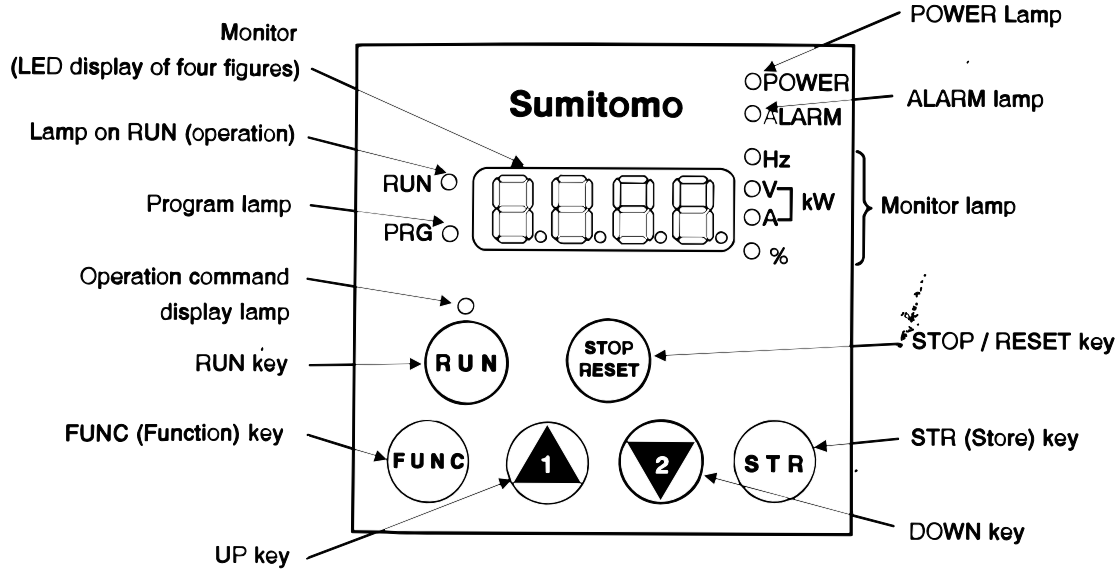

Name	Contents
Monitor	Display of frequency, output current and set value
Lamp on RUN (Operation)	Light on when the inverter is running
Program lamp	Light on when displaying set value of each function in monitor section Light will flash On and Off as a warning (when set value is incorrect)
POWER lamp	Power lamp of control circuit
ALARM lamp	Light on when the Inverter trips
Monitor lamp	Lamp display state of monitor section. Hz : Frequency V : Voltage A : Current kW : Electric power % : Rate
Operation command Display lamp	Light on only when operating command (RUN/STOP) is set in operator
Run key	Run command to start the motor. But this is only valid when operation command is from the operator. (Be sure that the operation command display lamp is illuminated.)
Stop (stop/reset) key	This key is used to stop motor, or reset an alarm.
FUNC(Function) key	The key containing monitor mode, basic setting mode, extension function mode.
STR (Store) key	The key to store the data set. (On changing set value, must be pushed or value is lost.)
UP/DOWN key	The keys to change extension function mode, function mode and set value.

Figure 4.

When AC power is applied to the VFD, the red LED "POWER" will illuminate.

When the FUNC key is depressed, the Basic Setting Mode is selected. The UP/DOWN arrows can then be used to select a particular Function Number. The STR key is then depressed to read the value in memory. If the number in memory is to be changed, the UP/DOWN keys (arrow to the right) are used to change the value. The STR key is then depressed to store the new value. The FUNC key is then depressed to display the Function Number and the UP/DOWN arrows are used to step to the next Function Number. The FUNC key is depressed to exit the program mode.

The HF-430 Operate and Maintenance Manual further describes the Digital Key Pad and the Function and Run modes of operation.

During startup, the Sumitomo HF-430 VFD is programmed to ramp the pump up to set speed in 30 seconds. A ramp rate lower than 30 seconds can be programmed into the VFD, if desired. However, a ramp rate of less than 5 seconds could cause an overcurrent shutdown during initial acceleration and should not be used. The set speed and ramp rate are programmed into the VFD and can be changed as necessary. Refer to the VFD manual for information to reprogram the VFD.

Appendix A summarizes the VFD settings as recommended for the unit as shipped to NASA-MSFC.

4.0 MAINTENANCE

4.1 VFD MAINTENANCE

The variable frequency drive was manufactured by Sumitomo Heavy Industries. VFD maintenance if covered in section 5.1 of the Sumitomo HF-430 VFD manual. If VFD troubles occur, refer to the VFD manual and/or contact the Sumitomo representative in your area.

4.2 REPLACING THE PUMP ASSEMBLY

- W A R N I N G -

BEFORE PERFORMING ANY MAINTENANCE ON THE PUMP, ENSURE THAT ALL ELECTRICAL POWER TO THE UNIT IS TURNED OFF, LOCKED OUT AND TAGGED. FAILURE TO DO SO COULD RESULT IN PERSONAL INJURY OR EQUIPMENT DAMAGE.

The pump is designed so that all electrical connections are

external to the dewar. The dewar must be drained or valved-off before the pump can be replaced with a spare pump. The following steps describe the removal and reinstallation of the liquid nitrogen (hydrogen) pump.

Removal of the Pump

1. Ensure all electrical power is turned off.

2. Disconnect the electrical cable on the pump housing (removal of insulation might be required to reach connector).

3. Drain or valve-off the dewar from the pump.

4. Carefully cut the tubing about 1-inch beyond the inlet and discharge port weld.

Installation of a Reconditioned Pump

1. Install the motor electrical connector onto the motor receptacle.

2. While viewing the pump inducer, check motor rotation. Rotation should be counter clockwise. If rotation is backwards, swap any two leads between the motor and the VFD.

3. Orient the pump into it original position. Butt-weld the inlet and discharge ports back into the system piping.

5. Reinstall pump insulation.

6. Pump air out of the liquid nitrogen loop.

7. Refill the dewar with liquid nitrogen.

4.3 REPLACING THE BEARINGS

The BNHP-08B pump is designed for long-life and trouble-free operation. No periodic maintenance is required. However, after sufficient run-time, components will wear.

The pump bearings have an estimated life of over 10,000 hours under normal use at a rotational speed of 3100 rpm. If the pump has been operating for over 10,000 hours or contaminants have caused early bearing failure, motor bearing replacement is required.

Due to the welded housing on the pump, field replacement of the bearings is not possible. The pump must be returned to Barber-

Nichols for refurbishment.

4.4 OTHER MAINTENANCE

The pump assembly should be returned to Barber-Nichols for any maintenance. There are no field serviceable parts accessible without cutting open pump.

5.0 PARTS LISTS

5.1 PARTS LIST FOR LIQUID NITROGEN PUMP BNHP-08B-000

Item	Qty	Description
1	1	Impeller Housing
2	1	Diffuser Housing
3	1	Pump Exit
4	1	Motor Shaft
5	1	Impeller
6	1	Inducer
7	1	Front Bearing Housing
8	1	Diffuser
9	1	Rear Bearing Housing
10	1	Electrical Enclosure
11	1	Motor Pin
12	2	Impeller Pin
13	1	Diffuser Pin
14	1	Bearing Shim
15	1	Impeller Shim
16	1	Inducer Screw
17	1	#6-32 x .250 SHCS
18	1	Motor
19	1	Electrical Feed-thru
20	2	Ball Bearings
21	1	Wave Spring
22	2	#10-32 x 2.50 SHCS
23	1	Belleville Washer
24	2	Belleville Washer
25	1	Belleville Washer

5.3 PARTS LIST FOR OVERHAUL KIT BNHP-08B-100

Item	Qty	Description
15	1	SR3-SST5 Ball Bearing
16	1	SR8-SST5 Ball Bearing
17	1	Wave Spring Washer
19	6	Belleville Washer
20	1	Belleville Washer
24	1	Spiral Retaining Ring

APPENDIX A: VFD PARAMETER SETTINGSAPPENDIX A: VFD PARAMETER SETTINGSAPPENDIX A: VFD PARAMETER SETTINGSAPPENDIX A: VFD PARAMETER SETTINGSAPPENDIX A: VFD PARAMETER SETTINGS

The VFD has been programmed to run the BNHP-08B-000 Liquid Nitrogen (Hydrogen) Pump at a design speed of 3100 rpm. The following table summarizes the settings of the Sumitomo HF4302-A40-W VFD as shipped to Marshall Space Flight Center.

The parameters shown in the table below are those changed to make the VFD compatible with the pump motor. Any parameters which do not appear in the table are still the factory default values.

DRIVE PARAMETER SETTINGS

Code	Function Name	Setting
A001	Frequency Setting Selection	02
A002	Operation Setting Selection	02
A003	Base Frequency	400
A004	Maximum Frequency	400
A038	Jogging Frequency	20
A061	Frequency Maximum Limiter	125
A082	Motor Voltage Selection	200
B012	Electronic Thermal Level	1.6
B083	Carrier Frequency Setting	8.0

APPENDIX B LAYOUT DRAWING FOR BNHP-08B PUMP

NOTES:

1. TWO-PLANE BALANCE PER TABLE 1 (SEE BELOW. BALANCE IN ORIENTATION SHOWN. MAXIMUM DEPTH OF MATERIAL REMOVAL 0.050 IN NOTED AREAS.
2. WIRE CONNECTOR AND VFD PER SCHEMATIC TBD.
3. PRESSURE/LEAK TEST PER BNWI-1089.
4. ELECTRO ETCH PER TABLE 2 (SEE BELOW). ETCH DATA ON O.D OF ITEM #2.

REVISIONS				
ZONE	LTR	DESCRIPTION	DATE	APPROVED

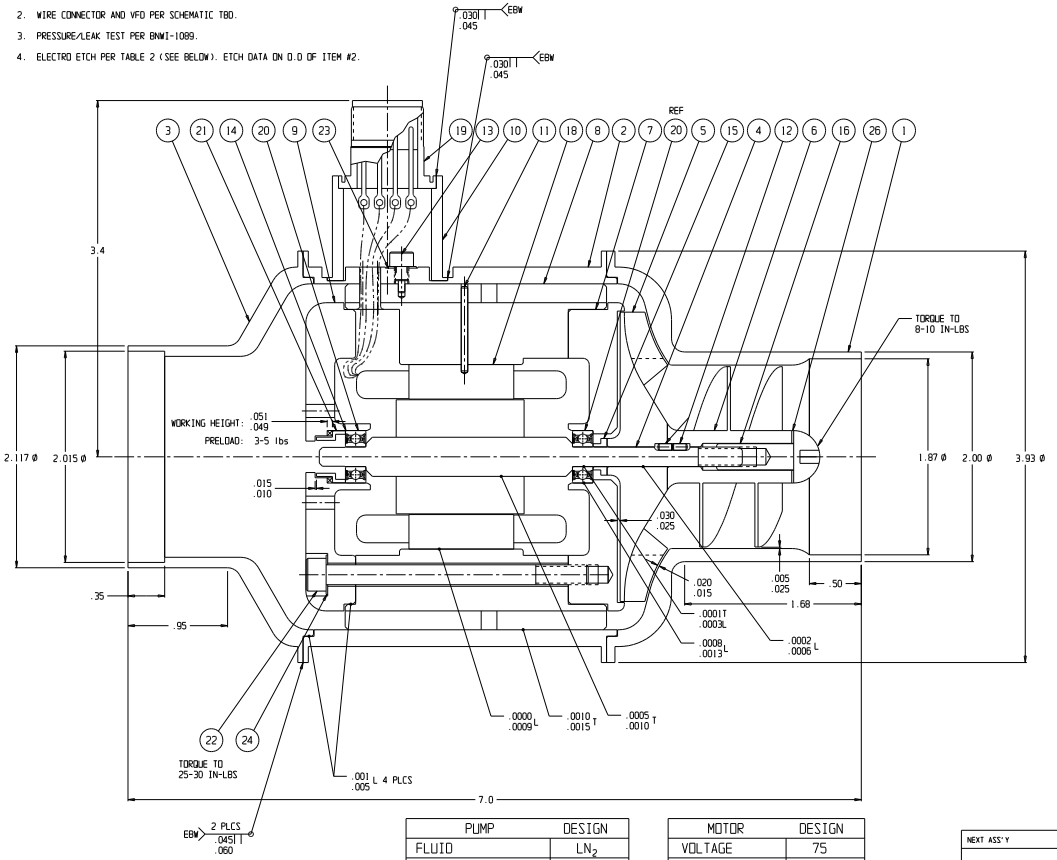

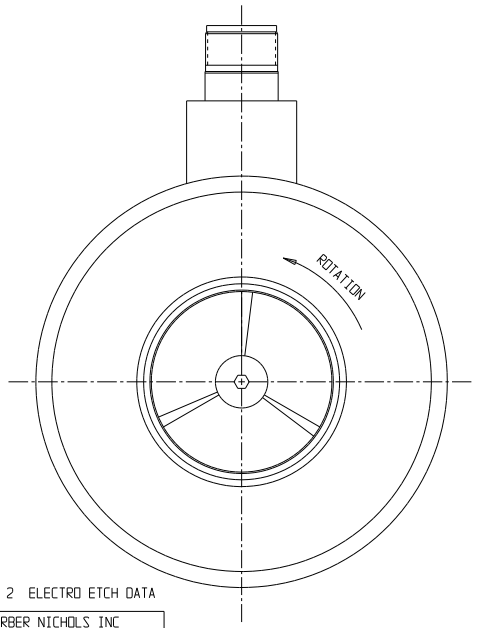

TABLE : 1 BALANCE REQUIREMENTS

	BP 1	BP 2
ROTOR WEIGHT @ BEARING (lbs)	.106	.385
TOLERANCE (gm-in)	.037	.140
SERVICE SPEED (RPM)	3100	
ISO 1940/1-1986(E) GRADE	G 2.5	

PUMP	DESIGN
FLUID	LN_2
FLOW RATE (GPM)	30
SPEED (RPM)	3100
INLET TEMP (°F)	-314
INLET PRES (PSIA)	23
INLET PRES (PSIG)	50
DELTA P (PSID)	5
HEAD RISE (FT)	14

MOTOR	DESIGN
VOLTAGE	75
HP	.12
Hz	108
AMPS	1.6
PHASE	3Ø

TABLE : 2 ELECTRO ETCH DATA

BARBER NICHOLS INC
LN2 PUMP
PART NO. BNHP-088-000
SERIAL NO. _____
FLOW RATE : 30 GPM
HEAD RISE : 14 FT
MAX DP PRESS : 50 PSIG

NEXT ASS'Y	ITEM NO.	QTY	PART NO.	DESCRIPTION	SPECIFICATION

UNLESS OTHERWISE SPECIFIED
INTERPRET PER ANSI Y14.5-1982
TOLERANCES ON DECIMALS: 1 PLACE 2 PLACE 3 PLACE
mm ± .76 ± .38 ± .13
INCH ± .030 ± .015 ± .005
ANGULAR DIMENSIONS ±2°
SURFACE ROUGHNESS 3.2um(125 µ")
REMOVE BURRS
ALL FILLET RADII XXXXX
BREAK EDGES XXX MAX.

THIRD ANGLE PROJECTION
MATERIAL: SEE BOM
HEAT TREATMENT: ----
PROCESS: ----

	APPROVED	DATE
DWN	T LIEURANCE	07-22-03
CHK		
QA		
PRJ		
MFG		
AERO		
MISC		

CADFILE: T:\BNHP-088 CURRENT UPDATE: BNHP-088-000 07-22-03

Barber Nichols

TITLE: LH2/LN2 PUMP

SIZE	CODE IDENT NO.	DRAWING NO.
D	57377	BNHP-088-000

SCALE 2:1 WT ACT CALC SHEET 1 OF 1

MSFC-11595

APPENDIX C: BARBER-NICHOLS WARRANTY

The following warranty is extended to purchaser on new products manufactured by Barber-Nichols Inc. (Barber-Nichols):

Barber-Nichols warrants all components, except for bearings, and materials of its manufacture against defects in workmanship and materials for 12 months from date of delivery to purchaser, FOB Arvada, Colorado. Barber-Nichols will repair or replace, FOB Arvada, Colorado, such components or materials as Barber-Nichols finds defective.

This warranty is limited to the repair or replacement of defective components or materials, subject to the conditions stated herein. This warranty does not cover the cost of labor to remove or reinstall Barber-Nichols' product from or into any other product into which it has been incorporated or made a part of.

Barber-Nichols shall not be responsible for any consequential or incidental damages incurred as a result of any defect in components or materials or loss arising from any cause by reason of the operation or failure of the operation of Barber-Nichols' product.

No claim shall be made pursuant to this warranty until the full price of the shipment of which any unit or units with defective components or materials is a part has been paid.

THIS WARRANTY IS THE ONLY WARRANTY APPLICABLE TO BARBER-NICHOLS' PRODUCT AND EXCLUDES ALL OTHER WARRANTIES, EXPRESSED OR IMPLIED, INCLUDING WARRANTIES OF MERCHANTABILITY, FITNESS FOR A PARTICULAR PURPOSE AND AGAINST INFRINGEMENT.

THIS WARRANTY IS VOID IF:

BARBER-NICHOLS'PRODUCT HAS BEEN DAMAGED BY FREEZING, FIRE OR ANY OTHER CONDITIONS NOT ENCOUNTERED IN ORDINARY USE.

BARBER-NICHOLS' PRODUCT IS NOT INSTALLED, OPERATED, MAINTAINED OR SERVICED IN ACCORDANCE WITH BARBER-NICHOLS' SPECIFICATION.

BARBER-NICHOLS' PRODUCT IS DAMAGED DUE TO DIRT, AIR, MOISTURE OR OTHER FOREIGN MATTER ENETERING THE PRODUCT.

BARBER-NICHOLS' PRODUCT IS DAMAGED DUE TO IMPROPER HANDLING, IMPROPER STORAGE OR FAIURE BY PURCHASER OR ITS CUSTOMER TO USE REASONABLE CARE TO PROTECT THE PRODUCT DURING THE WARRANTY PERIOD.

APPENDIX C—MULTIPURPOSE HYDROGEN TEST BED INSTRUMENTATION

Appendix C contains the instrumentation database document from appendix B of NASA/TM—2003–212926[2] that describes the MHTB instrumentation used in the spray bar performance testing.

Multipurpose Hydrogen Test Bed (MHTB)
Instrumentation Data Base

James Martin/EP25

This document details the instrumentation use on the Multipurpose Hydrogen Test Bed hardware. This includes instrumentation used on the tank interior/exterior, tank insulation/penetrations, tank support system and environmental shroud. This document is dedicated primarily to instrumentation which was installed during fabrication and assembly of test hardware, however, some facility instrumentation is noted if it is mounted in close proximity to the test hardware.

The breakdown of test article instrumentation is outlined by the following categories:

1) MHTB Program Over View and Hardware Description
2) MHTB Tank General Instrumentation Layout
3) MHTB Thermal Control System Instrumentation
4) MHTB Support Leg Penetration Instrumentation
5) MHTB Vent Penetration Instrumentation
6) MHTB Fill / Drain Penetration Instrumentation
7) MHTB Pressurization Penetration Instrumentation
8) MHTB MLI Interstitial Pressure Probe Instrumentation
9) MHTB Manhole Cover and Pump Out Penetration Instrumentation
10) MHTB Internal Rake and Fluid Instrumentation
11) MHTB Environmental Shroud Instrumentation
12) MHTB Zero-g Thermodynamic Vent System Instrumentation

Related Documents

1) MHTB Test Requirements Document (EP25 (93-25))
2) MHTB Thermal Control Subsystem (TCS) Test Plan (EP25 (94-04))
3) MHTB Pre-Installation Operations Document (EP25(94-13))
4) MHTB Thermodynamic Vent System (TVS) Test Plan (EP25(94-12))
5) MHTB Thermodynamic Vent System Installation Procedure

1) MHTB Program Over View and Hardware Description

The MSFC has established a technology/advanced development program to address the area of Cryogenic Fluid Management (CFM) for orbital applications, an area common to practically all future space programs. As part of this activity a test bed, termed the multipurpose hydrogen test bed (MHTB), was devised such that a variety of CFM subsystems could be integrated and evaluated in a ground based test environment. To minimize the reliance on scaling analyses in extrapolating overall performance data, the test bed is representative in both size and shape to that of a full scale space transfer vehicle liquid hydrogen tank. Current plans baseline testing of two key technology needs in representative spacecraft thermal and vacuum environments. The first involves evaluation of a foam multilayer insulation (FMLI) thermal control concept. This concept incorporates a spray on foam insulation (SOFI) attached to the surface of the test bed tank and is in turn covered with a 45 layer variable density multilayer insulation (MLI) blanket. This blanket is constructed of double aluminized mylar (DAM) sheets separated by Dacron netting. The second, an active tank pressure control system, is referred to as a zero-g thermodynamic vent system (TVS). This hardware will be installed after completion of the TCS test phase and consists of a tank internal spray bar/heat exchanger and tank external recirculation pump, Joule Thompson valve and back pressure orifice. More information regarding exact details of each test program can be found in the respective subsystem test plans.

The MHTB tank is constructed of aluminum 5083 and has a cylindrical shape with both a height and diameter of 3.05 m (10 ft) and elliptical domes as shown in figure 84. The tank has an internal volume of 18.09 m^3 (639 ft^3) with a surface area to volume ratio of 1.92 l/m (0.58 l/ft). The tank was designed and constructed per the ASME code (section VIII, Division 1) for a working differential pressure of 344 kPa (50 psig). The tank's total weight is 1270 kg (2800 lbm). The tank is equipped with a variety of penetrations, supporting hardware, and technology subsystems illustrated in figure 84.

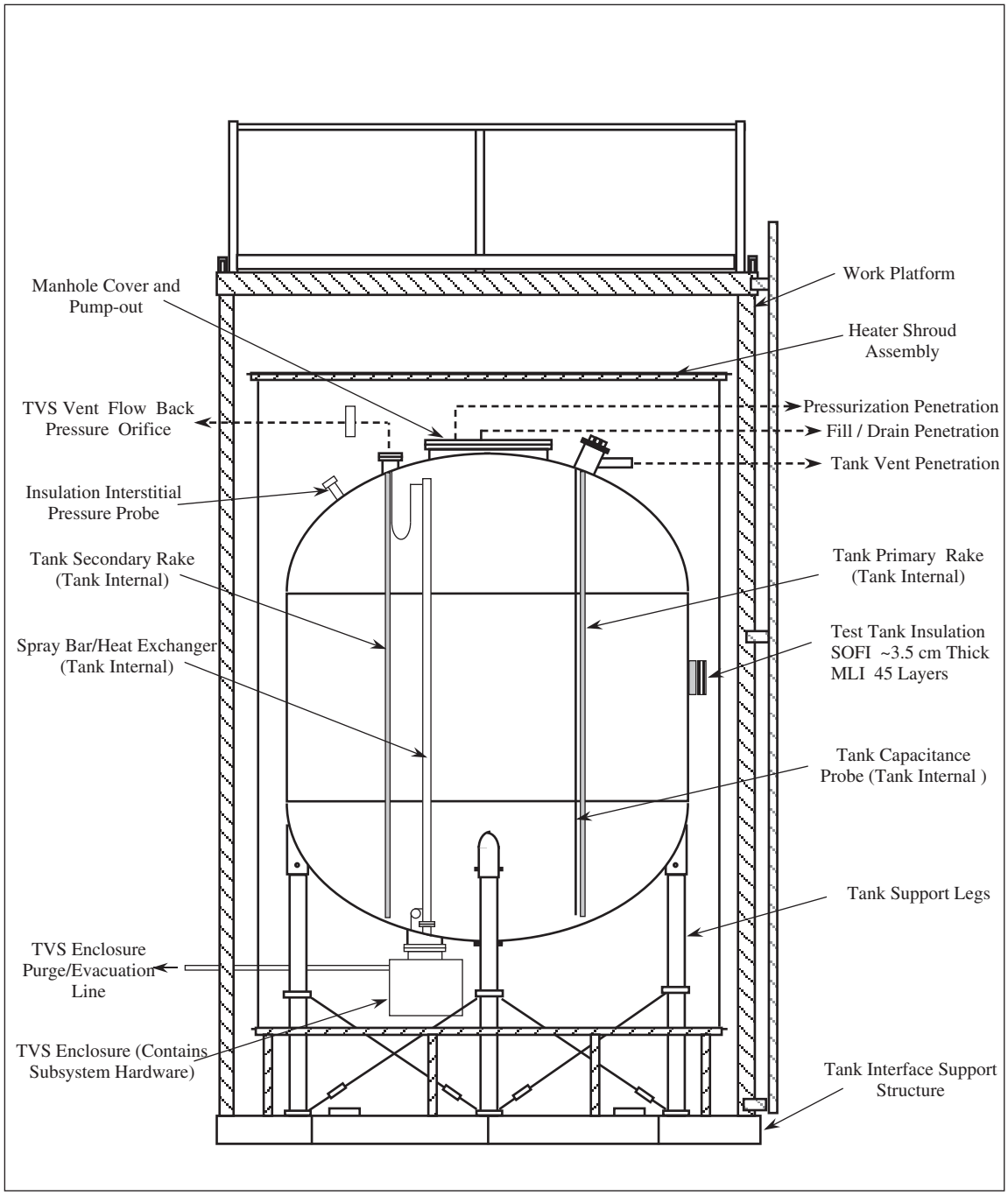

Figure 84. General MHTB tank schematic.

2) General MHTB Tank Instrumentation Layout

The general layout of instrumentation on the test bed is illustrated in figures 85–87. These figures represent the top, front and bottom views of the test tank without insulation to avoid confusion. However, the seams between major MLI blanket assemblies are indicated by dotted lines. A detailed description of instrumentation numbers and profiles shown on these figures is discussed in later document sections and Appendix A. Most of the instrumentation is composed of silicon diodes and thermocouples for measurement of thermal gradients (several pressure transducers are present). Typically, silicon diodes (Lakeshore type DT-470-11A) temperature transducers are placed in areas of lowest temperatures because they possess a higher accuracy at these temperatures when compared to thermocouples. Typical low temperature areas include the tank aluminum shell and SOFI material covering the tank. Thermocouples (Type E) are used in regions of higher temperature, such as within the MLI or on surfaces somewhat distant from the test tank contact point, where their accuracy becomes somewhat improved. The bulk of the instrumentation leads for components residing on the upper bulkhead and barrel section were routed toward the tank vent flange, while those on the lower bulkhead were routed out leg #1. There were some exceptions to this rule. Some of the penetration instrumentation was easier to route out along the respective penetration rather than snaking it to the vent or leg #1 area.

The tank orientation with respect to the vacuum chamber is such that the 0^{o} reference is directed from the test tank center through the secondary instrumentation rake penetration toward the chamber door. Positive angle measurement from this reference is taken in a clockwise location from a vacuum chamber perspective looking down on top of the test article. The complete MHTB instrumentation data base is included in Appendix A of this document.

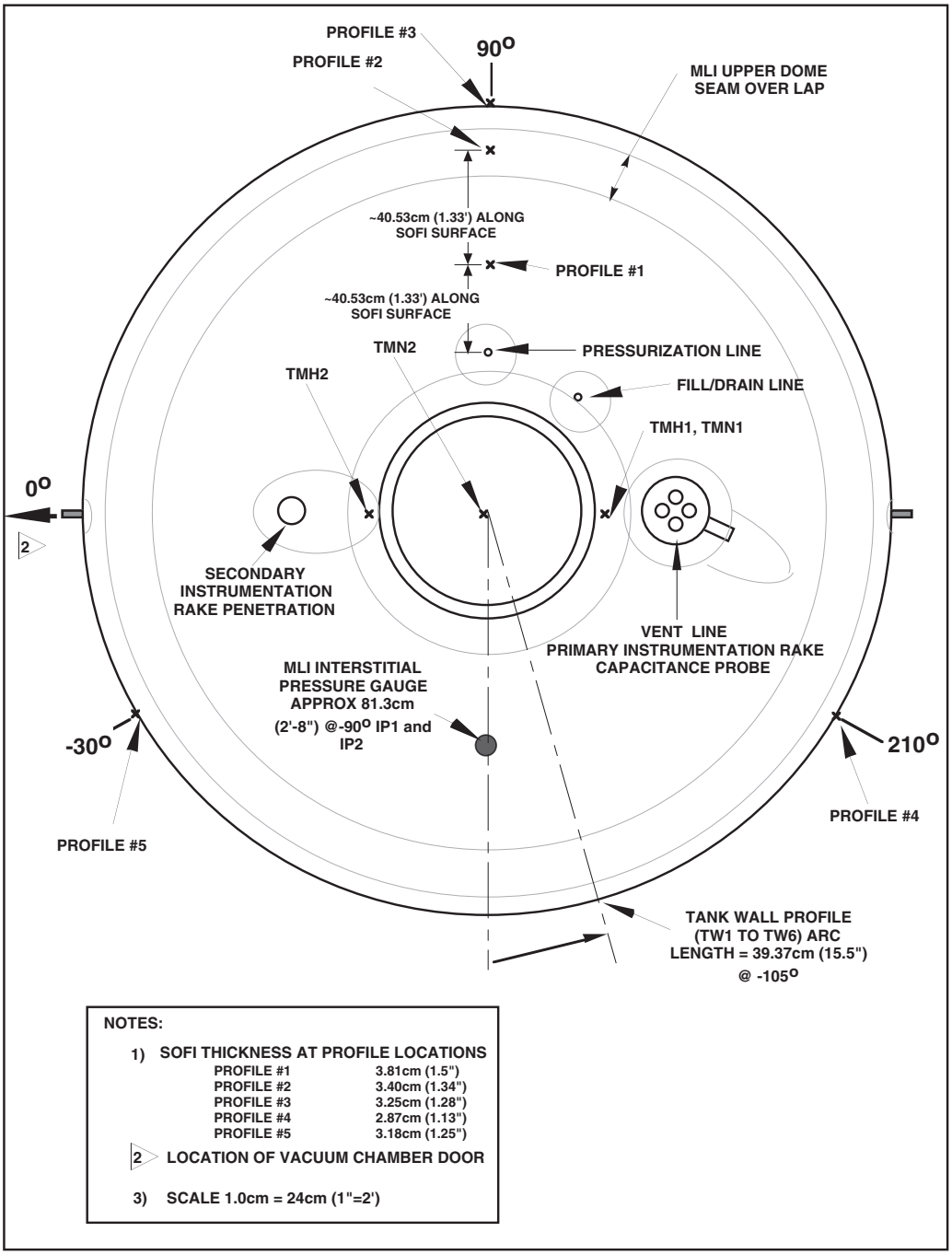

Figure 85. MHTB tank instrumentation top view.

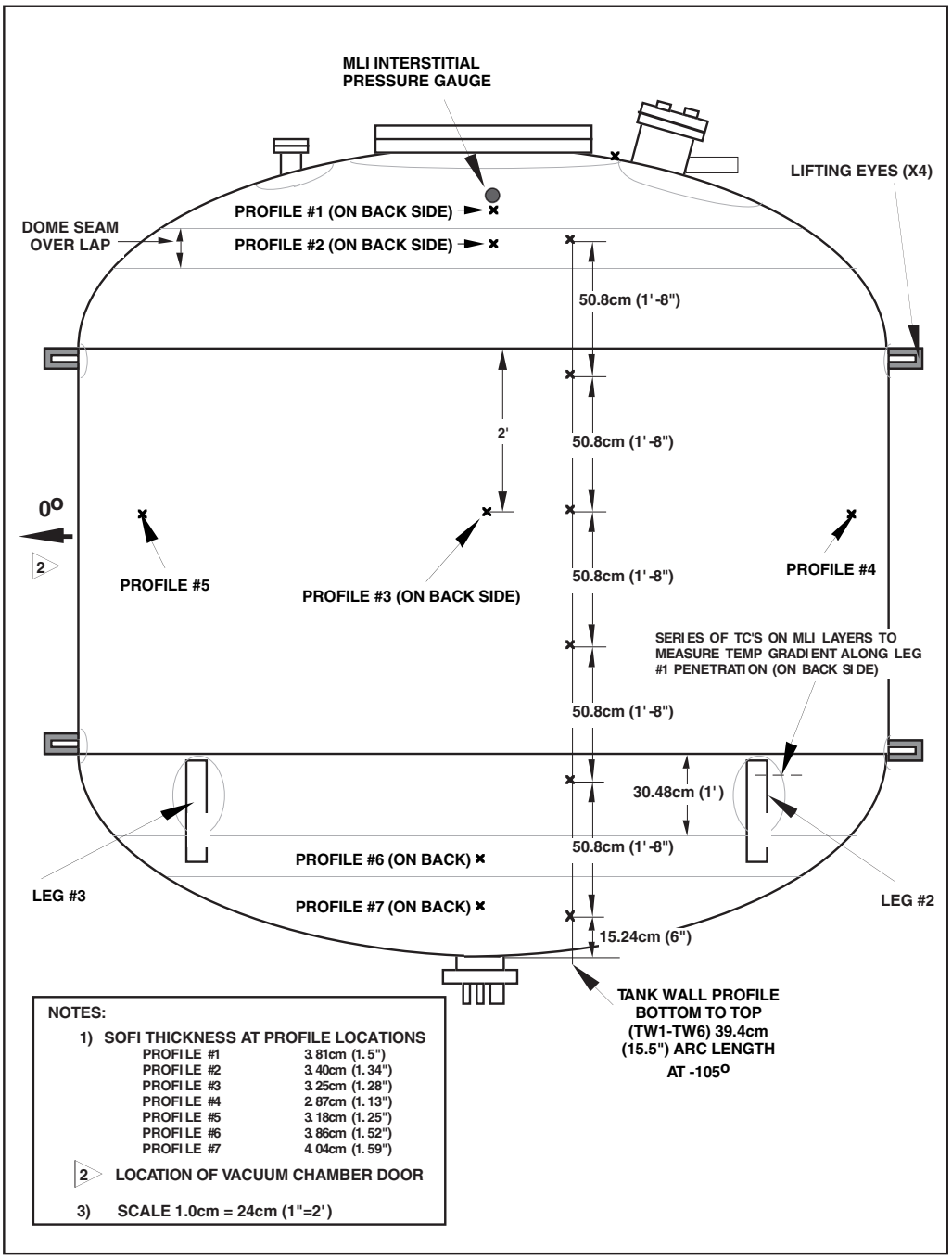

Figure 86. MHTB tank instrumentation side view.

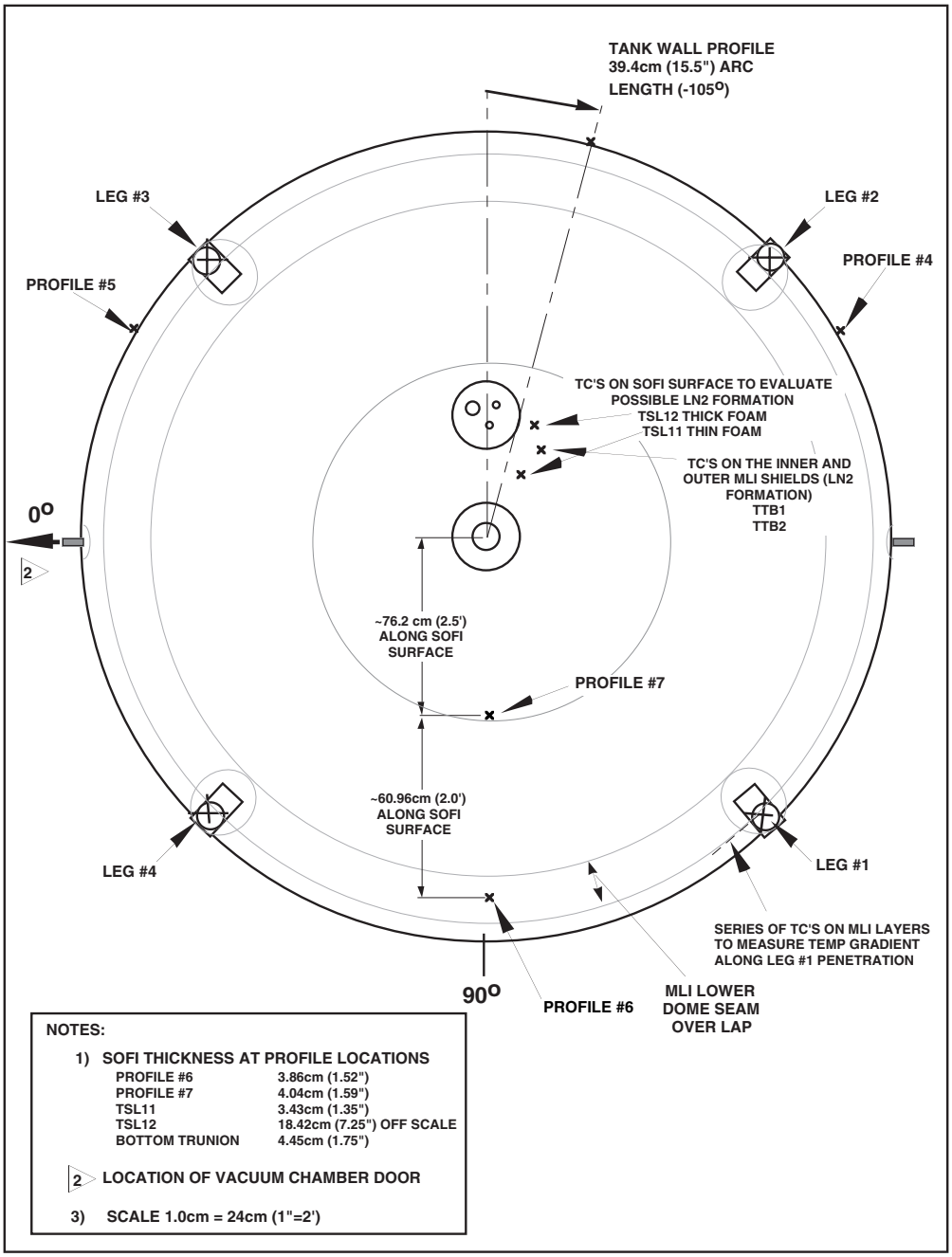

Figure 87. MHTB tank instrumentation bottom view.

3) MHTB Thermal Control System Instrumentation

A total of seven instrumentation profiles are incorporated into the test tank FMLI insulation with each profile composed of one silicon diode and four thermocouples. Figure 88 illustrates the typical location of each piece of instrumentation within the insulation layers. The diode (TSF#) was attached to the foam surface using a cryogenic epoxy (Lakeshore Stycast) while the thermocouples (TM#, TMI#, TMM# and TMO#) were attached to the MLI shields by using a piece of aluminized tape. In an effort to limit heat leak along the thermocouple leads toward the bead attachment point, approximately 5.08cm (2") of lead wire was spiraled around the bead (and placed under the tape). Additionally, each thermocouple lead was routed out (toward the exit point) along the same MLI shield to which it was attached. The thermocouples TM# were attached to the outer surface of the inner most MLI shield. The thermocouples TMI# were attached to the outer surface of the 10 MLI shield (interface between low and medium density MLI spacing). The thermocouples TMM# were attached to the outer surface of the 25 MLI shield (interface between medium and high density MLI spacing). The thermocouples TMO# were attached to the outer surface of the outer most MLI shield (shield 45 of the high density MLI spacing). The aluminized tape used to attach the thermocouples was manufactured by Lamart Corporation and was type #326L. This tape is electrically conductive on the exterior surface and has the same approximate surface emissivity as the DAM. The tape was purchased from:

Can-Do Incorporated
P.O. Box 4366
Nashville, Tn 37204
Tele. (615) 383-1775

At each instrumentation profile the SOFI thickness was measured using a Kaman eddy current device. Figures 85–87 indicate the SOFI thickness measured at each profile location. These thicknesses will be used in determining the thermal performance of the foam insulation. Data concerning each piece of instrumentation attached to the tank insulation is included in Appendix A.

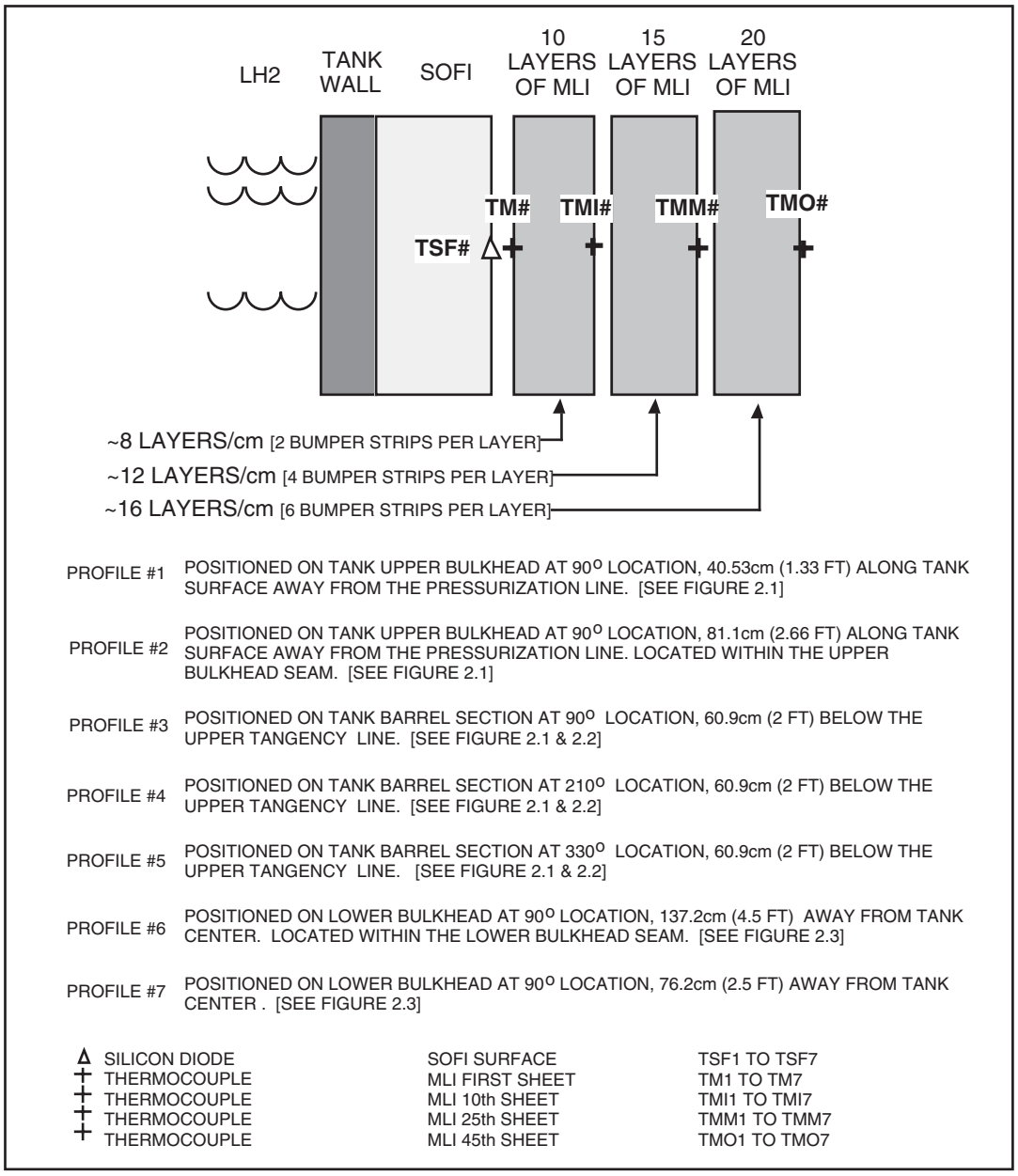

Figure 88. Typical insulation instrumentation profile.

4) MHTB Support Leg Penetration Instrumentation

The MHTB is supported by four legs as shown in figures 86 and 87. Each leg is comprised of two composite sections joined in the center by a stainless steel union. Each leg end is also equipped with stainless steel end caps which mount to the test tank and interface support structure. Two of the four tank legs are instrumented one of which, leg #1, is heavily instrumented as shown in figure 89. Silicon diodes (TSL1 and TSL2) and thermocouples (TSL5 through TSL10) are attached to the composite material (diodes closest to the tank) for determination of heat input along the support. Diodes TSL3 and TSL4 have been placed on leg #3. Each leg is equipped with a heat guard to reduce the amount of heat input. Legs #1 and #3 are instrumented with diodes (HG1 and HG3, respectively) to measure the heat guard boundary temperature. The SOFI surface (TSL17, TSL18 and TSL19) and MLI (TL13 through TL19) are also instrumented for determination of the insulation temperature profile. There are also thermocouples (TSL14 on leg #1 and TSL15 on leg #3) attached to the innermost layer of crumpled MLI (against foam) which occupies the hollow interior of the legs. These measurements will be used to determine if condensation of the insulation gaseous nitrogen (GN_2) purge gas occurs within the legs. A foam plug approximately 10.16cm (4") thick was poured into the top section of each leg's interior (above the MLI) to prevent potential condensation. The outer surface of each leg was also closed out with pour foam starting at the tank SOFI and extending out over the composite to a distance of approximately 15.24 cm (6"). Average foam thickness was based on the applied foam circumference measurements and determined to be 3.81 cm (1.5") for legs 1, 3 and 4 and 4.445 cm (1.75") for leg #2. The leg stainless steel center joint and interface support structure attachment point were instrumented with thermocouples for legs #1 (TLB1 and ISS1) and #3 (TLB3 and ISS3). Appendix A contains, in a data base format, additional information concerning the tank leg instrumentation.

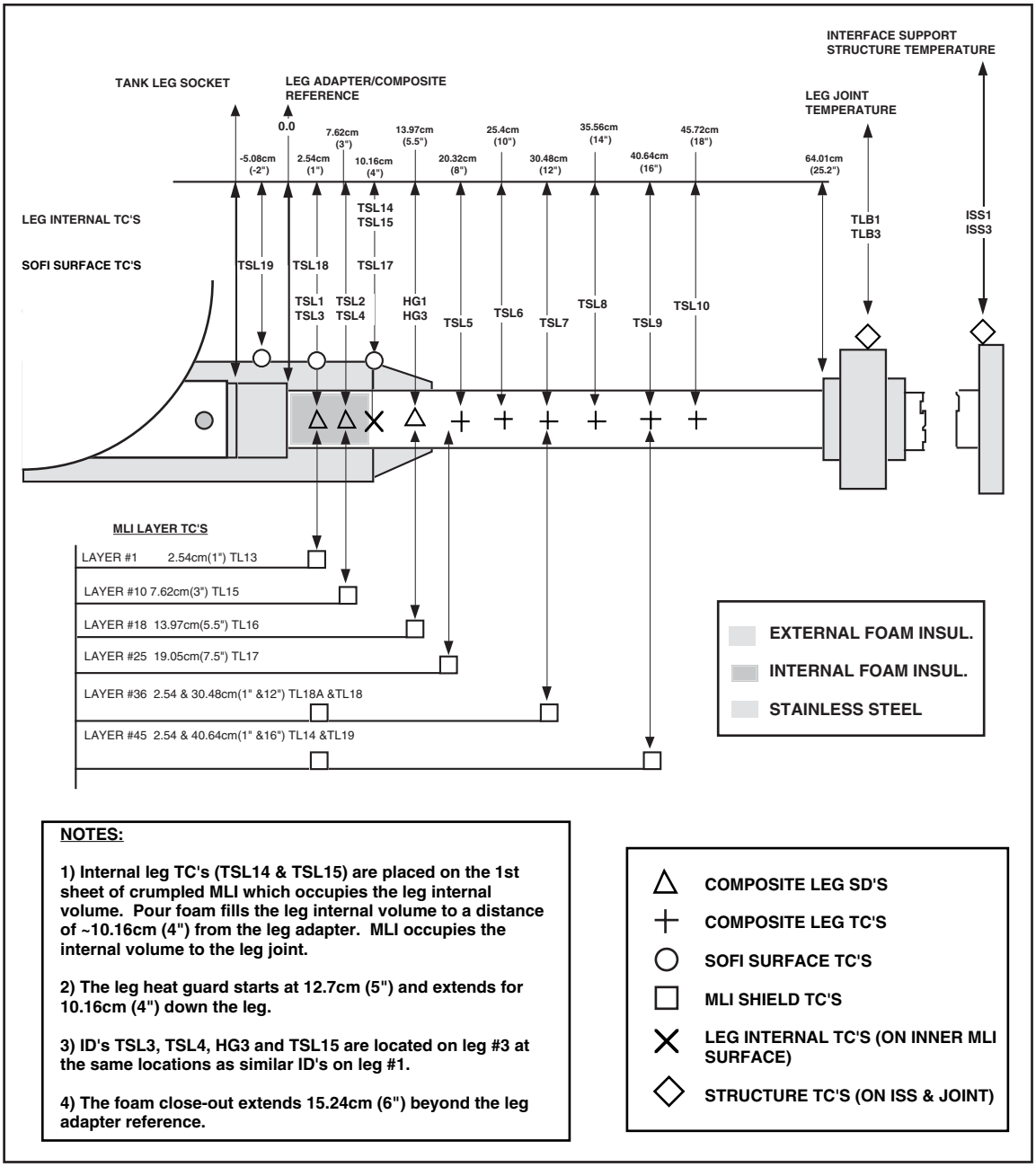

Figure 89. Leg No. 1 instrumentation locations.

5) MHTB Vent Penetration Instrumentation

The MHTB tank internal volume is vented through a 5.08 cm (2") diameter tube connected to a 20.32 cm (8") tank penetration (Conflat type flange) as illustrated in figure 90. The vent tube transitions to a vacuum jacketed pipe assembly approximately 30.48 cm (12") from the tank penetration. The penetration and tube are closed out with foam extending out over the vacuum jacketed pipe section approximately 40.64 cm (16") from the tank penetration. Average thickness of this foam based on the measured circumference is 6.98 cm (2.75"). Three silicon diodes are place along the length of the tube for determination of heat input (TVL1 and TVL2) and evaluation of the heat guard (HG7) operation. The vent tube foam surface is instrumented with two thermocouples (TVL6 and TVL7) to assist in evaluation of heat input through the foam. The vent penetration top flange contains a tank ullage pressure measurement port and 1.27 cm (0.5") diameter sampling tube which is equipped with two thermocouples (TUP1 and TUP2). The surface temperature of the top flange is measured by a silicon diode (TVL3). Internal to the tank, the vent flange supports a capacitance probe (CAP1) and an instrumentation rake. Two diodes (TVL4 and TVL5) are supported by the rake at the 99.4% tank fill location. These diodes are positioned just below the vent penetration (inside the test tank) and provide a measurement of the out flowing gas temperature. Details regarding the instrumentation rakes will be described in a later section. Appendix A contains, in a data base format, additional information regarding this instrumentation.

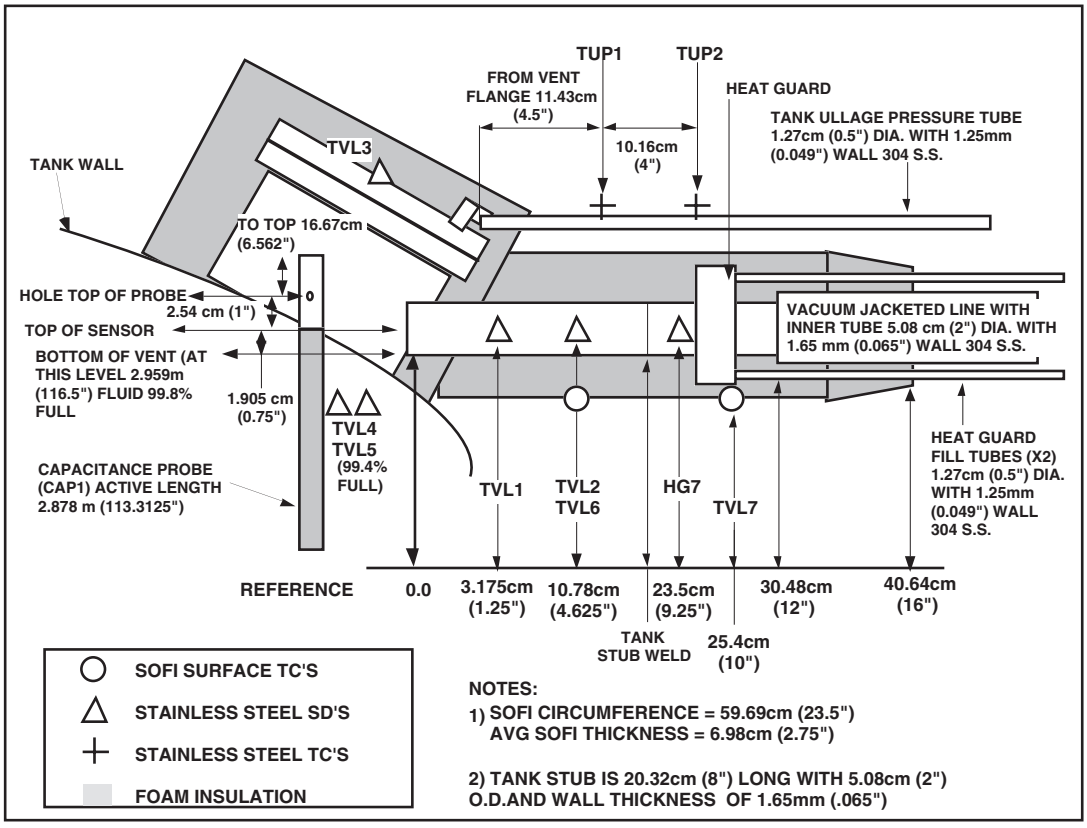

Figure 90. MHTB tank vent penetration instrumentation.

6) MHTB Fill/Drain Penetration Instrumentation

The MHTB LH_2 fluid service is provided through a 2.54 cm (1") diameter fill/drain tube attached to the test tank with an aluminum to stainless steel transition joint as illustrated in figure 91. The fill/drain tube transitions to a vacuum jacketed pipe assembly 16.51cm (6.5") from the tank penetration. A foam close-out is applied to the line and extends out over the vacuum jacketed pipe section approximately 35.56 cm (14") from the tank penetration. The average foam thickness around the fill/drain line is 6.604cm (2.6") based on the measured circumference. The tube is instrument with three silicon diodes placed along its length to determine heat input (TFD1 and TFD2) and operation of the heat guard (HG6). The outer surface of the foam is also instrumented with two thermocouples (TFD3 and TFD4) to assist in evaluation of heat input through the foam. Appendix A contains, in a data base format, additional information regarding this instrumentation.

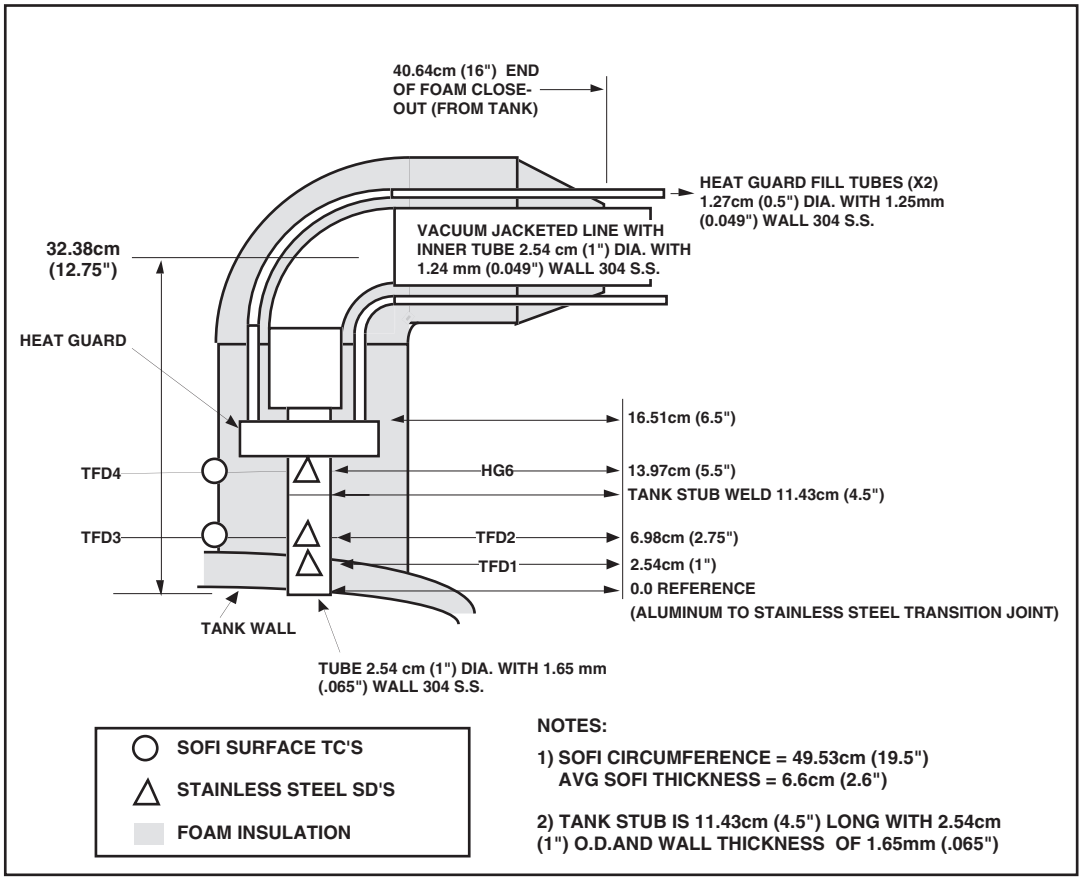

Figure 91. MHTB tank fill/drain penetration instrumentation.

7) MHTB Pressurization Penetration Instrumentation

The MHTB tank internal volume is pressurized using a 2.54 cm (1") diameter tube attached to the tank with an aluminum to stainless steel transition joint as illustrated in figure 92. The pressurization tube transitions to a double walled jacketed pipe assembly (used for gas conditioning purposes) 32.385 cm (12.75") from the tank wall. A foam close-out extends out over the jacketed pipe section approximately 40.64 cm (16") from the tank penetration. The average foam thickness around the pressurization line is 3.556 cm (1.4") based on the measured circumference. Three silicon diodes are place along the length of the tube, between the tank and heat guard, for determination of heat input (TPL1 and TPL2) and evaluation of the heat guard (HG5) operation. The line is also equipped with two thermocouples, (TPS1) used to measure the temperature of the pressurant gas flow within the line, and (TPS2) used to measures the pressurization line outer jacket temperature. The outer surface of the foam close-out is also instrumented with two thermocouples (TPL3 and TPL4) to assist in evaluation of heat input through the foam. Appendix A contains, in a data base format, additional information regarding this instrumentation.

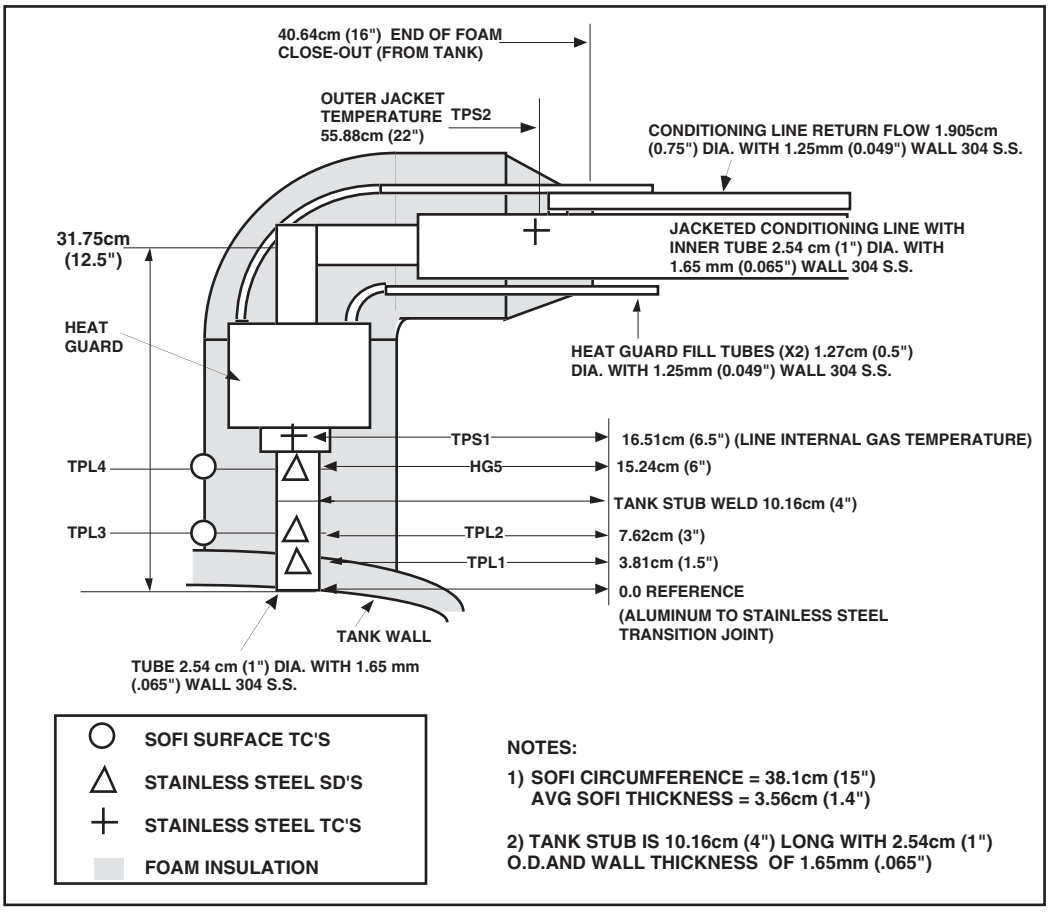

Figure 92. MHTB tank pressurization penetration instrumentation.

8) MHTB MLI Interstitial Pressure Probe Instrumentation

The gas pressure at the foam/MLI interface is measured with two pressure sensors mounted on top of a 5.08 cm (2") diameter thin wall probe that has a length of 22.86 cm (9") as illustrated in figure 93. This probe rests on the tank SOFI surface and is supported by the MLI which is taped out layer by layer to the surrounding MLI and to the probe body so as to prevent leakage of trapped MLI gases. The probe is also equipped with a 6.35mm (0.25") diameter sampling port for obtaining both dew point levels (using a hydrometer) and gas species samples (using a residual gas analyzer) from within the MLI. The two pressure transducers, a Gran Philips 275 (IP1) and a cold cathode (IP2), cover a complete pressure range from 760 to 10^{-7} torr. The Gran Philips gauge is remote mounted (for easier access) on top of the heater shroud and connected to the probe body using a flex hose. The probe body tube is equipped with three thermocouples placed along its length (IPP1, IPP2 and IPP3) to determine heat input through the probe. This probe, if necessary, shall be supported off of the tank heater shroud structure using stainless steel wire and springs to absorb transportation loads. The dew point measurement within the MLI is taken with a facility supplied Endress Hauser Model #2200 Hydrometer (DEW1). The sensing head for this unit is located in the MLI gas sample tube. Appendix A contains, in a data base format, additional information regarding this instrumentation.

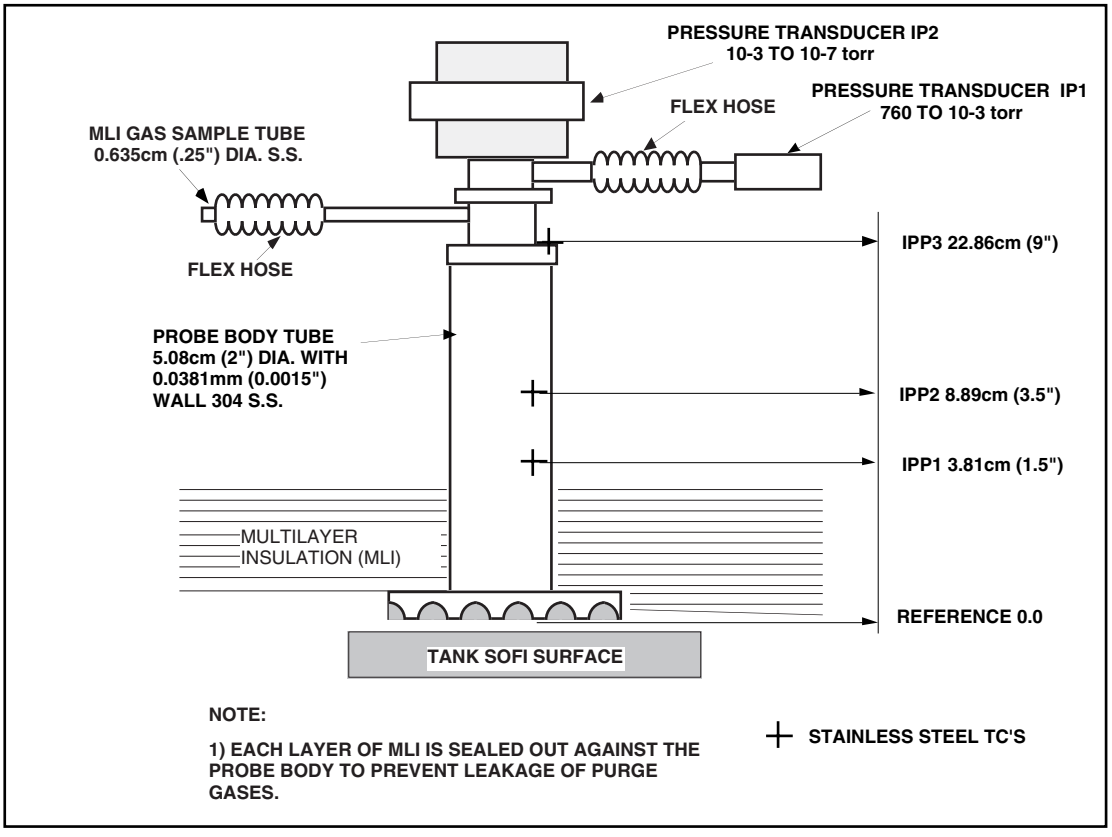

Figure 93. MHTB MLI probe instrumentation.

9) MHTB Manhole Cover & Pump Out Penetration Instrumentation

The MHTB tank is equipped with two manhole covers (inner and outer) to control potential leakage resulting in the degradation of insulation performance. Figure 94 illustrates the manhole cover set-up. The inner cover is equipped with two silicon diodes (TMN3 and TMN4) adhesively bonded to its inner surface with cryogenic epoxy (Lakeshore Stycast). The outer manhole cover exterior surface is equipped with a silicon diode (TMN2) bonded to its center with a single diode (TMN1) and two thermocouples (TMH1 and TMH2) bonded to its flange area. These temperature measurements will be used to assess the total thermal capacitance carried by the massive tank manhole system. The gas volume trapped between the inner and outer manhole covers is connected to a stainless steel evacuation line (flex hose) which is used to intercept potential leakage from the inner cover if it should occur. This flex line is equipped with two thermocouples (TCP1 and TCP2) attached to determine heat input. The spatial distance between the thermocouples is 5.08 cm (2"), however, the flex hose has a 3 to 1 contraction ratio yielding a material length of 15.24 cm (6"). The entire surface of the outer manhole cover is covered with foam insulation at an approximate thickness of 3.175cm (1.25"). The evacuation line is routed along the vent line and as such, is buried beneath the vent line foam insulation. Appendix A contains, in a data base format, additional information regarding this instrumentation.

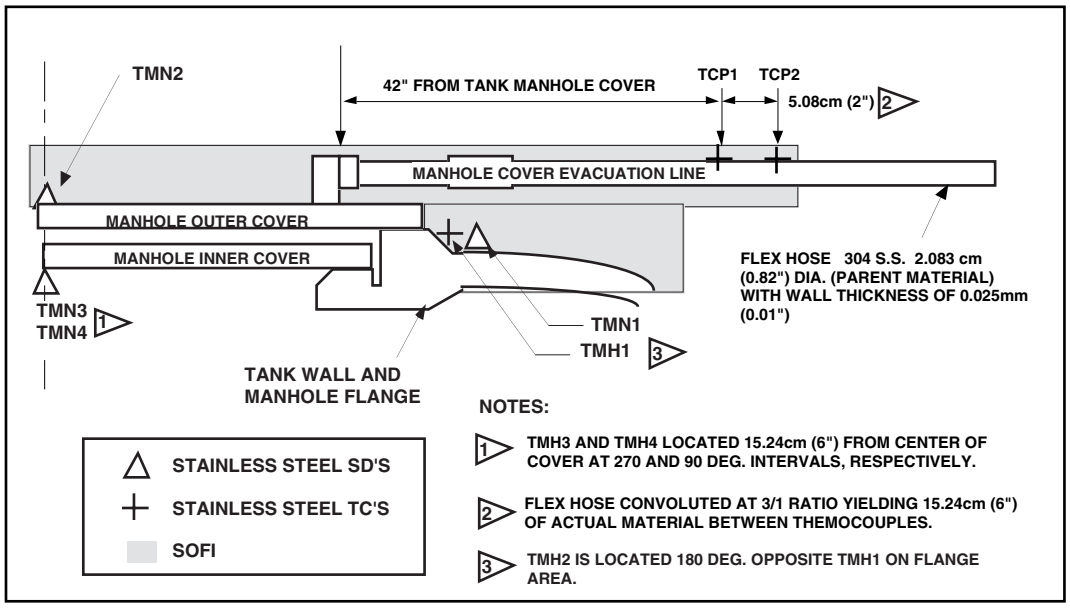

Figure 94. MHTB manhole cover and pump-out port instrumentation.

10) MHTB Internal Rake and Fluid Instrumentation

The MHTB tank is equipped internally with two instrumentation rakes and a capacitance probe which are supported from the top of the tank and extend downward. The rakes are constructed from a Fiberglass Epoxy channel section and are equipped with silicon diodes attached at given intervals using nylon rod offsets and cryogenic epoxy as illustrated in figure 95. The purpose of the rakes is to provide measurement of the temperature gradient within both the tank ullage and liquid masses in addition to providing a rough check of the liquid level to verify the capacitance probe operation. The primary rake (TD1 through TD12) positioned at 180 degrees is connected to the vent flange, while the secondary rake (TD13 through TD24) is positioned at 0 degrees as illustrated in figure 85 and 96. The capacitance probe (CAP1) provides continuous liquid level measurement and is mounted to the vent flange at the 180 degree position beside the primary rake. All tank internal instrumentation is passed through the 20.32cm (8") vent flange using four 37 pin Deutsch connectors. The exception is the capacitance probe which is equipped with its own co-axial feed through mounted in a 1.27cm (0.5") conflat type connector and attached to the center of the 20.32cm (8") vent flange. Appendix A contains, in a data base format, additional information regarding this instrumentation. Appendix B contains an MHTB tanking table with information regarding fill height, percent liquid/ullage volume and LH_2 mass.

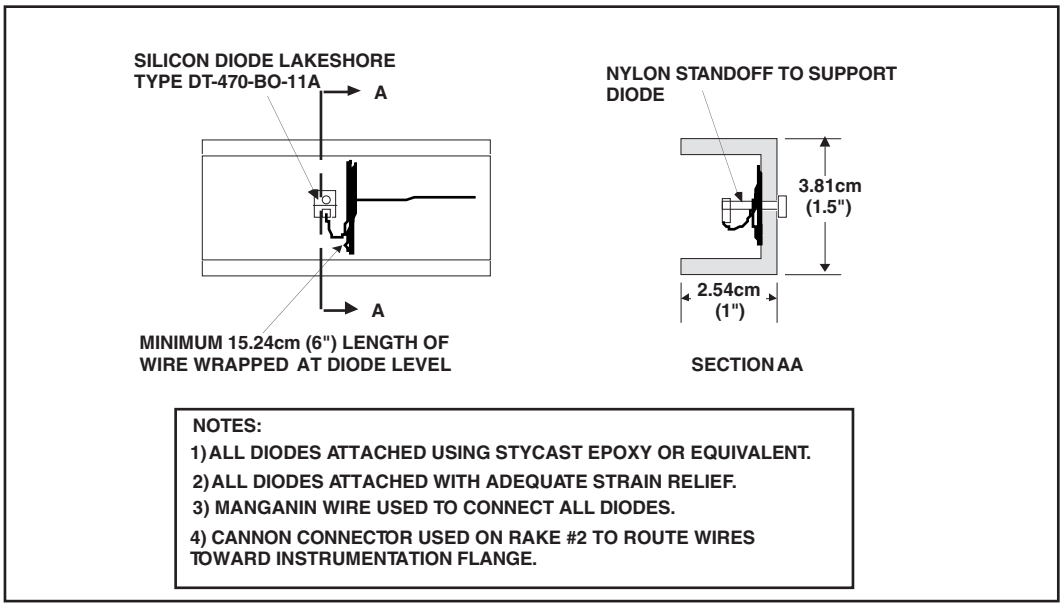

Figure 95. MHTB instrumentation rake silicon diode attachment.

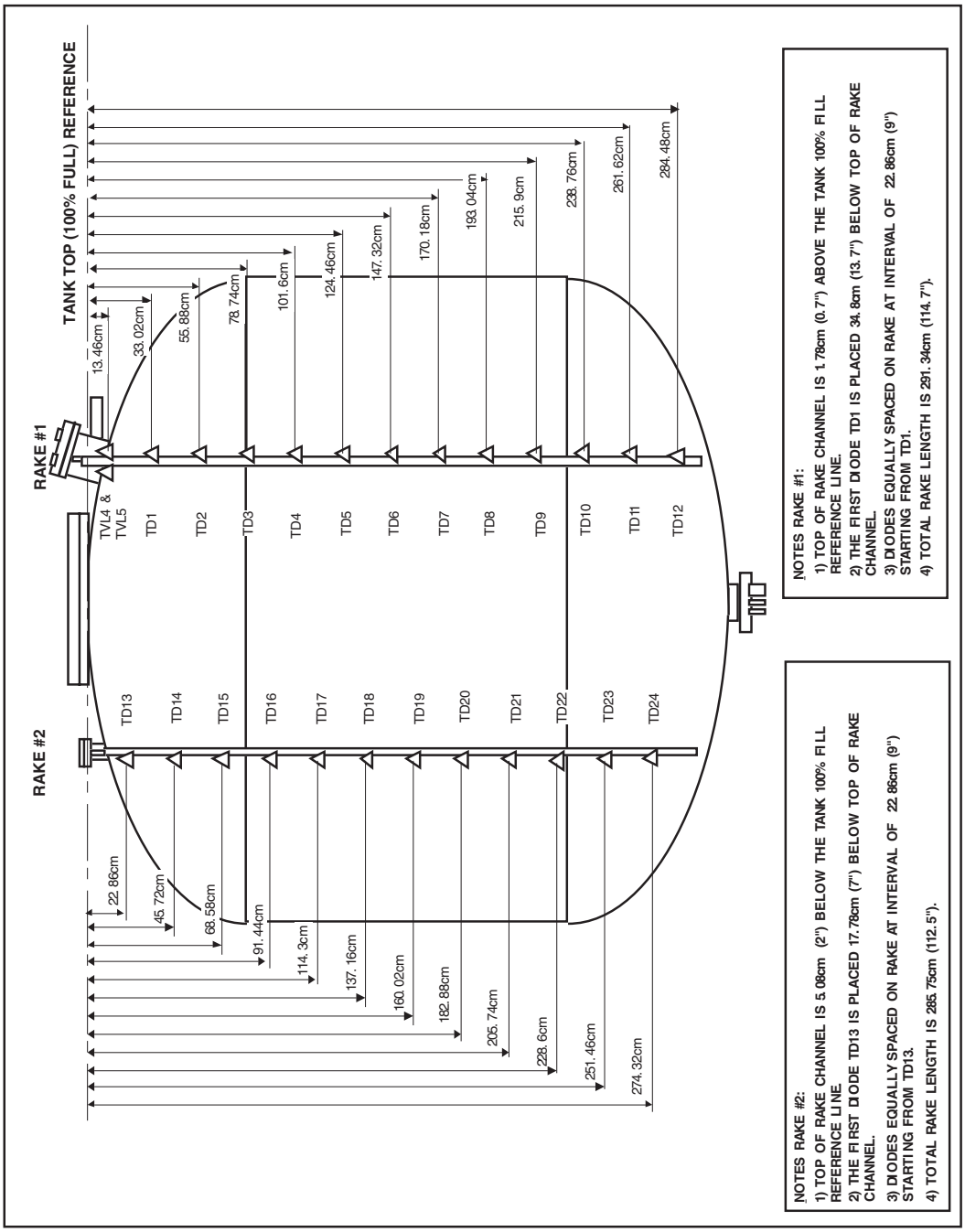

Figure 96. MHTB tank rake instrumentation layout.

11) MHTB Environmental Shroud Instrumentation

The MHTB tank and insulation systems are contained within a shroud structure that completely surrounds them and provides a warm boundary condition for which performance can be measured during testing. This structure is made completely of aluminum and is supported by the interface support structure as shown in figure 84. The shroud is composed of 17 individual panels each equipped with thermocouples attached to the inner surface of the shroud and placed beneath the electrical heating strip. These thermocouples are used with a closed loop control system to regulate each shroud panel's temperature. A minimum of two thermocouples are applied to each panel providing a primary and a backup in case of failure. Two panels #5 and #11 are equipped with additional thermocouples to provide data concerning shroud temperature gradients. Panel #11 has six thermocouples while panel #5 is heavily instrumented with 13 thermocouples since it was used during evaluation of the techniques used to assemble the shroud panels (documented in EP25(94-03)). The top shroud panels #1 through #4 are illustrated in figure 97. The typical side wall panel (5 through 12) instrumentation layout is provided in figure 98. The lower shroud panel layout (13 through 17) is illustrated in figure 99.

A series of 5 thermocouples are also placed within the annular region created between the vertical shroud panel #6 and the test tank insulation, at the 90 degree location. These thermocouples (HS18 through HS22) are spaced vertically along the panel at an interval of 60.96cm (24") with the thermocouple bead positioned approximately half way into the annular region. This instrumentation is used for measuring purge gas temperatures within the annulus. Vacuum chamber free air space temperatures are measured with facility provided thermocouples (CFA1, CFA2 and CFA3) mounted vertically at the 90 location and external to the test article shroud. These thermocouples are placed at 1.525m (5') intervals above the chamber floor. Purge gas dew point within the environmental shroud is measured with a facility supplied Endress Hauser Model #2200 Hydrometer (DEW2). The sensing head for this unit is located internal to the shroud and mounted on the lower shroud panel. Appendix A contains, in a data base format, additional information regarding this instrumentation.

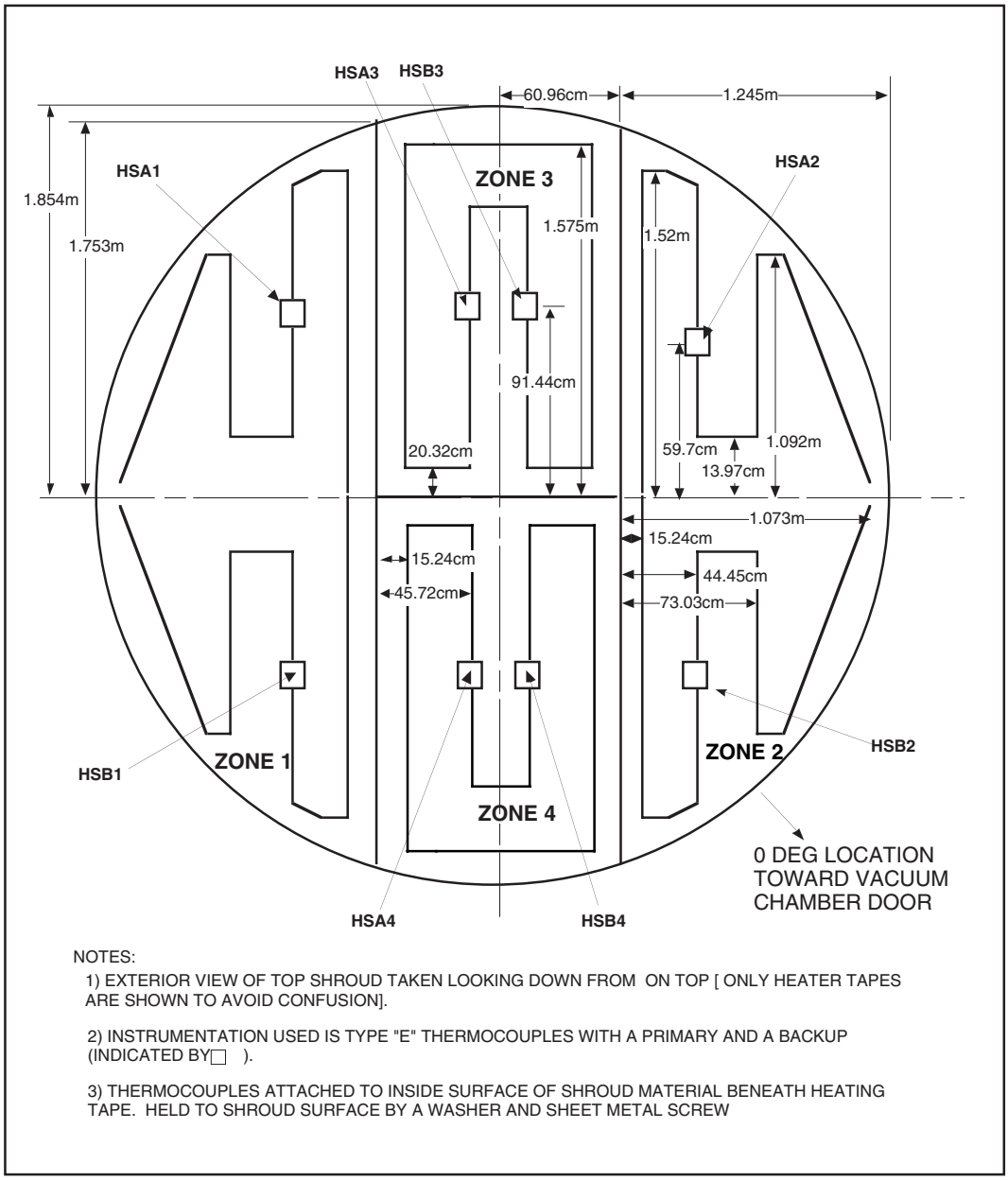

Figure 97. MHTB typical top environmental shroud panels.

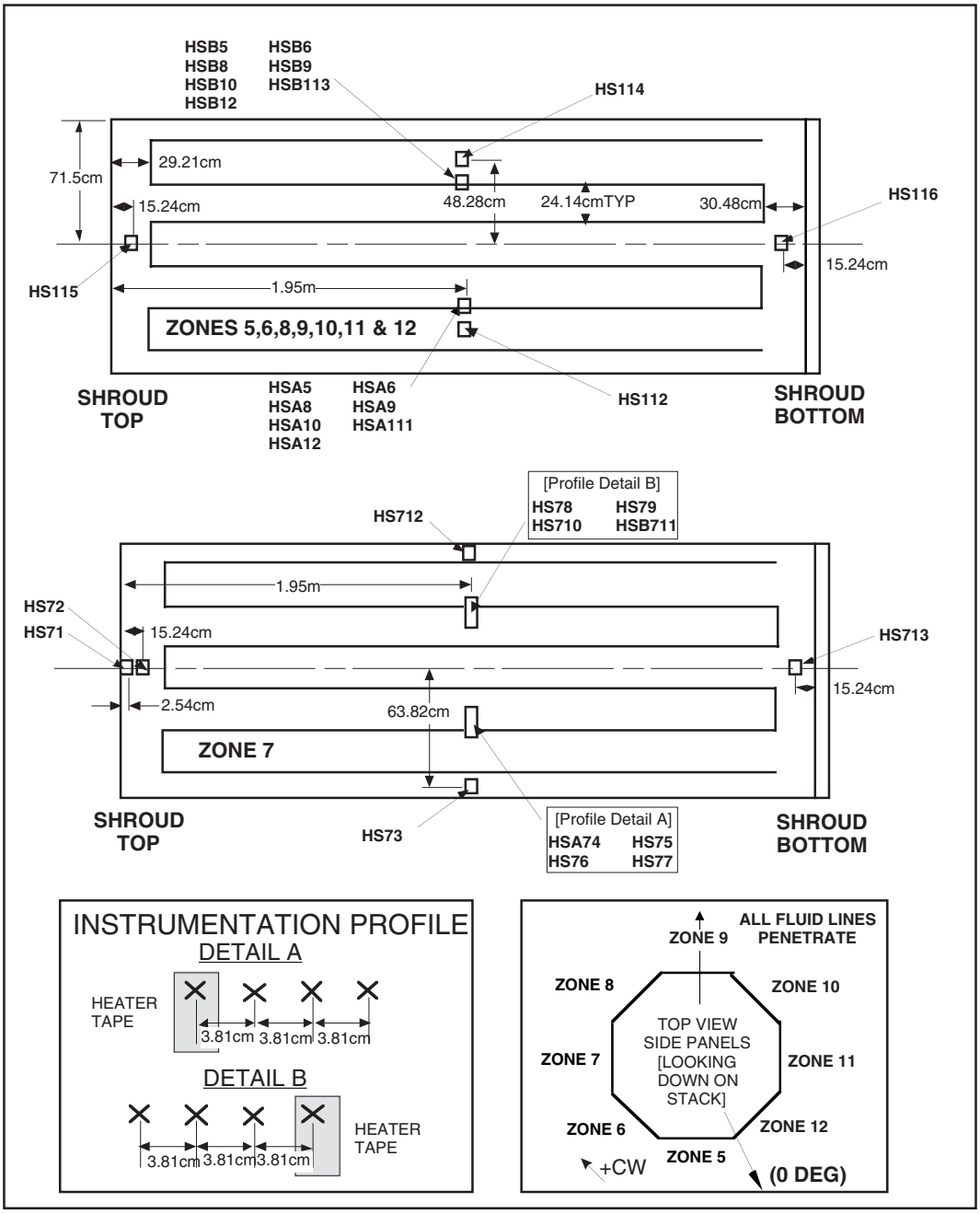

Figure 98. MHTB typical side wall environmental shroud panels.

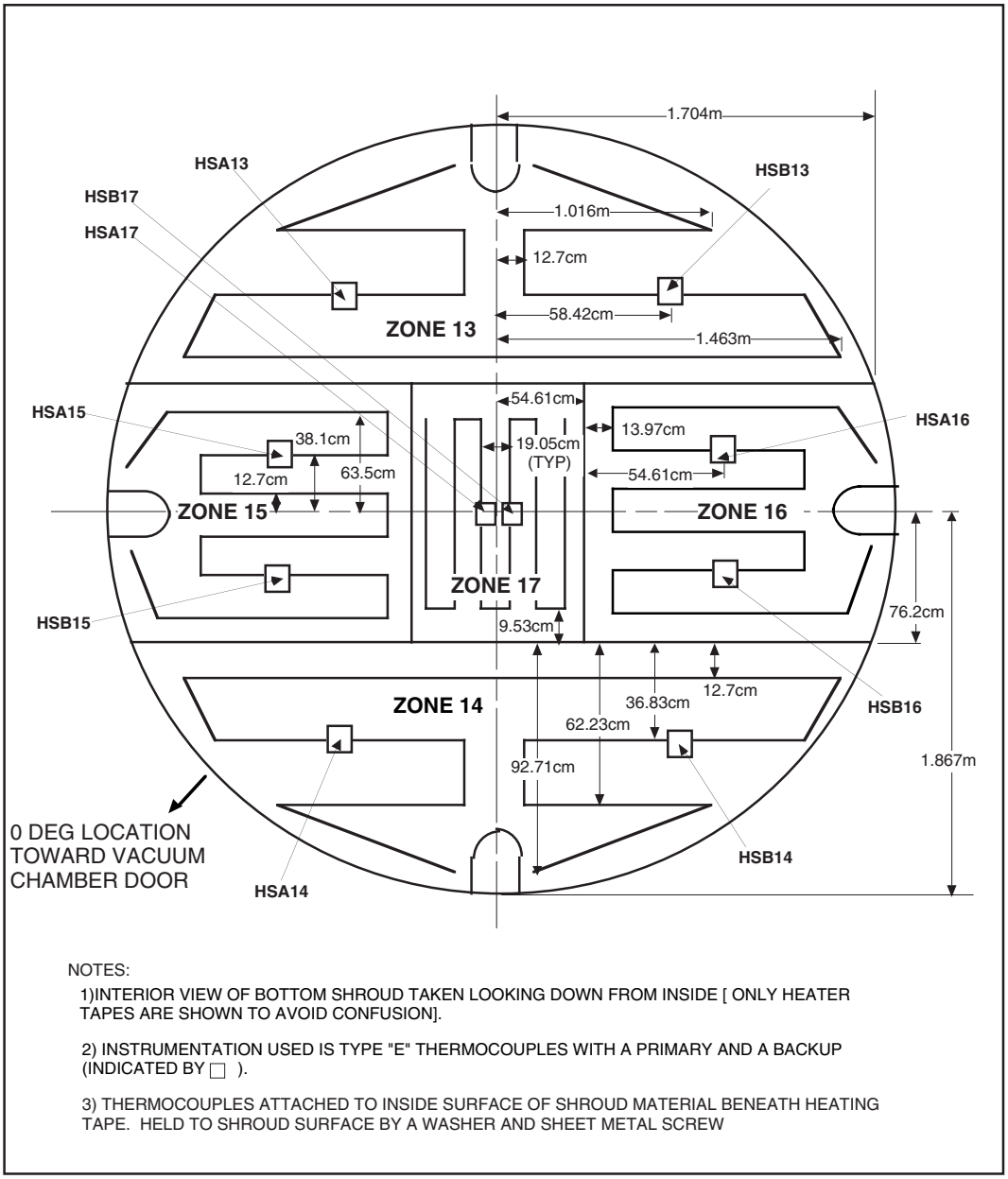

Figure 99. MHTB typical lower environmental shroud panels.

12) MHTB Zero-g Thermodynamic Vent System Instrumentation

The spray bar MHTB test phase requires that hardware related to the zero-g TVS be installed both internal and external to the MHTB test tank. Figure 84 illustrates the general hardware placement on the test tank while instrumentation placement on the hardware is outlined in figure 100. Attached to the lower MHTB tank bulkhead flange (external to the tank) is the vacuum tight TVS enclosure which contains the system control valving and recirculation pump. Instrumentation within the enclosure consists of thermocouples (T411, T412, T415, T416 and T417) pressure transducers (P402, DP400, P403, P404 and P405) and a flow meter (F401). Internal to the test tank is the heat exchanger/spray bar and a back pressure orifice. The spray bar is equipped with two silicon diodes (T413 and T414) and the orifice is instrumented with two diodes (T418 and T419) and two pressure transducers (P406 and P407). External to the MHTB tank, but still within the vacuum chamber, are temperature (diode T420) and pressure (P408) measurements on the TVS vent line to quantify the properties of the exiting gas flow. Instrumentation internal to the MHTB test tank will be routed through the 20.32cm (8") vent flange with the other internal instrumentation. The instrumentation within the TVS enclosure shall be routed through two Deutsch feed throughs and two thermocouple pull throughs. All thermocouples utilize an infinity meter for signal conditioning. The TVS enclosure shall be equipped externally with three thermocouples (T421, T422 and T423) mounted on the top, bottom and side of the enclosure, respectively. The enclosure internal pressure will be measured by two pressure transducers (P409 and P410). Appendix A contains, in a data base format, additional information regarding this instrumentation.

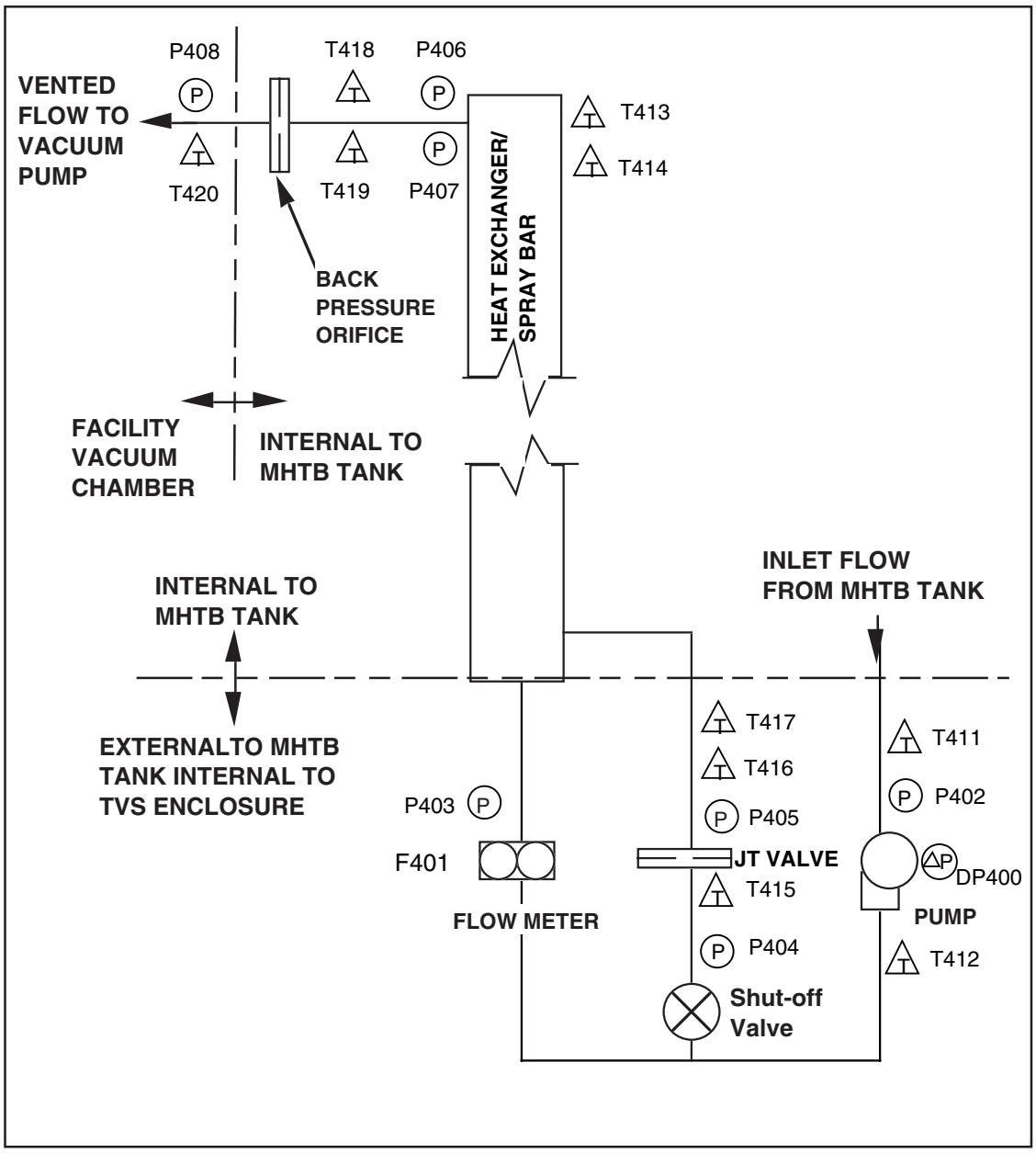

Figure 100. MHTB TVS instrumentation layout.

REFERENCES

1. Martin, J.J.; and Hastings L.J.: "Large-Scale Liquid Hydrogen Testing of a Variable Density Multilayer Insulation With a Foam Substrate," NASA/TM—2001–211089, NASA Marshall Space Flight Center, Huntsville, AL, 88 pp., June 2001.

2. Hastings, L.J.; Flachbart, R.H.; Martin, J.J.; et al.: "Spray Bar Zero-Gravity Vent System for On-Orbit Liquid Hydrogen Storage," NASA/TM—2003–212926, NASA Marshall Space Flight Center, Huntsville, AL, 160 pp., October 2003.

3. Flachbart, R.H.; Hastings, L.J.; Hedayat, A.; et al.: "Testing the Effects of Helium Pressurant on Thermodynamic Vent System Performance with Liquid Hydrogen," in *AIP Conf. Proc.*, AIP Publishing, Vol. 985, Melville, NY, pp. 1483–1490, doi:10.1063/1.2908510, 2008.

4. Flachbart, R.H.; Hastings, L.J.; Hedayat, A.; et al.: "Testing of a Spray-Bar Thermodynamic Vent System in Liquid Nitrogen," in *AIP Conf. Proc.*, AIP Publishing, Vol. 823, Melville, NY, pp. 240–247, doi:10.1063/1.2202422, 2006.

5. Jurns, J.M.: "Flow of Sub-Cooled Cryogens Through a Joule-Thomson Device—Investigation of Metastability Conditions," Master's Thesis, Cleveland State University, Cleveland, OH, 103 pp., December 2007.

REPORT DOCUMENTATION PAGE

Form Approved
OMB No. 0704-0188

1. REPORT DATE *(DD-MM-YYYY)*	2. REPORT TYPE	3. DATES COVERED *(From - To)*
01–07–2014	Technical Publication	

4. TITLE AND SUBTITLE

Liquid Methane Testing With a Large-Scale Spray Bar Thermodynamic Vent System

5a. CONTRACT NUMBER

5b. GRANT NUMBER

5c. PROGRAM ELEMENT NUMBER

6. AUTHOR(S)

L.J. Hastings,* L.G. Bolshinskiy,** A. Hedayat, R.H. Flachbart (retired), J.D. Sisco, and A.R. Schnell

5d. PROJECT NUMBER

5e. TASK NUMBER

5f. WORK UNIT NUMBER

7. PERFORMING ORGANIZATION NAME(S) AND ADDRESS(ES)

George C. Marshall Space Flight Center
Huntsville, AL 35812

8. PERFORMING ORGANIZATION REPORT NUMBER

M–1386

9. SPONSORING/MONITORING AGENCY NAME(S) AND ADDRESS(ES)

National Aeronautics and Space Administration
Washington, DC 20546–0001

10. SPONSORING/MONITOR'S ACRONYM(S)

NASA

11. SPONSORING/MONITORING REPORT NUMBER

NASA/TP—2014–218197

12. DISTRIBUTION/AVAILABILITY STATEMENT

Unclassified-Unlimited
Subject Category 20
Availability: NASA STI Information Desk (757–864–9658)

13. SUPPLEMENTARY NOTES

Prepared by the Propulsion Systems Department, Engineering Directorate
*Alpha Technology Inc., **Jacobs Engineering MSFC Group

14. ABSTRACT

NASA's Marshall Space Flight Center conducted liquid methane testing in November 2006 using the multipurpose hydrogen test bed outfitted with a spray bar thermodynamic vent system (TVS). The basic objective was to identify any unusual or unique thermodynamic characteristics associated with densified methane that should be considered in the design of space-based TVSs. Thirteen days of testing were performed with total tank heat loads ranging from 720 to 420 W at a fill level of approximately 90%. It was noted that as the fluid passed through the Joule-Thompson expansion, thermodynamic conditions consistent with the pervasive presence of metastability were indicated. This Technical Publication describes conditions that correspond with metastability and its detrimental effects on TVS performance. The observed conditions were primarily functions of methane densification and helium pressurization; therefore, assurance must be provided that metastable conditions have been circumvented in future applications of thermodynamic venting to in-space methane storage.

15. SUBJECT TERMS

liquid methane in-space propulsion, on-orbit liquid methane pressure control, in-space liquid methane storage, upper stage cryogenic fluid management

16. SECURITY CLASSIFICATION OF:			17. LIMITATION OF ABSTRACT	18. NUMBER OF PAGES	19a. NAME OF RESPONSIBLE PERSON
a. REPORT	b. ABSTRACT	c. THIS PAGE			STI Help Desk at email: help@sti.nasa.gov
U	U	U	UU	120	19b. TELEPHONE NUMBER *(Include area code)* STI Help Desk at: 757–864–9658

National Aeronautics and
Space Administration
IS20
George C. Marshall Space Flight Center
Huntsville, Alabama 35812